Enhancing the stability of probiotics: Freeze-drying and encapsulation

Bai, Shuai

2024

Enhancing the stability of probiotics: Freeze-drying and encapsulation

Enhancing the stability of probiotics: Freeze-drying and encapsulation

Shuai Bai Palmkron

LUND
UNIVERSITY

DOCTORAL DISSERTATION

Doctoral dissertation for the degree of Doctor of Philosophy (Ph.D.) at the Faculty of Engineering at Lund University to be publicly defended on Friday 2nd of February at 09.15 in Lecture Hall A, Kemicentrum, Lund

Faculty opponent
Professor Petra Först

Food Process Engineering, Technical University of Munich (TUM)
Munich, Germany

Organization:
LUND UNIVERSITY

Division of Food and Pharma

Document name: Doctoral dissertation	**Date of issue:** 02-02-2024
Author: Shuai Bai Palmkron	**Sponsoring organization:** BioGaia AB

Title: Enhancing the stability of probiotics: Freeze-drying and encapsulation

Abstract: This research dives into the intricate world of freeze-drying, an essential process in pharmaceutical and probiotic industries, to better understand the factors affecting probiotic stability during storage. The process of freeze-drying and the composition of freeze-dried products significantly affect the stability of probiotics, yet factors such as the material's encapsulation properties remain relatively unexplored, demanding further research.

This thesis will explore the effects of lyoprotectants, freezing, annealing, and drying on the structure of freeze-dried products. It aims to provide a comprehensive understanding of how varying conditions influence structural characteristics and their correlation with the storage stability of probiotics. We will also explore the key differences between vial and pellet formulations, and discuss topics critical for ensuring stability during storage such as glass transition temperatures.

The investigation uses techniques such as scanning electron microscopy (SEM) and X-ray micro-computed tomography (µCT) to investigate the structural attributes of freeze-dried material. The thickness of the encapsulating material is the central focus, revealing its crucial role in protecting the probiotic cells. The findings indicates that a notably thicker material provides increased protection, enhancing probiotic storage stability.

Keywords: Freeze-drying, lyophilization, L.ruteri, Probiotics, Lyoprotectant, Structure, Encapsulating material, Pore size, SEM, Tomography, Storage stability, DSC, Glass transition temperature, Amorphous sugars,

Classification system and/or index terms (if any)

Supplementary bibliographical information

Language: English

ISBN (pint): 978-91-8096-018-2

ISBN (digital): 978-91-8096-019-9

Recipient's notes	**Number of pages**: 68
	Security classification

Signature   Date 18-12-2023

Enhancing the stability of probiotics: Freeze-drying and encapsulation

Shuai Bai Palmkron

LUND
UNIVERSITY

*"Suckin' at something is the first step
to being sorta good at something"*
–Jake the dog

Table of Contents

Abstract

This research dives into the intricate world of freeze-drying, an essential process in pharmaceutical and probiotic industries, to better understand the factors affecting probiotic stability during storage. The process of freeze-drying and the composition of freeze-dried products significantly affect the stability of probiotics, yet factors such as the materials' encapsulation properties remain relatively unexplored, demanding further research.

This thesis will explore the effects of lyoprotectants, freezing, annealing, and drying on the structure of freeze-dried products. It aims to provide a comprehensive understanding of how varying conditions influence structural characteristics and their correlation with the storage stability of probiotics. We will also explore the key differences between vial and pellet formulations, and discuss topics critical for ensuring stability during storage such as glass transition temperatures.

The investigation uses techniques such as scanning electron microscopy (SEM) and X-ray micro-computed tomography (μCT) to investigate the structural attributes of freeze-dried material. The thickness of the encapsulating material is the central focus, revealing its crucial role in protecting the probiotic cells. The findings indicate that a notably thicker material provides increased protection, enhancing probiotic storage stability.

Popular scientific summary

The probiotic market reached a valuation of $60 billion in 2023, and this increase can be credited to the increasing interest in probiotic products among health-conscious consumers.

Probiotics are defined as: live microorganisms that confer health benefits when taken in adequate amounts. The live aspect of probiotics poses a unique challenge in industries where the storage stability of these live bacteria poses great difficulties.

Freeze-drying, also known as lyophilization, is the most commonly used technique to stabilize pharmaceutics and probiotics for long-term storage. This method removes water from the cell formulation by sublimation and preserves the viability of the bacteria by encapsulating dried cells within a protective material that maintains the structural integrity of the cell and protects it from changes during storage. The way freeze-drying is conducted has a significant impact on storage stability, presenting areas that need further research.

Unlike pharmaceutical ingredients such as proteins, probiotic cells are relatively large, ranging from 1 to 3 μm. To maintain the cells' integrity and viability during storage, these cells need to be well encapsulated inside a protective material. Structural properties, such as material stability during storage and material thickness, become crucial in this context. The traditional freeze-drying approaches based on much smaller pharmaceutical components may therefore not be suitable for the encapsulation of the larger probiotic cells.

The freezing step plays a crucial role in freeze-drying as the cooling rate affects the size of ice crystals. Very rapid cooling, such as quenching pellets in liquid nitrogen, results in small ice crystals while traditional freezing methods yield larger ones. Larger ice crystals facilitate more efficient drying and lead to a thicker encapsulating material, and are therefore preferred.

Annealing is a process where the sample is exposed to a temperature that encourages the growth of larger ice crystals and reduces smaller ones; the rate of the annealing process is faster for small ice crystals and decreases as their size increases. Annealing is therefore especially relevant for samples with small ice crystals, such as quenched pellets, and leads to reduced batch variations and enhanced encapsulation properties.

The final stage of freeze-drying is the drying process. Here, the goal is to preserve the product by removing the water while maintaining the integrity and viability of the cells. A challenge in this phase is the collapse of freeze concentrate due to insufficient mass transfer, common in non-annealed pellets, which can cause large deviations. Another challenge is the inhomogeneous heat transfer that leads to different drying rates amongst samples.

The different freeze-drying formats have different advantages but need to be handled in different ways, Pellets offer an increased surface area for better mass transfer, leading to a higher throughput compared to vial or tray drying, but pellets need to be annealed to create more efficient mass transfer and avoid collapse and deviations. Annealing is also crucial for creating a better encapsulating material for the cells. Freeze-drying in vials and trays is often less efficient but does not require annealing as the slow freezing already produces large ice crystals.

In summary, the freeze-drying of probiotics is a complex process that needs to be viewed differently from the freeze-drying of pharmaceutics. The encapsulation property is essential for probiotic storage stability and is a factor unique to probiotic products. As the market continues to grow, so does the incentive and need for research to develop more stable products.

Populärvetenskaplig sammanfattning

Probiotikamarknaden nådde en värdering på 60 miljarder dollar år 2023, och denna ökning kan tillskrivas det ökande intresset för probiotikaprodukter bland hälsomedvetna konsumenter.

Probiotika definieras som levande mikroorganismer som ger hälsofördelar när de tas i tillräckliga mängder. Att bibehålla vitaliteten hos probiotika utgör en unik utmaning inom branscher där lagringsstabiliteten hos dessa levande bakterier utgör en stor utmaning. Frystorkning är den mest använda tekniken för att stabilisera läkemedel och probiotika för långtidslagring. Denna metod avlägsnar vatten från cellformuleringen genom sublimation och bevarar bakteriernas livsduglighet genom att kapsla in torkade celler inom ett skyddsmaterial som bibehåller cellens strukturella integritet och skyddar den från förändringar under lagring. Sättet frystorkning utförs på har en betydande påverkan på lagringsstabiliteten och presenterar områden som behöver ytterligare forskning.

Till skillnad från farmaceutiska ingredienser som proteiner är bakterier relativt stora, varierande från 1 till 3 μm. För att bibehålla cellernas integritet och livsduglighet under lagring måste dessa celler vara väl inkapslade inuti ett skyddande material. De strukturella egenskaperna, såsom materialets stabilitet under lagring och materialets tjocklek, blir avgörande i detta sammanhang. De traditionella frystorkningsmetoderna baserade på mycket mindre farmaceutiska komponenter kan därför vara olämpliga för inkapsling av de större bakterier.

Fryssteget spelar en avgörande roll i frystorkning eftersom nedkylhastigheten påverkar storleken på iskristallerna. En mycket snabb nedkylning, som att snabbt kylda pellets i flytande kväve, resulterar i små iskristaller medan traditionella infrysningsmetoder ger större kristaller. Större iskristaller underlättar effektivare torkning och leder till ett tjockare inkapslande material och föredras därför.

Temperering är en process där provet utsätts för en temperatur som främjar tillväxten av större iskristaller och minskar de mindre, hastigheten för tempererings processen är snabbare för små iskristaller och minskar när storleken ökar. Temperering är därför särskilt relevant för prover med små iskristaller, som snabbkylda pellets, och leder till minskad variation inom produktionen och förbättrade inkapslingsegenskaper.

Den sista fasen av frystorkning är torkningsprocessen, målet är att bevara produkten genom att avlägsna vattnet samtidigt som cellernas integritet och livsduglighet bibehålls. En utmaning i denna fas är kollapsen av fryskoncentrat på grund av otillräcklig massöverföring, vilket är vanligt förekommande i icke-tempererade pellets och kan orsaka stora avvikelser. En annan utmaning är den ojämna värmeöverföringen som leder till olika torkningshastigheter bland proverna.

De olika frystorkningsformaten har olika fördelar men måste hanteras på olika sätt. Pellets erbjuder ökad yta för bättre massöverföringseffektivitet, vilket leder till en högre genomströmning jämfört med vial- eller bricktorkning, men de måste tempereras för att skapa effektiv massöverföring och undvika kollaps och avvikelser. Temperering är också avgörande för att skapa ett bättre inkapslande miljö för cellerna. Frystorkning i vials och brickor är ofta mindre effektivt men kräver inte temperering eftersom den långsamma nedfrysningen redan producerar stora iskristaller.

Sammanfattningsvis är frystorkning av probiotika en komplex process som måste betraktas annorlunda än frystorkning av läkemedel. Inkapslingsegenskapen är väsentlig för probiotikas lagringsstabilitet och utgör en faktor som är unik för probiotikaprodukter. I takt med att marknaden fortsätter att växa ökar incitamentet och behovet av forskning för att utveckla mer stabila produkter.

Acknowledgement

Embarking on a PhD feels like rediscovering the wonder of childhood, the authentic curiosity of the endless possibilities waiting to be explored, and facing the challenges ahead with fearlessness and tenacity. While the PhD journey undeniably brings its share of challenges that can shatter this outlook on life, supportive and loving supervisors and colleagues have been my companion and guide, helping me navigate the rough truth of the real world without losing the bright optimism.

The proverb "It takes a village to raise a child" perfectly applies to my journey as a PhD student, and there are numerous people to whom I owe sincere gratitude. Foremost amongst them are my supervisors, similar role as parents you have been my greatest support and role models.

To **Björn Bergenståhl**, you are a true inspiration, not only are you a dedicated and inspirational supervisor, but also a genuine loving and caring individual. I once heard a quote saying "Don't look for the 'most brilliant' supervisor. Look for the person who is kind, who mentors you, and lifts you up." I consider myself lucky to have found someone who embodies both kindness and wisdom in you.

Marie Wahlgren, first I want to express my gratitude for believing in my capacity to do a PhD even when I doubted myself. You are one of the main reasons I embarked on this journey. Your genuine care for your students permeates and shapes all your actions, and much like a mother, you're not afraid to show some tough love, and I have always recognized that it stems from a place of honest concern for my own best.

Anna Fureby, navigating through a PhD project is a daunting task, and I'm happy to have you as my guide, you have the ability to shine a light on the path ahead which has been immensely valuable for the success of this project. Having scientific discussions with you is fun.

Sebastian Håkansson, Like Doc in "Canary Row" provided guidance, allocated resources, built up a community, encouraged analytical thinking and problem-solving and supported Mack's personal and professional development, you have done the same for this project and me. You have become Doc, and I'm gladly embracing the role of Mack under your guidance.

Emanuel Larsson, your knowledge and enthusiasm for tomography have significantly elevated this project. Your dedication and willingness to assist make you not only a great scientist but also a great supervisor.

To my colleagues at BCC-P **Nikhil Rao, Ludwig Ermann Lundberg, Krishnan Sreenivas**, and all associated supervisors, you have taught me so much about the intricate and fascinating world of microbiology. The enjoyable adventures we shared will be forever cherished.

To **Ekaterina Bogdanova**, **Vitaly Kocherbitov** and my other colleagues at NextBioForm, your help and knowledge have been immensely valuable.

To **Olexandr Fedkiv, Peter Eklöv**, **Peter Jensen**, and **Hilde Skar Olsen**, thank you for all your support, the department literally wouldn't be running without you. And thank you **Lars Nilsson,** the time we randomly meet in an airplane was the starting point of this incredible journey.

Maintaining a balance between life and work during a PhD can be challenging. A PhD student, much like a child requires moments of fun and relaxation to thrive. "All work and no play makes Jack a dull boy" rings true. Thankfully, I didn't go insane as Jack did in the movie, and my colleagues and fellow PhD students played a significant role in maintaining my sanity.

First, I would like to thank all my colleagues and friends at **BioGaia** for making me feel at home at the company. **Julia Thomasson** and **Veronika Ekdahl**, you two are just awesome, you always make me happy and relaxed, and the haunted house will always put a smile on my face. **James Lemanczyk** thank you for all your expertise, we still need to go out for cocktails.

To my fellow PhD students and colleagues in the department **Lingping Zhang, Johanna Hjalte, Shruti Lawani, Juanita Francis, Anna-Maria Börjesdotter, Ingrid Ramm, Anna Kjellström, Catalina Fuentes, Zandra Gidlöf, Amanda Västberg, Daniel Osanloo, Hans Bolinsson,** and **Jade Schut**, what a brilliant, compassionate and fun bunch of individuals. If supervisors are like parents, consider yourselves siblings, only without the fights. We nurture, care for, and supports each other. We can always share our frustration and joy, and then we can go out and have fun. I am genuinely happy and grateful to have known each one of you.

Lastly, I would like to express my deepest gratitude to my family. **Maria Palmkron,** you are my foundation, my pillar of strength. Your unwavering support, understanding and love have remained steadfast throughout this challenging journey. This achievement would not be possible without you, and I'm lucky to have you by my side. **Alva Palmkron** my beloved daughter, you are undeniably my proudest achievement. You bring everything into perspective, and when I hold you all frustration and worries vanish. Witnessing your joy and growth brings me more happiness than any academic accomplishment. I'm truly blessed to be your father; I love you dearly!

List of Papers

Paper I: **Temperature and Heat Transfer Control During Freeze-drying. Effect of Vial Holders and Influence of Pressure**

Shuai Bai Palmkron, Linnea Gustavsson, Marie Wahlgren, Björn Bergensthål, Anna Millqvist Fureby. (2022), In: *Pharmaceutical Research,* 39, 2597-2606. https://doi.org/10.1007/s11095-022-03353-4

Paper II: **Quantification of structures in freeze-dried materials using X-ray microtomography**

Shuai Bai Palmkron, Björn Bergenståhl, Sebastian Håkansson, Marie Wahlgren, Anna Millqvist Fureby, Emanuel Larsson. (2023), In: Colloids and Surfaces A: Physicochemical and Engineering Aspects, Volume 658, 130726. https://doi.org/10.1016/j.colsurfa.2022.130726

Paper III: **Quantification of structures in quenched annealed and nonannealed freeze-dried pellets using X-ray microtomography**

Shuai Bai Palmkron, Björn Bergenståhl, Sebastian Håkansson, Marie Wahlgren, Emanuel Larsson, Anna Millqvist Fureby, Manuscript

Paper IV: **The impact of annealing methods on the encapsulating structure and storage-stability of freeze-dried probiotic pellets.**

Shuai Bai Palmkron, Björn Bergenståhl, Sebastian Håkansson, Marie Wahlgren, Emanuel Larsson, Anna Millqvist Fureby, Manuscript

Paper V: **Microtomography for in-situ studies of the freeze-drying process**
Shuai Bai Palmkron, Hans Bolinsson, Jonas Engqvist, Björn Bergenståhl, Sebastian Håkansson, Marie Wahlgren, Emanuel Larsson, Anna Millqvist Fureby, Short communication Vinnova

Other related publications

Impact of pre-formulation hold time on long-term stability of *Limosilactobacillus reuteri* DSM 17938

Nikhil Seshagiri Rao, Shuai Bai Palmkron, Ludwig Ermann Lundberg, Krishnan Sreenivas, Christer Larsson, Björn Bergenståhl, Anna Millqvist Fureby, Ed WJ van Niel, Stefan Roos, Magnus Carlquist, Sebastian Håkansson.

Author's contribution to the papers

Paper I

I participated in the study design along with my supervisors. I performed the experimental work together with a master's student. I designed the equipment used to perform the experiments. I performed the data analysis as well as drafted the manuscript.

Paper II

I designed the study together with my supervisors. I performed the experimental work, I participated in DSC measurements. I participated in the tomographic measurements and performed the data analysis together with my supervisors. I performed the SEM measurements and did the analysis together with my supervisors. I performed the data analysis and wrote the first version of the manuscript.

Paper III

I designed the study with support from supervisors. I developed methods and protocols for pellet freeze-drying. I performed the DSC measurements. I participated in the tomographic measurements and performed the data analysis together with my supervisors. I performed the SEM measurements and did the analysis together with my supervisors. I performed the data analysis and drafted the manuscript.

Paper IV

I designed the study and experimental methods with support from my supervisors. I developed methods and protocols for pellet freeze-drying and the stability study. I performed all the experiments. I participated in the tomographic measurements and performed the data analysis together with my supervisors. I performed the data analysis and wrote the first version of the manuscript.

Paper V

I designed the study and performed the synchrotron tomographic measurements, and participated in the design of the sample environment. I participated in writing the short communication.

Abbreviations

BET	Brunauer-Emmet-Teller
CFU	Colony-forming unit
Cg'	Concentration of a maximally freeze-concentrated solution.
DSC	Differential scanning calorimetry
SEM	Scanning electron microscopy
SRµCT	Synchrotron-based X-ray micro-computed tomography
Tc	Collapse temperature
Tg	Glass transition temperature
Tg'	Glass transition temperature for maximally freeze-concentrated solution
TGA	Thermogravimetric analysis
µCT	X-ray micro-computed tomography

Introduction to the downstream process of probiotics

The market for probiotic products has been steadily growing in the last decades and as of 2023 is valued at 70 billion dollars (Prajapati *et al.*, 2023). The increasing interest in probiotic products is also shown in the number of papers published on this subject, which has grown from a few hundred at the turn of the millennium to close to ten thousand in the year 2022, data obtained from Scopus. One of the big research topics revolves around improving the downstream production process to increase storage stability, a matter of significant concern to the industry. Stability improvements not only reduce resource consumption but also elevate product quality and improve consumer trust (Jackson *et al.*, 2019). This thesis aims to provide a holistic approach to optimize the downstream process, thereby enhancing storage stability.

Probiotics are defined as: <u>Live</u> microorganisms that, when administered in adequate amounts, confer a health benefit on the host (Hill *et al.*, 2014). The challenges in this research lie in the initial word of this definition, the necessity of live microorganisms. To overcome the challenges associated with preserving the vitality of live microorganisms, researchers and industry turn to techniques like freeze-drying.

Freeze-drying or lyophilization is one of the most common ways to stabilize pharmaceutics such as proteins and high-value foods for long-term storage (Franks & Auffret, 2008; Gaidhani *et al.*, 2015; Tang & Pikal, 2004). The most common method to ensure the viability of probiotics is also to encapsulate the dried cells in a protective material. The way freeze-drying is conducted, as well as the composition of the encapsulating material, strongly affects the storage stability of probiotics.

While freeze-drying is a well-established technique for enhancing the stability of probiotics, the research is dominated and influenced by pharmaceutical applications. The most common approach in the pharmaceutical industry is to freeze dry in vials or trays at a low sample temperature to obtain an elegant freeze-dried cake without visible collapse (around 10–20% solute concentration) and with good rehydration properties (Liu, 2006). The research focus has been directed toward developing formulations and processes that protect the API (Tang & Pikal, 2004; Wang, 2000)

and increase the reproducibility, robustness and efficiency of the process (Foerst *et al.*, 2019b).

When developing a downstream process to enhance the storage stability of a probiotic product, it is essential to account for the specific properties and factors related to the bacteria, such as membrane/cell wall composition (Hansen et al., 2015), metabolic activity (Lundberg, 2023), oxygen sensibility (Rao et al., 2023) etc. This thesis will particularly address a factor that has been overlooked in academic research: the impact of bacteria size and the demands this puts on the encapsulating material. The methodologies and practices employed by the pharmaceutical field have influenced both the academic research into freeze-drying of probiotics and the practices within the probiotic industry. However, the question is whether a pharmaceutical methodology such as conservative freeze-drying results in an ideal structure necessary for effective encapsulation, especially for larger entities such as probiotic cells.

There has been limited emphasis on the encapsulation capacity of freeze-dried material in the pharmaceutical industry. This is primarily because the pharmaceutical ingredient is typically significantly smaller than the dimensions of the freeze-dried material and therefore always well encapsulated. The encapsulation capacity is therefore an issue unique to bacteria formulations. A typical freeze-dried material for pharmaceutical purposes produces an encapsulating material that is around 1µm thick, (**Paper II**) (Hottot *et al.*, 2004; Oddone *et al.*, 2017; Palmkron *et al.*, 2023); the approximate size of *Limosilactobacillus reuteri* is around 1-3 µm (Rao *et al.*, 2021). This implies that the cells may protrude beyond the material, experiencing inadequate encapsulation in the material that is supposed to protect them. The thickness of the freeze-dried material is an indication of encapsulation capacity and may therefore be a factor of importance.

Academic research has predominately emphasized production formats such as vials and trays, which are the most common formats in the pharmaceutical industry (Gan *et al.*, 2005; Patel & Pikal, 2011). Conversely, the probiotic industry predominantly employs pellets as the format. At the time of writing, only a handful of articles have discussed the freeze-drying of bacteria in pellet format (**Paper III, IV**) (Ekdawi-Sever *et al.*, 2003). It is crucial to acknowledge that the structure and handling of these formats significantly differ from one another. Consequently, optimization conducted for one format may not apply to the other. This thesis aims to explore the disparities between different formats concerning their handling, differences in structure, and the influence this has on storage stability. *Limosilactobacillus reuteri* DSM 17938 provided by BioGaia is used in all stability studies in this thesis.

Due to the relative neglect of encapsulation properties, there are currently no established methods available for the assessment of these properties regarding freeze-dried material. Previous studies to quantify freeze-dried material have been focused on pore size and not material thickness (Arsiccio *et al.*, 2019; Konstantinidis

et al., 2011; Qian & Zhang, 2011). The lack of quantification methods has presented a significant challenge in developing novel methods to quantify freeze-dried material. Methods assessed include Brunauer-Emmet-Teller analysis (BET), able to quantify surface areas and pore size distributions; freeze-drying and light microscopes for structural overviews and determination of collapse temperatures; scanning electron microscopy (SEM) for detailed cross-sectional images; and X-ray micro-computed tomography (μCT), that provides a comprehensive 3D structural map. The combination of SEM and μCT proved to be most promising as the high resolution of SEM gave a detailed overview while μCT provided data for quantitative analysis.

State diagrams such as the one shown in Figure 1, serve as an essential tool in the designing of a downstream process. The diagram provides information on how changes in temperature and water content affect the state of the formulation. It can portray the trajectory and alterations in the formulation throughout different process steps. State diagrams can be used to showcase the behaviour and stability of a dried formulation (Chapter 1). Additionally, they offer insights into the implications of different cooling rates during freezing and provide an understanding of optimal annealing conditions (Chapter 2) and freeze-drying conditions (Chapter 3). State diagrams will be used throughout this thesis to illustrate different process steps.
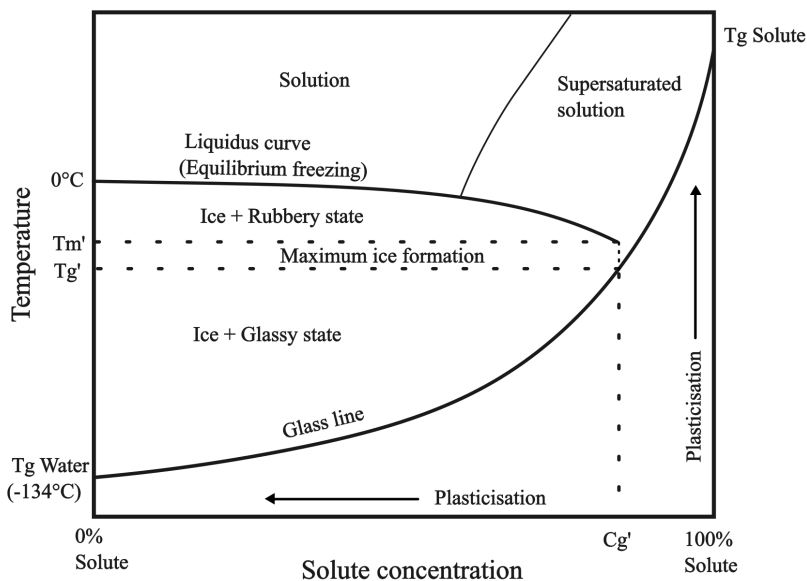
Figure 1: Typical state diagram of an amorphous formulation consisting of sugars. The diagram can provide an overview of how changes in temperature and water content affect the state of the formulation. It can provide information on the storage stability of the solute (Tg solute), optimum freeze-drying conditions (Tg'), freezing, and annealing trajectories (liquidus and glass curve).

The aim of the thesis

The objective of this thesis is to provide an overview of the various stages of the probiotic downstream process, focusing on understanding factors influencing probiotic stability during storage. The study will investigate how lyoprotetants, freezing, annealing, and drying affect the encapsulating properties of the structure of the freeze-dried material and evaluate their implications on the storage stability of the probiotics.

The encapsulation properties of the material are a relatively unexplored topic, and the aim is to shed a light on their role in preserving probiotics during storage. This study will also compare the differences between vial and pellets freeze-drying formats. The investigation on the freeze- dried structure utilizes techniques such as scanning electron microscopy (SEM) and X-ray micro-computed tomography (μCT), with focus on thickness of the encapsulating structure.

The primary goal is to establish a correlation between different process condition, characteristics of the dried material, and storage stability.

Chapter 1:

Formulation

Introduction

The most studied way to improve the stability of probiotic products is to find an appropriate mix of agents. In the literature, this protective agent is variably referred to as a cryoprotectant or lyoprotectant, indicating its role in protecting the cells during freezing, drying, and often also storage. In this thesis, I will exclusively use the term lyoprotectant for constituents aimed to protect the cells and the term formulation for compositions of both lyoprotectants and stabilizers. The formulation aims to relieve as much stress as possible during the downstream process and provide stability during the storage (Kiepś & Dembczyński, 2022). A well-designed formulation should consider all the stresses posed by freezing, drying, and storage to ensure good storage stability with high colony-forming unit (CFU) and cell viability over time. The cells undergo various kinds of stress during the downstream process including osmotic, freezing, drying and storage. This thesis will focus on the two primary stresses that have the most significant impact on stability: drying and storage.

Lyoprotectant

The drying process imposes significant stress on the cells, especially on the membrane. The cell membrane consists of a lipid bilayer where the polar headgroups are oriented toward the polar water. Removing the water during drying will disrupt the orientation and cause aggregation of the (acyl chains) polar headgroups (Santivarangkna, 2015). To be able to maintain the orientation and integrity of the cell membrane, a substitute for the water is needed. The requirements for such a substance are that it needs to be polar (hydroxyl group) in its dry state and be sufficiently small to provide support between the polar headgroups on the membrane. This is called the water replacement theory (Aschenbrenner *et al.*, 2015). Some also hypothesize that it is beneficial if the lyoprotectants can accumulate inside the cells for protection against freezing and dehydration (Duong *et al.*, 2006;

Termont *et al.*, 2006; Tymczyszyn *et al.*, 2007). Common substances used for this purpose are non-reducing disaccharides such as trehalose and sucrose. Other small polar molecules such as glutamate, can also serve as suitable candidates (Aschenbrenner *et al.*, 2015). To maintain the polarity in the dry state, the dried formulation must be in its amorphous form. This is the reason many monosaccharides are unsuitable as protectants as they tend to crystalize during handling/freezing and lose their hydrogen bond capacity (Dixit *et al.*, 2011; Mehta *et al.*, 2013; Santivarangkna *et al.*, 2011). The freeze-dried material discussed in this thesis will solely be of amorphous form. The reason non-reducing sugars such as sucrose and trehalose are commonly used is to avoid Maillard reactions, as this degrades the cells and produces water, which is detrimental to stability (Chen *et al.*, 2023; Montel Mendoza *et al.*, 2014). A formulation comprising only lyoprotectant, such as disaccharides, often exhibits high freeze-drying survival. However, to address other stresses encountered during storage, a more complex composition is required in the formulation design.

The primary challenge arises during storage, when the dried product is exposed to oxygen and experiences fluctuations in humidity and temperature (Celik & O'Sullivan, 2013; Kurtmann *et al.*, 2009; Montel Mendoza *et al.*, 2014). An increase in temperature and moisture level plasticizes the material and can lead to loss of stability. Maintaining the stability of the amorphous encapsulating material throughout the storage is crucial, and stabilizers play an essential role in preserving a static and stable product (Pehkonen *et al.*, 2008). Figure 2 shows freeze-drying survival and storage stability for small polar molecules (sucrose and glutamate) with and without stabilizers (maltodextrin).

The freeze-drying survival rates vary between 60% to 30% for all the formulations without a noteworthy pattern. However, on examining the storage stability an interesting trend emerges, indicating that lyoprotectants alone (sucrose and glutamate), as well as stabilizers alone (maltodextrin), are insufficient to maintain viability during storage. However, when combined, the formulation exhibits increased stability over time (Oluwatosin *et al.*, 2022; Yang, 2021). Understanding the importance of combining lyoprotectants with stabilizers depends on grasping an essential aspect of formulation – the glass transition temperature of the dried product.
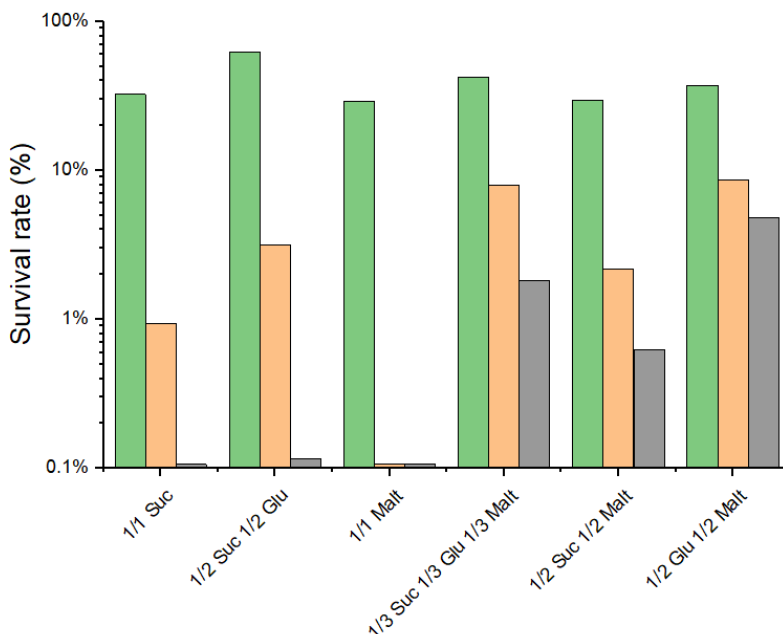
Figure 2: Freeze-drying survival and storage stability of lyoprotectants sucrose and glutamate in combination with stabilizer maltodextrin stored at 37°C (In vials). Samples contain 10% solute and 10^{10} cells/ml. The CFU was measured after freeze-drying (green column), 19 days of storage (orange column), and 42 days of storage (grey column). Samples containing solely lyoprotectants or stabilizers respectively, had poor storage stability, while the combination of both significantly increased the storage stability (Values based on CFU of biological duplicates) (Yang, 2021).

Glass transition temperature of the dried formulation

The glass transition temperature (Tg) is the temperature at which an amorphous material undergoes a transition from a hard brittle state to a rubbery viscous state. The Tg signifies a change in the material's physical properties. When the storage temperature is below the Tg, the material remains rigid/static and glassy/amorphous. But if the storage temperature is above the Tg, the material becomes more flexible and can undergo physical changes that lead to storage collapse and eventually crystallization (Bhugra *et al.*, 2007; Harnkarnsujarit *et al.*, 2012; Mathlouthi, 1995; te Booy *et al.*, 1992), which is detrimental to viability. The Tg is dependent on the formulation and the moisture content of the product. Since the freeze-dried material is often hygroscopic, this may result in an increase in the moisture content during storage and a decrease in Tg (Ghorab *et al.*, 2014; Mathlouthi, 1995). Hence, it is advisable to design a formulation with a high Tg that can withstand increases in moisture content and temperature and to store the product in a dry environment. A

rule of thumb is to design a formulation with a Tg 50°C higher than the storage temperature (Craig *et al.*, 1999; Hancock & Zografi,1997).

While disaccharides serve as effective protectants against drying, formulations relying solely on them often show a rapid decrease in survivability during storage. This arises from the fact that a dried formulation consisting of disaccharides has a low Tg even at low moisture contents (Roe & Labuza, 2005). Figure 3 shows the structural stability during storage at 37°C for samples containing sucrose, glutamate (lyoprotectants) and maltodextrin (stabilizer). Samples with lyoprotectants alone are unstable during storage and lead to storage collapse and loss of viability, while mixtures of lyoprotectants and stabilizers remain intact during storage and can maintain better viability (Yang, 2021). Stabilizers alone do not provide good stability against storage (see Figure 2) and are only added to sufficiently increase the Tg of the dried product.
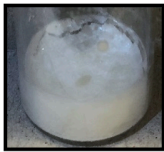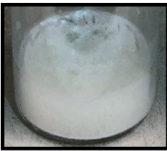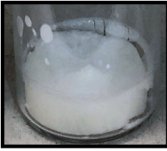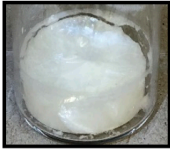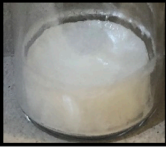
Composition	After freeze-drying	After 19 days of storage

Figure 3: Structural stability during storage for formulations containing sucrose and glutamate, with and without stabilizer maltodextrin stored at 37 °C. Samples contain 10 % solute and 1010 cells/ml. Primary drying was done at 10 Pa at -30 °C, and secondary drying was done at 20 °C at the same chamber pressure. The sample without stabilizer undergoes storage collapse while samples with stabilizers remain intact.

The best way to understand the Tg of a formulation and the effects of mixing ingredients is by studying the state diagram shown in Figure 4. An increase in water content and temperature plasticizes the material and a pure sucrose formulation with low Tg (around 60°C) quickly plasticizes with increased moisture content and temperature (Roe & Labuza, 2005). While short sugars such as sucrose prove to be unstable during storage, a longer polysaccharide with high Tg, such as maltodextrin, offers stability. By combining the two constituents, a formulation with both protective properties and stability can be achieved (Rodríguez Furlán et al., 2011; Yang, 2021)

Mixing lyoprotectants with a stabilizer such as a maltodextrin also increases the glass transition temperature of the freeze concentrate (Rodríguez Furlán et al., 2011), which is an important aspect of freezing, annealing, and drying and will be discussed in later chapters.
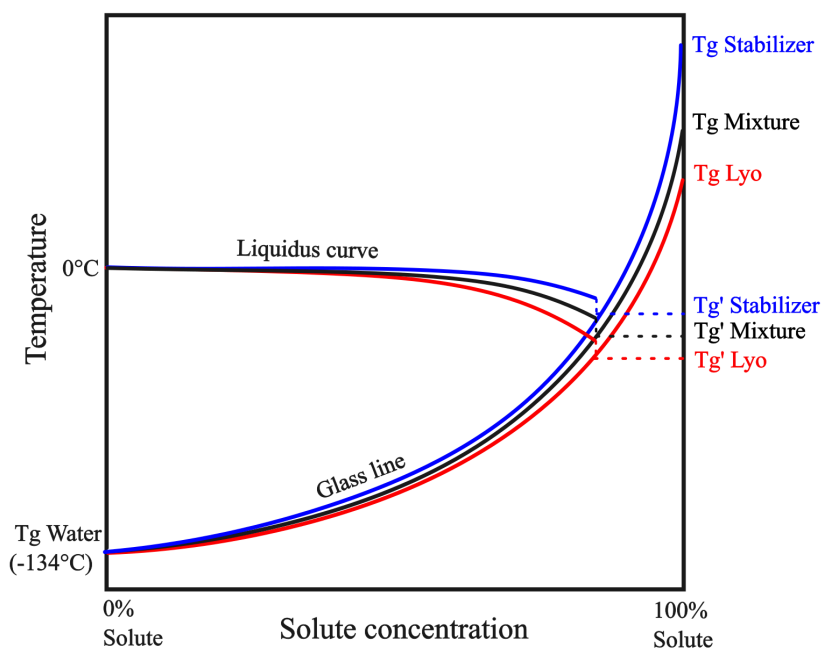
Figure 4: State diagram of lyoprotectant such as sucrose (Red), Stabilizer such as maltodextrin (Blue), and a mixture of both (Black). lyoprotectant has a low Tg and therefore has poor storage stability. The Tg can be increased by adding a stabilizer which increases the Tg, thereby increasing the storage stability. The Tg' is also increased when stabilizers are added; this will facilitate the freeze-drying process (Chapter 3).

Handling

The harvested cells are metabolically active; this needs to be considered when the cells are dispersed in the formulation. If the formulation consists of sugars, which often is the case, enzymes such as glucansucrase and other metabolic activity in the cells will start to convert it into other components (Lundberg, 2023; Seshagiri Rao, 2023). This changes the composition of the formulation and can significantly alter the stability of the final product. To avoid alterations in the composition by metabolic activity a formulation containing cells needs to be frozen as soon as possible. The holding time from when cells are dispersed in the formulation to being frozen can greatly affect the storage stability of the product. Figure 5 illustrates the storage stability of a formulation containing cells and sucrose that has been directly frozen, maintained at room temperature for 3 hours, and maintained at room temperature and replenished with sucrose. It clearly shows the negative effect of the lyoprotectant conversion, where the survival rate (CFU/g) of samples maintained at room temperature rapidly declined (Seshagiri Rao, 2023).
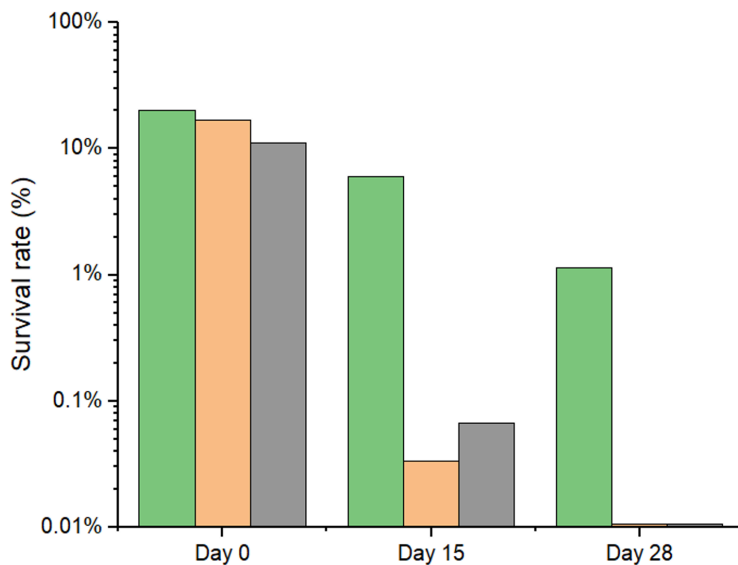
Figure 5: The effect of hold time on the storage stability of freeze-dried bacteria. Fresh cell culture is dispersed in a formulation containing 10% sucrose, 1/3 of the suspension is directly frozen (green column), 1/3 is left at room temperature for 3h and then frozen (orange column). The last 1/3 is left at room temperature for 3h and then replenished with sucrose (grey column). The samples were then freeze-dried, and storage stability was conducted at 37°C. The 3h hold time had a detrimental impact on the storage stability (value based on the CFU of biological triplicates).

Production formats: Vial/Tray Vs Pellets

There are two common ways to freeze dry the cell suspension, using vials/trays or pellets (drying in vials and trays are similar processes). The predominant format in the pharmaceutical industry and academic research involves vials or trays, where the formulation is filled to a hight of approximately 1cm to prevent excessive resistance (see Chapter 3). Subsequently these vials or trays undergo freezing either inside a freeze dryer or a freezer, with a relatively slow cooling rate of 1–5°C/min. Both vials and trays are frozen in similar manners, yielding comparable structures (Badal Tejedor *et al.*, 2020; Bagad *et al.*, 2017; Béal & Fonseca, 2015; Champagne *et al.*, 1996; Fonseca *et al.*, 2015; Giulio *et al.*, 2005). The other approach of preparing the formulation involves freezing drops of formulation rapidly by quenching them in liquid nitrogen which results in very rapid freezing, up to 300°C/min (Oetjen & Haseley, 2007). While pellets are a common format used in the probiotic industry, they also find applications in the formulation of diagnostics (Erber & Lee, 2015) and, in some cases, proteins (Olbrich *et al.*, 2019). The significant increase in the surface area of pellets, compared to trays and vials, increases the efficiency of pellets freeze-drying as more surface area is exposed to the vacuum. This increases the freeze-drying capacity and increases the throughput of the downstream process.

However, major differences exist between pellet and vial/tray formats in both performance as well as in structure and material properties (Palmkron *et al.*, 2023) (**Paper III**). Acquiring knowledge of the differences between each format is essential for ensuring the stability and reproducibility of the product. Although the pellet is a common format in the probiotic industry, there are only a few scientific articles published on the topic (Aschenbrenner *et al.*, 2015; Ekdawi-Sever *et al.*, 2003).

This thesis will explore how pellets differ from vials/trays in freezing, annealing, and drying (Chapters 2 and 3) and examine differences in the structure of the freeze-dried product (Chapter 4).

Chapter 2

Freezing and Annealing

Introduction

Freezing is the first step of freeze-drying, and the moment when most of the water is separated from the formulation. During freezing, the sample is separated into several phases, consisting of pure water as ice and a freeze-concentrated formulation with cells dispersed in it. Annealing is a process in which the frozen sample is exposed to a temperature where the size of the ice crystals can be altered. Understanding the dynamics of freezing and annealing is essential, as it significantly impacts both the freeze-drying process and the structure of the dried product.

Impact on ice

Nucleation is the initial step in the formation of ice crystals; aggregations of tiny clusters of water molecules act as the starting blocks for the ice crystals. When the nuclei are sufficiently large, ice crystals will start to form. The number of nuclei in the solution will determine the size of the ice crystals, where a higher number of nuclei will result in smaller ice crystals. The number of nuclei is determined by the degree of undercooling, which is the temperature difference between the thermodynamic ice formation temperature (freezing point -0 °C) and the actual temperature when the water crystallizes. Factors such as cooling rate and available surfaces (presence of particles) affect the degree of undercooling; the presence of particles will facilitate the nucleation and decrease the undercooling (heterogeneous nucleation) (Jameel & Searles, 2010; Nakagawa *et al.*, 2007). Very quick cooling such as quenching the formulation in liquid nitrogen, results in the highest undercooling and smallest ice crystals. A slow cooling rate such as freezing the vial/tray in a pre-cooled freezer or freeze dryer normally results in lower undercooling and larger ice crystals (Hottot *et al.*, 2004). The crystallization process is a stochastic process, and it can be difficult to ensure uniformity amongst the samples in a freeze-drying batch (Vali, 1994).

Directional freezing introduces a temperature gradient to the sample, causing the cooler section to crystallize first. Consequently, ice crystals begin to grow in the direction of the temperature gradient, leading to oriented ice crystals (Zhang &

Cooper, 2007). This phenomenon is commonly observed in quenched pellets, resulting in anisotropic structures with ice crystals pointing towards the centre.

The size of ice crystals will affect many aspects of the downstream process. A larger ice crystal size creates larger pores, decreasing the diffusion resistance during drying compared to small ice crystals, which create small and narrow pores (Assegehegn *et al.*, 2019; Hottot *et al.*, 2004). Large crystals are therefore often preferred as this increases the drying rate. A common method in the industry to maximize the ice crystal size is to minimize the undercooling. This is achieved by introducing nucleation points, which can be done by spraying the samples with a mist of ice crystals when the sample temperature has dropped below the freezing point. The low undercooling results in larger ice crystals and facilitates drying (Palmkron *et al.*, 2023; Searles *et al.*, 2001). Larger ice crystals also occupy less surface area compared to small ones, which leads to a thicker freeze-concentrated material in between the ice crystals, which eventually leads to a thicker dried material. The material thickness is one of the main topics in this thesis and will be described more in detail in the following chapters.

Impact on freeze concentrate and glass transition temperature

When nucleation/crystallization occurs, water from the formulation starts to diffuse to the ice crystal, concentrating the formulation. With increasing concentration, the rate of water diffusion from the freeze concentrate to the ice crystals decreases. At a slow cooling rate (equilibrium freezing rate), water molecules can diffuse from the freeze concentrate to the ice crystals, ultimately reaching the maximally freeze-concentrated solution (Cg') of approximately 80% for a sugar-water mixture (Roos, 1997). The Tg of this freeze-concentrated solution is called the glass transition temperature of a maximally freeze-concentrated solution (Tg') and depends on the composition of the formulation. The freeze concentrate solidifies at a temperature below Tg', and further concentration of the formulation is not possible (Roos, 1997). The Tg' is a crucial factor to consider in maintaining structural integrity during the drying process. Frozen samples are recommended to be stored at temperatures below Tg' (often -80°C) to avoid changes in the sample.

Rapid cooling leads to non-equilibrium freezing, where the water from the freeze concentrate is unable to diffuse to the ice crystals before the temperature has declined below its Tg. This is the case when freezing is done by quenching droplets of formulation in liquid nitrogen (-195.8°C). The unfrozen water trapped in the freeze concentrate leads to a lower Tg and Cg compared to the maximally freeze-concentrated solution (Tg' and Cg') (Charoenrein & Harnkarnsujarit, 2017). A rapidly frozen sample that has not reached the Tg' is called a non-relaxed sample and is characterized by a high volume ratio of freeze concentrate with lower Tg and a low volume ratio of small ice crystals compared to a maximally freeze-concentrated sample.
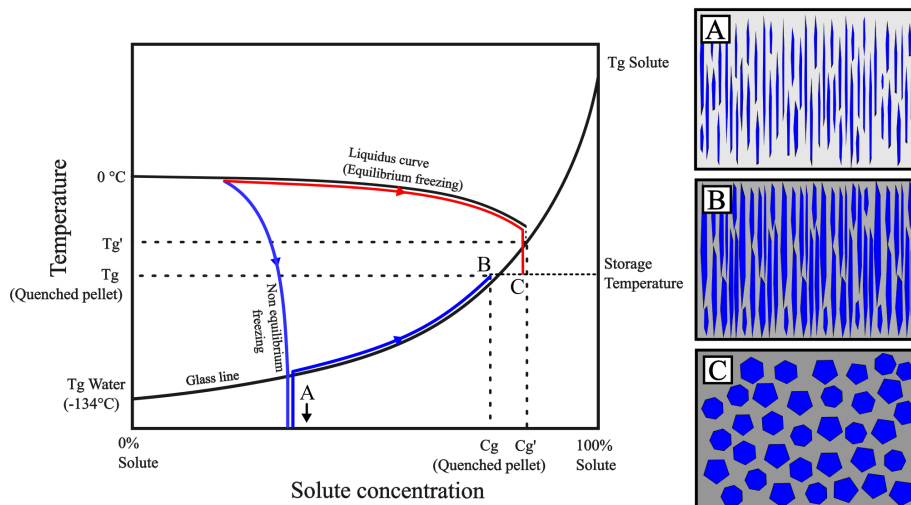
Figure 6: This state diagram depicts the freeze concentrate trajectory at different cooling rates, accompanied by images illustrating the composition. In the images, blue sections represent ice crystals, and grey areas are the freeze concentrate, with darker shades indicating a higher concentration of solute. The blue line in the state diagram represents a rapidly cooled sample at a non-equilibrium freezing rate, resulting in small ice crystals and low Tg (A). The red line represents a slow cooling at an equilibrium freezing rate, leading to larger ice crystals and a freeze concentrate at Tg' (C). In storage, the rapidly frozen sample undergoes relaxation (see next paragraph), resulting in larger ice crystals and Tg equal to the storage temperature (B), while the slowly frozen sample remains unchanged.

Understanding the influence of cooling rate on the Tg is essential when designing the downstream process. The state diagram depicted in Figure 6 illustrates the trajectory of various cooling rates and their effects on the composition and Tg of the sample.

The different production formats give rise to different cooling rates. Vials and trays placed in a pre-cooled freeze dryer or freezer typically experience a cooling rate of 0.5–5 °C/min. In contrast, the temperature of pellets quenched in liquid nitrogen rapidly drops to -196°C. The impact of the cooling rate on the Tg of the freeze concentrate can be measured using differential scanning calorimetry (DSC). DSC measurements of different cooling rates and their impact on the Tg in a 10% sucrose solution are shown in Figure 7. This shows that an increase in cooling rate from 0.5–20°C/min results in a small decrease in Tg (Yang, 2021).

Due to the difference in freezing rate between vials and pellets, it is crucial to handle them in very different ways. The different freezing methods also exert different kinds of stress on the bacteria (Béal & Fonseca, 2015).
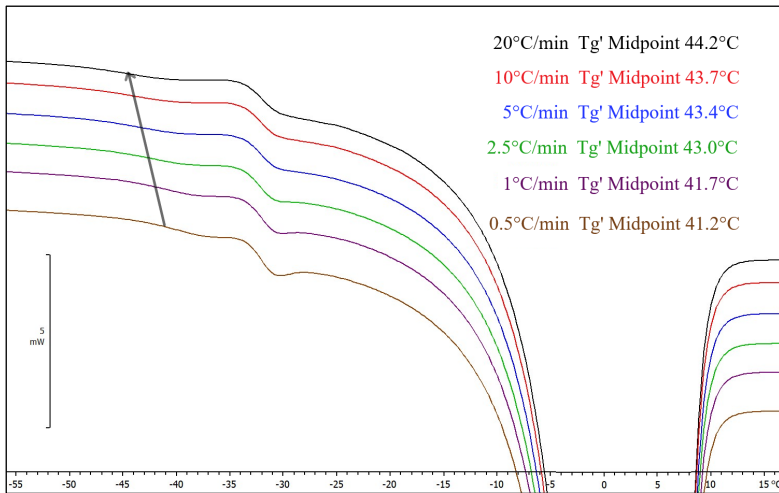
Figure 7: DSC measurement of Tg' at different cooling rates for a 10% sucrose solution. The Tg' was measured using the ISO standard (ISO 11357–2:1999). An increase in cooling rate decreases the Tg' of the freeze concentrate.

Annealing and relaxation

As previously discussed, larger ice crystals are often preferred in the sample as this decreases drying resistance and enables a shorter primary drying process (Tang & Pikal, 2004; Wang, 2000), as well as leading to thicker dried material. It is therefore beneficial to have larger ice crystals. The technique used to increase the size of ice crystals is called annealing.

In the pharmaceutical field, annealing is often referred to as the crystallization of bulking agents such as Mannitol and Glycine (Dixit *et al.*, 2011). However, the focus of this chapter will solely be on the annealing of ice crystals. Annealing of ice crystals involves subjecting the frozen sample to a temperature just above the Tg of the freeze concentrate, maintaining the sample in the rubbery state. The process encourages larger ice crystals to grow while the small crystals shrink and disappear. This process is driven by Ostwald ripening (Kharatyan *et al.*, 2022). The annealing process benefits from factors such as high Laplace pressure, large surface area of the ice crystals, and short distance between the ice crystals (Kharatyan *et al.*, 2022). Smaller ice crystals have a higher Laplace pressure and offer a larger surface area that also results in a thinner freeze-concentrate material compared to larger ice crystals. Hence, smaller ice crystals rapidly diffuse to larger ones, As the small crystals disappear, and larger crystals grow, the rate of annealing rapidly decreases. Therefore, the annealing process is particularly relevant for quenched pellets with small ice crystals (Lifshitz & Slyozov, 1961). The effect of annealing is less prominent in vial freezing as the ice crystals formed during slow cooling are already relatively large. (Kabalnov *et al.*, 1987b; Lifshitz & Slyozov, 1961). The dynamics

16

of annealing have been investigated using SRμCT. This reveals a rapid decrease in the annealing rate as the ice crystals increase in size, demonstrating the limitations of the process, as it becomes impractical to further anneal a sample beyond a certain ice crystal size (**Paper V**).

The annealing process has both been shown to increase the drying rate as well as reduce batch-to-batch variations (**Paper IV**). However, there are instances where extensive annealing has caused a global collapse in formulations with low solute concentrations (<10%). This is caused by insufficient material to uphold a continuous network, leading to freeze-dried material suspended in the air after drying (Yang, 2021).

The freeze concentrates of a rapidly frozen sample such as pellets are non-relaxed samples, (see previous section, Impact on freeze concentrate and glass transition temperature). These contain unfrozen water or water available for freezing and therefore have a lower Tg compared to the Tg'. The non-relaxed sample can reach the Tg' by relaxation. Relaxation is performed by maintaining the sample temperature above the Tg, allowing the freeze concentrate to liquefy and release the trapped water, so increasing the concentration and the Tg of the freeze concentrate. The relaxation also increases the size and volume fraction of ice crystals. When the Cg' (at temperature Tg') is reached, the total volume of ice crystals cannot be further increased (Roos, 1997; Roos & Drusch, 2016a). The relaxation of freeze concentrate transfers water molecules from the freeze concentrate to the ice and should not be confused with annealing and Oswald ripening, where the water molecules are transported in between ice crystals and where the driving force is the ice-liquid surface energy (Kabalnov *et al.*, 1987a; Lifshitz & Slyozov, 1961). When the sample temperature is above the Tg of the freeze concentrate, diffusion can occur simultaneously between ice crystals, as well as between freeze concentrate and ice. This makes it difficult to distinguish the difference between ice crystal growth (relaxation) and recrystallization (annealing). How annealing, and relaxation procedures influence the freeze concentrate is illustrated in Figure 8.

In the case of samples with small ice crystals, temperature increases will result in rapid changes in the structure and composition of the freeze concentrate (**Paper V**). The rapid dynamics of annealing and relaxation underscore the challenges associated with the handling of quenched pellets. The rate of annealing decreases over time, making the process more controllable. Avoiding relaxation/annealing can therefore be challenging and cause batch-to-batch variations. Annealing/relaxation should therefore be done deliberately for non-relaxed samples to avoid deviations.
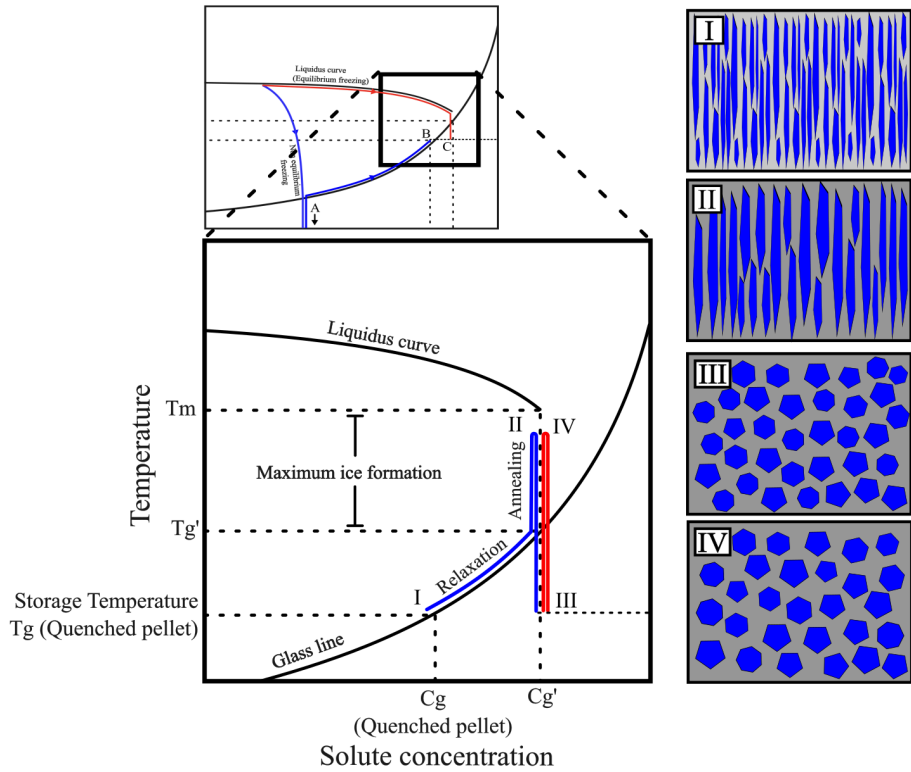
Figure 8: This state diagram illustrates the freeze concentrate trajectory during relaxation and annealing, extending from Figure 6. In the images, blue represents ice crystals, and grey indicates freeze concentrate, with darker shades indicating a higher solute concentration. The blue line in the state diagram represents the relaxation and annealing for a rapidly cooled, non-relaxed sample like a pellet. As temperature rises from point I, the relaxation process progresses until reaching Tg', after which further temperature increases to point II (above Tg') facilitates annealing. Relaxation and annealing of a non-relaxed pellet lead to a rapid increase in ice crystal size. The red line represents a slowly cooled sample with larger ice crystals. A temperature increase from point III to annealing temperature at point IV results in an increase in ice crystal size, though not as drastic as a non-relaxed sample with small ice crystals.

Chapter 3

Drying

Introduction

The goal of the drying process is to preserve products while removing moisture for long-term storage. It aims to achieve products with low water content while ensuring the product remains structurally intact and chemically stable over time. Freeze-drying often consists of two steps; the first step is primary drying where the ice crystals sublimate and are removed from the sample, leaving a cake/pellet of freeze-concentrated material. The next step is to remove the moisture in the freeze-concentrated material; this is called secondary drying. A successful freeze-drying protocol removes the ice while keeping the freeze-concentrated structure intact, avoiding collapses. Collapses during drying result in diversions in structure and moisture content and are therefore important to avoid. Another common issue that causes inhomogeneity is the deviation of water content between samples (**Paper I**). The deviations in structure and water content derive from poor mass and heat transfer control. The mass and heat transfer are affected by the freeze-drying protocol and setup, as well as the structure of the frozen formulation. This chapter aims to provide an understanding of how different protocols, setups, and structures of the sample can affect the result of the dried product.

Primary drying

The frozen sample consists of two phases, the freeze-concentrated formulation and ice. Primary drying involves the removal of frozen water from the material through sublimation, leaving a matrix of freeze-concentrated material (Patel *et al.*, 2010). The main contributing factor to the material structure is the ice crystal structure; this was confirmed by investigating the primary drying *in situ* using synchrotron-based microtomography (SRµCT) and revealed that well-designed primary drying does not significantly alter the structure of the freeze concentrate. The structure of the freeze-dried material is therefore mainly a consequence of freezing and annealing parameters (**Paper V**).

The ice crystals sublimate at the sublimation front, which is the surface exposed to the vacuum. The temperature at the sublimation front is dependent on the chamber pressure (vapor pressure over ice), the shelf temperature, and the mass transfer resistance originating from the structure of the sample. An increase in resistance, either due to high solute concentration or high tortuosity, will lead to an increase in pressure at the sublimation front, which in turn increases the temperature and the potential of collapse (**Paper III, IV**).

The temperature at the sublimation front must be below the collapse temperature (Tc) to maintain the structure of the material. Tc determines the maximum allowable temperature to maintain structural stability for amorphous formulation during drying (Mujat *et al.*, 2012; Roos & Drusch, 2016a). Tc is often a few degrees above Tg' and is dependent on molecular weight and the viscosity of the solute, where a higher molecular weight/viscosity leads to a higher Tc (Fonseca *et al.*, 2004; To & Flink, 1978).

A sample with low mass transfer resistance decreases the drying time and facilitates maintaining a low temperature at the sublimation front. Therefore, a low-resistance sample is less prone to collapse (**Paper III, IV**). Samples with large ice crystals (and low solute concentration) tend to have low mass transfer resistance and can be achieved by freezing the sample with a slow cooling rate, or by annealing (See Chapter 2).

Understanding the heat and mass transfer and the influence of structure allows for the optimization of the freeze-drying process while maintaining structural integrity.

Mass and heat transfer during primary drying (the role of mass transfer in collapse)

A common issue in freeze-drying is inhomogeneous drying and deviations between samples. This arises from the limited control of temperature and heat transfer. This can be especially relevant for demanding samples with low Tc that require a low temperature and chamber pressure during drying (Rambhatla & Pikal, 2003; Wegiel *et al.*, 2018). These conditions can lead to uneven heat distribution and poor temperature control. The uneven heat transfer leads to non-uniform drying and reduced reproducibility (Rambhatla & Pikal, 2003) (**Paper I**). Understanding heat transfer will aid in the designing of a reliable freeze-drying cycle.

The heat transfer during freeze-drying can be described by means of three mechanisms: direct contact conduction, convection/conduction through rarefied vapor, and radiation. Direct contact is constant and unaffected by pressure, while conduction/convection through vapor depends on factors like distance, temperature, and pressure. Radiation depends on the chamber pressure and the temperature of

surrounding surfaces including the walls and door of the freeze dryer. By comparing sublimation rates of water with the equilibrium temperature (non-sublimating oil sample), it becomes possible to differentiate between conduction and radiation (**Paper I**). Figure 9 illustrates the heat flux of radiation and conduction experienced by vials standing directly on the shelf and vials inside a vial holder. It shows that 65–75% of heat is transferred by conduction while 25–35% is due to radiation from the surrounding surfaces. This shows that radiation significantly influences freeze-drying.

Lower chamber pressures increase the influence of radiation heat transfer from surrounding surfaces, particularly affecting the samples at the perimeter and leading to deviations in drying rate between samples in the middle of the freeze dryer and those close to the wall. This effect is further enhanced by low shelf temperatures as this leads to a larger temperature difference between the walls/door and shelf (**Paper I**).

The influence of radiation is especially relevant when freeze-drying samples with bad contact with the shelf, such as with syringes and pellets. The minimal contact between the shelf and pellet means that the heat transfer mainly occurs through radiation. This allows for significantly higher shelf temperatures while maintaining the vapor pressure temperature at the sublimation front, which prevents collapse during drying (**Paper III**). The temperature gradients inside the sample will also differ for vials/trays and pellets. In vials, the heat is applied from the bottom through the ice. For pellets, the drying process is radial, progressing from the surface to the centre, with heat conducted from the surface of the pellet (Trelea *et al.*, 2009).

Using vial holders to shield radiation helps reduce vial-to-vial variations but other issues, such as uneven contact between vial and vial holder, raise other complications causing deviations between samples (Brülls & Rasmuson, 2002; Daller *et al.*, 2020; Rambhatla & Pikal, 2003) (**Paper I**). Figure 10 illustrates the sublimation rate of individual vials standing directly on the shelf and vials standing in a vial holder.
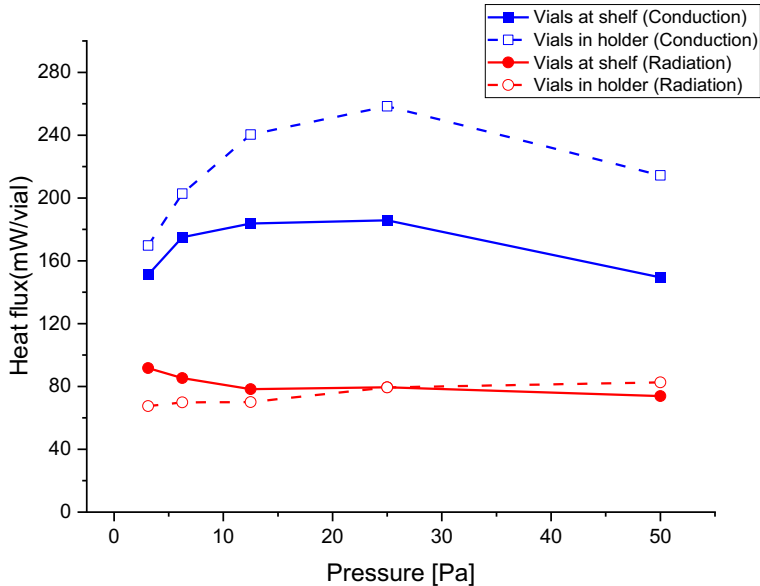
Figure 9: The heat flux contribution from conduction (blue), and radiation (red) for vials standing on the shelf (continuous line) and vials inside a vial holder (dashed line). The values are an average of all vials standing at -10 °C. 25–35 % of the heat flux arrives from the radiation.

There are several ways to avoid deviations amongst the samples. Samples in the middle of the shelf have a homogenous sublimation under all conditions. Therefore, to obtain homogenous freeze-drying, placing samples close to the walls and door should be avoided. The impact of radiation is less influential at higher pressures and at shelf temperatures closer to the surrounding temperatures. Designing a formulation with higher Tc can therefore be advantageous as this enables freeze-drying at a higher shelf temperature and chamber pressures (Fonseca *et al.*, 2004; Yang, 2021)

The impact of radiation can also be utilized in freeze-drying, such as in the case of freeze-drying pellets. As the heat transfer solely derives from radiation, it is possible to raise the shelf temperature to match the surrounding surface, resulting in homogenous heat transfer without the risk of collapse (**Paper III, IV**) (Trelea *et al.*, 2009).
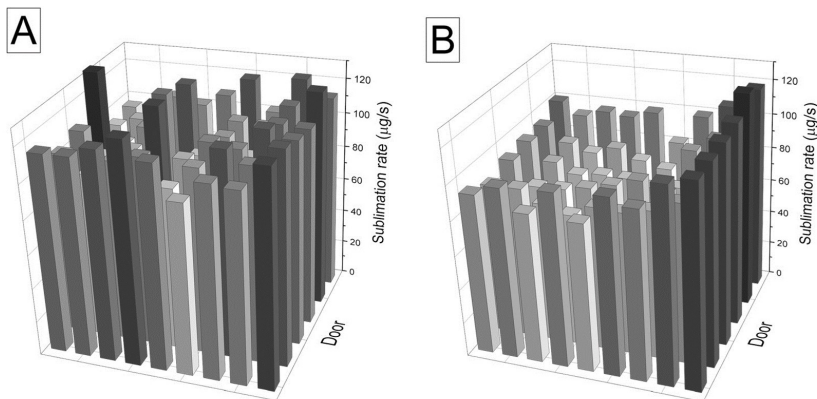
Figure 10: The sublimation rate of individual vials standing in a vial holder, A, and vials standing directly on the shelf, B. The shelf temperature is -15 °C with a chamber pressure of 12.5 Pa.

Designing a drying protocol/avoiding collapse

There are different causes of collapse. As mentioned in Chapter 1, a freeze-dried material with low Tg can cause storage collapse. Chapter 2 describes collapse due to extensive annealing and low solute concentrations. Collapse can also occur during drying if the temperature at the sublimation front exceeds the Tc (Fonseca *et al.*, 2004; Levi & Karel, 1995).

Collapse leads to an inhomogeneous structure in the sample where collapsed domains have large pores and thick materials while the intact parts have smaller more monodispersed pore size and thinner material (**Paper III, IV**). A partial collapse in a small region of the sample that does not influence the overall shape and size of the sample is termed microscopic collapse, while a larger collapse that is visually noticeable is termed macroscopic collapse. Collapses can cause deviations both amongst samples and between batches, and as this is a difficult process to control, a well-designed freeze-drying protocol should avoid collapse. However, there are instances where collapse is deliberately induced to enhance the storage stability of probiotics (Yde *et al.*, 2018). Figure 11 shows pellets and vials with and without macroscopic collapse. Microscopic collapse can only be investigated by dividing the sample and investigating the internal structure see Chapter 4.

Provided that the chamber pressure is kept below the vapor pressure temperature of Tc, the collapse occurs due to an insufficient mass transfer. During drying, as ice sublimates and water vapor seeks to exit the sample, a high resistance within the material can elevate pressure at the sublimation front and subsequently raise the temperature. This plasticizes the freeze-concentrated material and causes movements and collapse (Pikal & Shah, 1990).

Intact sample   Macroscopic collapse
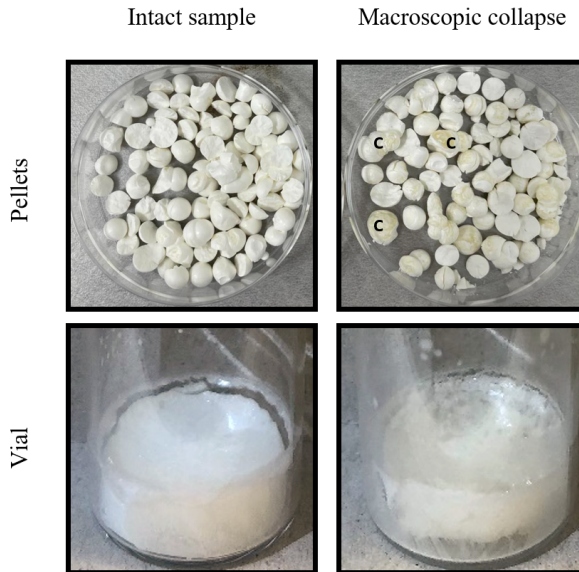
Pellets

Vial

Figure 11: Comparison between intact samples and samples with macroscopic collapse. The collapse in pellets is shown as indentations or bubbles (marked C), while the collapse in the vial is shown as shrinkage of the entire cake.

A high mass transfer resistance can be found in structures with very small ice crystals, leading to an increase in the tortuosity, or a high material concentration that makes it challenging to create pores/channels through the material (or a combination of both) (Harnkarnsujarit *et al.*, 2012; To & Flink, 1978). The resistance also increases as dry material accumulates in front of the sublimation front and collapse is therefore more likely as the drying progresses. The requirement of maintaining the temperature below Tc at the sublimation front makes it more challenging to freeze dry formulations with low Tg/Tg' such as formulations with only sucrose and quenched non-relaxed pellets. A non-relaxed quenched pellet has small ice crystals and a high proportion of freeze concentrate with low Tg, and is therefore prone to extensive collapse, as shown in the work by Ekdawi-Sever (Ekdawi-Sever *et al.*, 2003).

Relaxation and annealing can minimize the risk of collapse during drying by increasing the Tg and the size of the ice crystals. Collapse can also be avoided by increasing the Tc (and Tg') of the formulation by mixing in stabilizers (such as maltodextrin), thereby allowing for a higher sample temperature during drying without the risk of collapse (To & Flink, 1978). To conclude, collapse is most prominent for samples with low Tg, high solute concentrations, fine structures (small ice crystals), and high fill heights.

A primary drying program can vary significantly depending on the factors previously mentioned. Typically, the chamber pressure is set to a few degrees below

24

the vapor pressure of Tg'. This means that a sucrose formulation with a low Tg' needs to have a lower chamber pressure compared to a maltodextrin formulation with a higher Tg (Pikal & Shah, 1990; Tang & Pikal, 2004). The shelf temperature is set depending on the heat and the mass transfer of the sample. A sample with conduction to the shelf (vial and trays) needs a lower shelf temperature compared to samples with solely radiation as the means of heat transfer (**Paper III, IV**) (Aschenbrenner *et al.*, 2015; Trelea *et al.*, 2009). Samples with high mass transfer resistance such as formulations with high solute concentrations, non-annealed pellets, and vials with high fill volume need a lower shelf temperature to avoid collapse, while samples with low mass transfer resistance (annealed pellets) can have significantly higher shelf temperatures without the risk of collapse (**Paper III**). The end of primary drying occurs when all available ice has been removed.

Secondary drying

After all available ice has been removed in primary drying, a matrix of freeze-concentrated material containing a high proportion of bound water (approximately 25%) is left (Patel *et al.*, 2010). The goal of secondary drying is to remove the remaining moisture inside the freeze concentrate. The water is removed by desorption and dependent on diffusion rates. The shelf temperature is therefore often raised to facilitate diffusion (Pikal *et al.*, 1990). The drying rate depends on the area of the freeze-dried material and the thickness of the material; a larger surface area (smaller pores) and thinner material facilitates the drying process (opposite of primary drying) (Pikal *et al.*, 1990). Therefore, a sample with large pores and thick material takes a longer time to dry compared to small pores and thin material. The drying rate decreases as water is successively removed and it is impractical to remove all water in the material. The moisture content will determine the Tg of the dried material and is therefore an important parameter for storage stability. (see Chapter 1), It has also been shown that too low moisture content can be detrimental to cell survival. A common moisture content to aim for is 1–6% (Pikal & Shah, 1997; Pikal *et al.*, 1990). Figure 12 illustrates the residual moisture of pellets with different material thicknesses, freeze-dried under the same conditions. It shows a clear correlation between residual moisture content and material thickness, where thicker material leads to higher residual moisture (**Paper IV**).
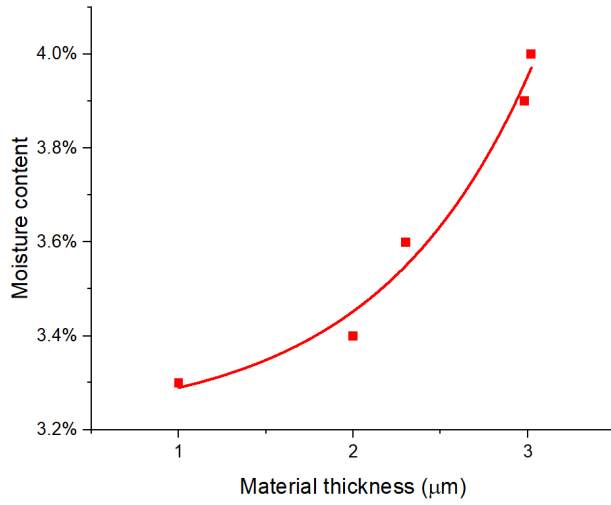
Figure 12: Correlation between material thickness and the residual moisture content of pellets. The pellets are freeze-dried at 30°C and 30Pa for 36h. The residual moisture is measured using thermogravimetric analysis (TGA). A thicker material results in higher residual moisture.

Chapter 4
The structure of dried material

Introduction

After freeze-drying, the cells are encapsulated in an amorphous protective material often consisting of a non-reducing sugar such as sucrose, that protects the cell membrane integrity from desiccation (Santivarangkna *et al.*, 2008), and a longer oligomer/polymer, such as maltodextrin, to increase storage stability. The factor that has been less considered in the probiotic community is the thickness of the encapsulating material. Since the bacteria are of similar size to the wall thickness of a typical freeze-dried formulations, a thicker material should be better at encapsulating the bacteria and be less sensitive to structural changes during storage. Sugars in a glassy state also provide a good barrier towards oxygen and act as a buffering material for humidity (Roos & Drusch, ; Santivarangkna *et al.*, 2011). Therefore, a thicker protective material is expected to provide better protection of cells and a slower loss of viability during storage.

Figure 13 depicts SEM images of a typical freeze-dried material in vials, with 10% solute concentrations, featuring silicon particles 2µm in diameter (simulating bacteria). The material thickness is approximately 1–2 µm. Notice how the particles are protruding from the material, providing limited protection (**Paper II**, Yang, 2021). Provided that a well-designed freeze-drying program is used (see Chapter 3), factors that influence the material thickness (excluding collapse) are solute concentration and size of ice crystals, where high solute concentration and large ice crystals result in thicker material (**Paper III, IV**).

600 X   200 X
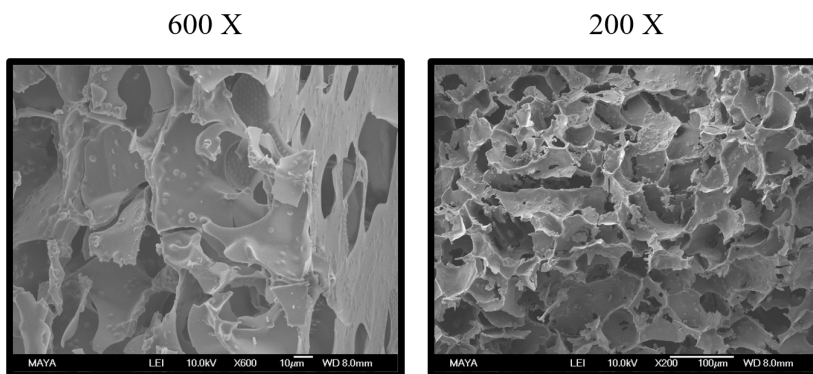
Figure 13: SEM images of material freeze-dried in vials, containing 10% maltodextrin and silicon particles 2 μm in diameter. The material thickness is approximately 1–2μm and the particles encapsulated in the material are protruding from the matrix, providing limited encapsulation.

Collapse is another occurrence that leads to changes in material structure and is described in detail in Chapter 3. It is important to distinguish the difference between storage collapse and drying collapse. Storage collapse is caused by instability of the material during storage (low Tg) and is often detrimental to storage stability. While drying collapse is caused by insufficient control during drying, this material can still be stable and provide good protection during storage (Yang, 2021; Yde *et al.*, 2018). The collapse studied in this thesis is solely collapse due to drying conditions.

The degree of collapse is difficult to control and causes deviations between samples and batches and should therefore be avoided. Instead, the material thickness should be modified by altering the ice crystal structure and solute concentration (**Paper III, IV**).

Analysis methods

Scanning electron microscopy (SEM) is a qualitative method that provides topographic images with high resolution. Estimations of pore size can be carried out provided that the images provide a good overview. It is more challenging to estimate the material thickness using SEM, as there is a limited amount of broken or cracked material. The material thickness can therefore only be roughly estimated using SEM.

X-ray micro-computed tomography (μCT) is a technique able to obtain a 3D map of the sample structure. These tomographic images can be used for quantitative evaluations, and the data has been shown to correspond well to SEM images. Figure 14 illustrates a 3D-rendered image of freeze-dried material. In recent years,

tomography has been used in several different applications to study freeze-dried structure and the focus has primarily been on pore size (Foerst *et al.*, 2019a; Gruber *et al.*, 2021; Nakagawa *et al.*, 2018; Thomik *et al.*, 2022). Pore size is an important factor when it comes to drying rates and is quantified using a method called water-shedding. This method is described in detail in **Paper II**.

Figure 14: Tomographic 3D image of 10% maltodextrin freeze-dried in vial. The 3D-rendered image can be used to quantify material properties.

When it comes to the encapsulation capacity of bacteria, the material thickness is the most relevant factor to investigate. Unfortunately, very little studies have been done of material thickness (**Paper II, III, IV**). The material thickness is quantified using a method called local thickness and is described in detail in **Paper II**.

μCT can be a time-consuming method in terms of image acquisition as well as image analysis. A single sample can take several hours to scan, and setting the correct threshold for segmentation can be challenging for structures at the limit of pixel size and resolution. It is therefore suitable to combine tomographic images with SEM images when conducting a comprehensive assessment of the material structure (Vásárhelyi *et al.*, 2020). While increasing the μCT resolution is possible, it comes at the cost of much longer scanning times, and therefore synchrotron-based μCT (SRμCT) is a better option (**Paper V**). The limitations of μCT become evident when trying to visualize and analyze intricate structures with thin material such as the material from a quenched pellet. Thin structures finer than the voxel length may not be accurately depicted and may affect the quantitative analysis, and image analysis of such a sample should be avoided. The obtained tomographic 3D data provides a number distribution of spherical blobs with different diameters able to fit inside the material. The number distribution can then be converted into a volume-weighted distribution. The volume-weighted distribution is more relevant, as it better predicts the volume/thickness in which the cells are encapsulated (**Paper II, III, IV**). The

size distributions presented in this chapter will exclusively be in volume-weighted distribution.

Vial vs Pellets

Vial

Investigating the SEM images of samples frozen and dried in vials it becomes apparent that there are two levels of structure (for a non-annealed sample), a honeycomb structure that is <10µm and larger pores >30µm. The pores are connected via holes in the wall material, termed connecting pores. The connecting pores have smooth edges, suggesting that holes are created under rubbery conditions (temperature and water content just above the Tg line). For all the ice to be sublimated, all pores need to be exposed to the vacuum, indicating a continuous void in the freeze-dried material (**Paper II**) (Tang & Pikal, 2004). As long as the sample temperatures are kept below Tc, the main contributing factor to the material matrix is the ice structure (**Paper V**). Therefore, two distinct different freeze-drying protocols can result in similar dried structures, if they were frozen/annealed in the same way. The similarities in structure can be confirmed when looking at SEM and tomographic data sets on pore structure (**Paper II**). Annealing vial samples with already large ice crystals (>30µm) is a slow process, the main difference being the elimination of the small honeycomb structures. This can be observed in both the SEM images and the tomographic data (**Paper II**). Nakagawa et al. have conducted similar annealing experiments that show the annealing of ice crystals from <10 µm to >50 µm (Nakagawa *et al.*, 2018). The slow dynamics of annealing large ice crystals showcase the limit of this process, as it becomes impractical to further anneal a sample beyond a certain ice crystal size (see Chapter 2) Figure 15 illustrates SEM images of 10% maltodextrin freeze-dried in vials, with and without annealing.

Before annealing   After annealing

200 X

600 X
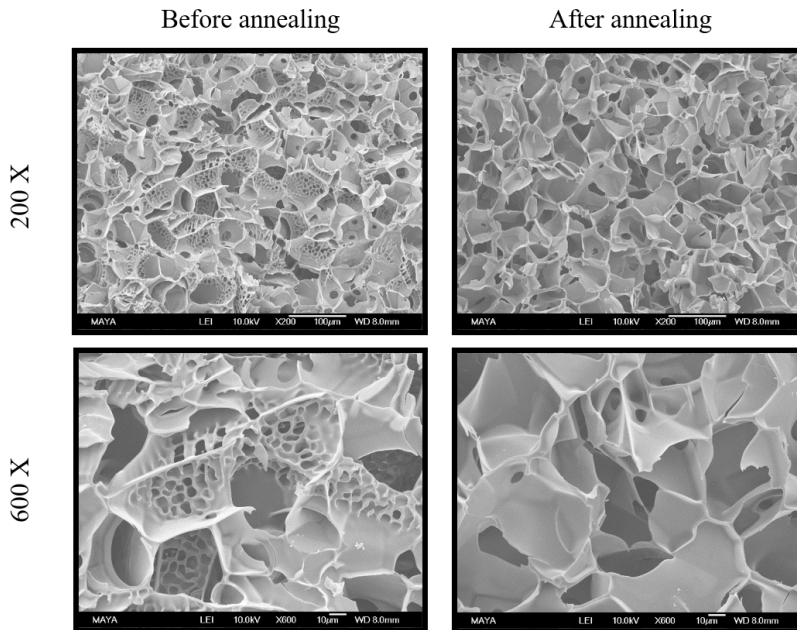
Figure 15: 10% maltodextrin formulation freeze-dried in vials, before and after annealing. Notice how the overall size of the pores is similar for both samples, but the honeycomb structures have vanished in the annealed sample.

Investigating the tomographic data of the pore size from **Paper II**, a size distribution of 10–80 µm can be estimated where the mode is dominated by pores around 20–30 µm; this is in good agreement with the SEM images. However small details such as wall protrusions and honeycomb structures (seen both in SEM and tomography slices) were not detected as pores in the tomography data (water-shedding method). The pore size is directly correlated to the material thickness (provided there is no collapse) with smaller more numerous pores resulting in a thinner freeze-dried material. The average material thickness can therefore by estimated based on the pore size (**Paper II**). The size distribution of material thickness can be determined through direct measurement (local thickness method, **Paper II**).

Figure 16: Tomography 2D slice and size distribution (volume weighted) illustrating the material thickness of annealed and non-annealed material freeze-dried in vials, consisting of 10% maltodextrin. The measured thickness is colored according to size, a more yellowish hue represents thicker material. The thickest material structure can be found in the annealed sample, especially at the intersection between pores. The annealed sample has a lower ratio of material <2.5µm and a higher ratio of material >2.5µm (**Paper II**).

Upon comparing the material thickness of annealed and non-annealed samples from **Paper II**, it becomes clear that the annealed sample contains slightly thicker material, see Figure 16. The increase in thickness for the annealed sample is likely due to the presence of thick corners which are more pronounced in the annealed sample and these features can be visualized in the tomography slices.

Pellets

Apart from the studies in this thesis, limited research has been conducted on the freeze-drying of probiotics in pellet format (Ekdawi-Sever *et al.*, 2003). Due to the small ice crystals of quenched pellets, the dynamics of annealing are much more rapid compared to annealing samples frozen in vials. The influence of rapid freezing and relaxation/annealing on ice crystal structure and freeze concentrate is discussed in Chapter 2. When investigating the SEM images and tomography data of pellets from **Paper III** and **Paper IV**, it becomes evident that longer annealing results in a higher ratio of larger pores. Figure 17 illustrates the size distribution of pores for annealed pellets. Notice that the size of the pores ranges from 10µm–40µm after

annealing, which is still smaller than the pores in the slowly frozen vial sample (**Paper II, III**).

As the size of the ice crystals grows, the thickness of the material also increases. Figure 18 shows the distribution of material thickness, where the increase in material thickness due to annealing can clearly be distinguished. The structure of the non-annealed sample was too fine with a material thickness <1 µm and too thin to be accurately analysed using lab based µCT.
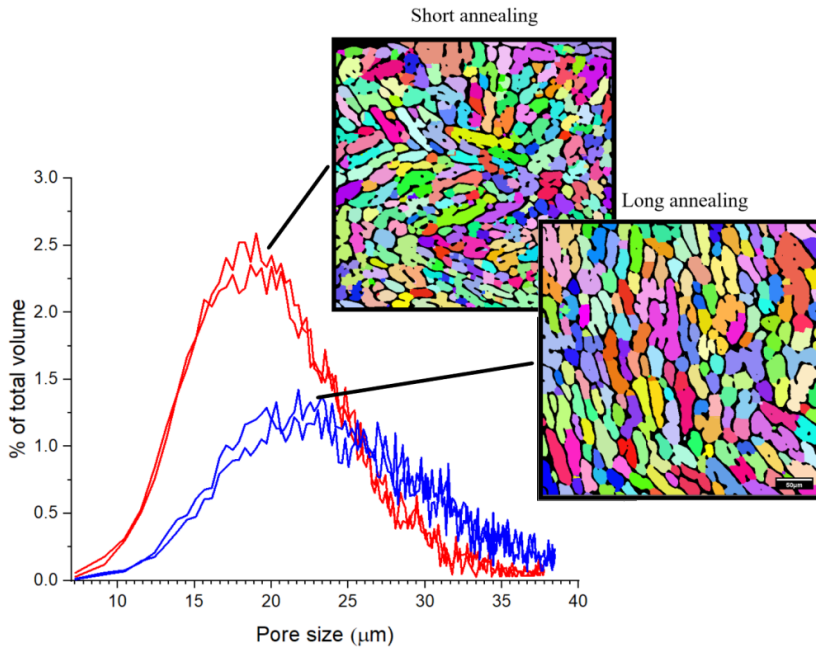
Figure 17: Tomography 2D slice and size distribution (volume weighted) illustrating the pore size of short and long annealed freeze-dried pellets. The formulation consisted of 1/3 maltodextrin, 2/3 sucrose and 20% dry matter. Each coloured domain corresponds to a detected pore. The long-annealed sample had a lower ratio of smaller pores <25µm and a higher ratio of larger pores >25µm (**Paper III**).

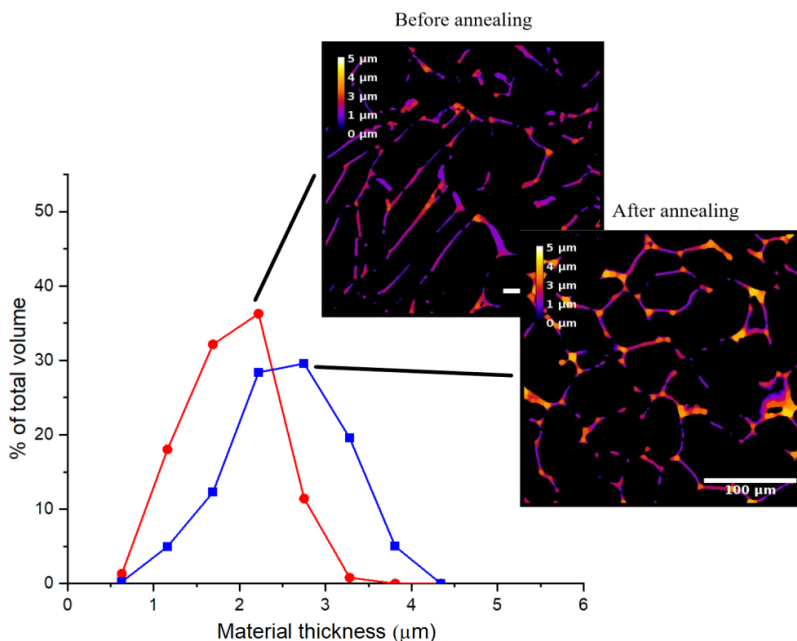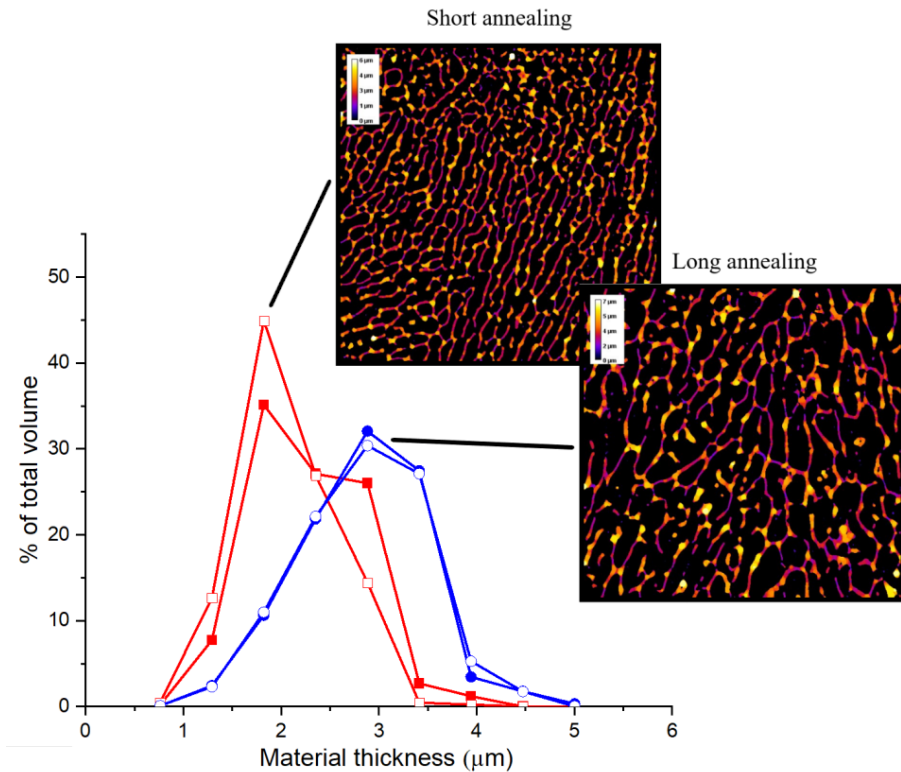**Figure 18:** Tomography 2D slice and size distribution (volume weighted) illustrating the material thickness of short and long annealed freeze-dried pellets. The formulation consisted of 1/3 maltodextrin, 2/3 sucrose, and 20% dry matter. The measured thickness is coloured according to size, where a more yellowish hue represents thicker material. The thickest material structure can be found in the annealed sample, where the long-annealed sample has a lower ratio of material <2.5µm and a higher ratio of material >2.5µm (**Paper IV**).

As µCT has limitations in resolution, finer structures need to be examined using SEM, Figure 19 presents SEM images of pellets previously described. Including the non-annealed pellet that underwent relaxation for 10 min at -30°C. The structures exhibit a lamellar-like pattern directed toward the middle of the pellet, a result of directional cooling (Chapter 2). The non-annealed (relaxed) pellet displays the finest structure, while increased annealing leads to a coarser structure.

34

	No annealing	Short annealing	Long annealing
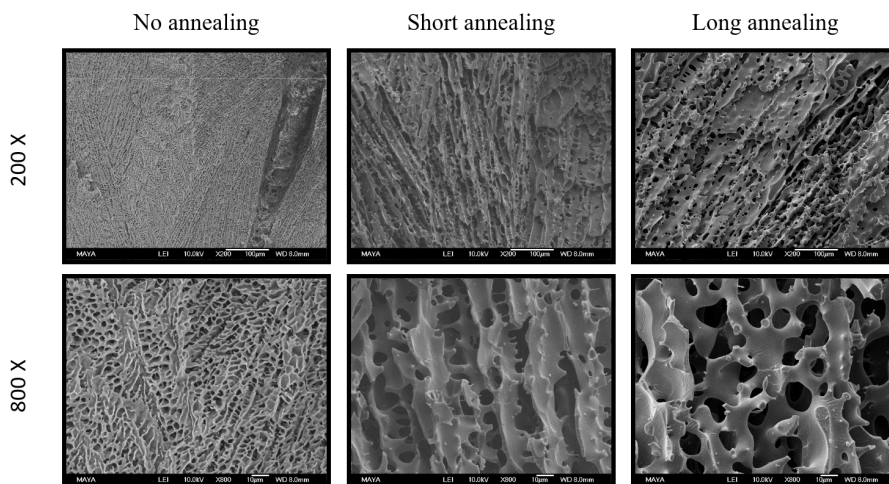
Figure 19: SEM images of freeze-dried pellets at various degrees of annealing. The formulation consisted of 1/3 maltodextrin, 2/3 sucrose and 20% dry matter. The non-annealed (relaxed) pellet has a very fine structure with small pores and thin material, and the annealed pellet has a coarser structure, where more annealing leads to larger pores and thicker material. All samples show anisotropic structure, where the material points towards the centre of the pellets (**Paper IV**).

When it comes to the non-annealed pellets, large variations in structure often emerges between batches. Some have a uniform structure with smaller pores and very thin material, but some batches show large macroscopic collapses with large cavities and much thicker material. The large deviation in structure between different non-annealed batches is likely due to the deviation in residence time inside the pre-cooled freeze dryer before drying (-30˚C in **Paper III** and **Paper IV**). The low Tg in combination with very small ice crystals (Chapter 2) leads to a high mass transfer resistance in a plasticized material, which leads to collapse (Chapter 3). When the pellets are allowed to relax, the Tg and the ice crystal size are increased (Chapter 2), reducing the risk of collapse, and the pellets can stay intact. The rate of relaxation in dependent on temperature and formulation. For formulations containing sucrose or trehalose, a residence time of around 10 min at -30˚C is sufficient to relax the freeze concentrate and avoid collapse (Ekdawi-Sever *et al.*, 2003) (**Paper III, IV**). Depending on the residence time and temperature during relaxation, a wide range of collapse can occur (within 10–20 min). The rapid dynamics of relaxation even at low temperature makes it challenging to control the degree of collapse and this should therefore not be considered to be a reliable method for modifying material thickness (Ekdawi-Sever *et al.*, 2003).

Collapse due to mass transfer resistance, as discussed in Chapter 3, can still occur for relaxed pellets due to small ice crystals and high solute concentration (**Paper IV**). These collapses are less extensive and often microscopic. The risk of collapse during drying diminishes for annealed samples except for extensive annealing in

combination with low solute concentration (see annealing collapse, Chapter 2) Figure 20 shows the difference between a collapse caused by insufficient mass transfer causing local microscopic collapse and extensive global collapse caused by a low amount of dry matter and extensive annealing. The macroscopic global collapse caused by insufficient relaxation is illustrated in the work by Ekdawi-Sever et al (Ekdawi-Sever *et al.*, 2003).

Collapse changes the material thickness significantly, but often results in inhomogeneity/polydispersity both within the sample as well as between samples and batches. This makes a collapsed sample difficult to assess and replicate. The annealing process is a more controlled way of varying the material thickness and is therefore a more suitable process to test the hypothesis of whether a better encapsulation (thicker material) provides better storage stability.
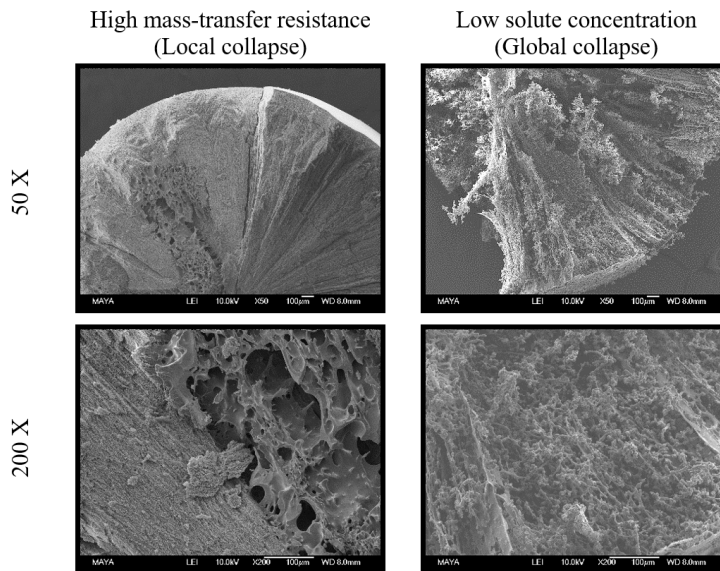
Figure 20: SEM images of freeze-dried pellets with collapsed structures. The pellet on the left is a non-annealed pellet with high solute concentration (30%) which causes a local microscopic collapse due to insufficient mass transfer. The pellet on the right has low solute concentration (10%) and is annealed extensively, causing a global macroscopic collapse.

Chapter 5
Storage stability

Enhancing the storage stability of probiotic products is a well-researched topic. Besides optimizing formulations, factors such as water activity, storage conditions, moisture content and freeze-drying parameters have been investigated and correlated to storage stability (Higl *et al.*, 2007; Kurtmann *et al.*, 2009; Rascón *et al.*, 2018; Zayed & Roos, 2004). Storage stability studies have been conducted on freeze-dried material with different material thickness and there are even patents for enhanced stability of collapsed pellets (Yde *et al.*, 2018). However, there has been no aim to correlate the stability improvements with the enhanced encapsulating capacity. Correlating storage stability with encapsulation capacity is therefore a novel way to assess a freeze-dried product. The material thickness is a measure of encapsulation capacity and is varied in a controlled manner using annealing (**Paper IV**).

Pellets is the chosen format to test this hypothesis for two reasons. The first is that pellets are the most common format used in the probiotic industry. The second is that it is possible to alter the structure and material thickness of pellets, as annealing is most effective for smaller ice crystals.

To assess the storage stability of bacteria with varying structures, three distinct annealing protocols were devised. The first protocol was aggressive and fast while the second was milder and longer (to simulate storage conditions in freezers). Based on the pore size and material thickness, the milder and longer protocol gave rise to a more annealed pellet (thicker material and larger pores). These two annealing conditions were then compared to relaxed and non-relaxed pellets; with the relaxed pellet giving rise to the thinnest material while the non-relaxed pellet has an inhomogeneous collapsed structure with thick material. Furthermore, to examine the impact of oxygen on storage stability, the pellets were stored in both oxygen-rich and low-oxygen environments. The samples were then stored at 37°C and the CFU counted for each timepoint (**Paper IV**).
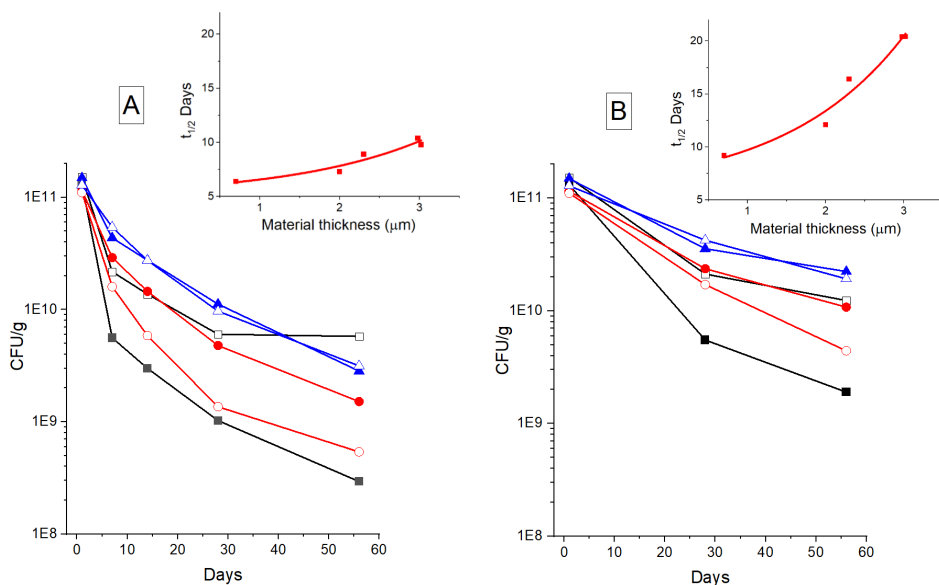
Figure 21: Storage stability in CFU/g and in half-life (t1/2) as a function of material thickness of freeze-dried bacteria in pellets stored at 37°C. The formulation consists of 20% solute with 2/3 sucrose, 1/3 maltodextrin and 2•1011 cells/ml. A: samples stored in an oxygen-rich environment and B: samples stored in a low-oxygen environment. Relaxed non-annealed pellet (black ■) non-relaxed collapsed pellet (black □) Short annealed pellet (red ●○) Long annealed pellet (blue △▲). The storage stability increases with increasing material thickness (more annealing) and is clearly illustrated in the half-life figure.

The viability of the bacteria during storage is shown in Figure 21. The results strongly indicate that a thicker material offers greater protection during storage. The most collapsed pellet (non-relaxed pellet) and most annealed pellet (mild and long) demonstrated the highest stability.

The inhomogeneous structure of the collapsed pellet also suggests that some cell portions are surrounded by thicker material, while others are embedded in thinner material. Consequently, as the cells within the less protective thin material lose their vitality, those within the thicker material remain stable. This effect is evident in Figure 21, where the collapsed pellet experiences an initial rapid decline in viability, followed by stabilization over time. This behaviour of a collapsed sample has been observed in previous work but further research is needed for confirmation (Yang, 2021).

One of the attributes that improved the stability is likely due to the increased protection against oxygen, as reactive oxygen species (ROS) is known to have a detrimental effect on the stability of freeze-dried bacteria (Kurtmann *et al.*, 2009; Wang *et al.*, 2022). In alignment with this hypothesis, pellets stored in a low-oxygen

environment exhibited better stability compared to those stored in the presence of oxygen. The encapsulating material composed of amorphous sugars is characteristically hydrophobic; as such, the material should repel the relatively hydrophobic oxygen (Roos & Drusch, ; Santivarangkna *et al.*, 2011). Therefore, increased thickness of the encapsulating material serves as a more efficient barrier against oxygen. Ekdawi-Sever et al previously discovered that a collapsed pellet had higher storage stability but correlated this with water content (water content shows a covariance with material thickness, see Chapter 3). In their study, water content ranged from 1–8%, whereas in the current investigation, water content variation was minimal (3.3–4%) and therefore considered to have a low impact on storage stability. The different preparation methods not only affect the material thickness and moisture content but also influence the drying rate and stress levels during annealing and drying. As a result, these factors together contribute to the overall stability.

In addition to the improved storage stability, another significant advantage of annealing is the enhanced control of freeze-drying, resulting in a more consistent and reproducible product. An annealed sample encounters less risk of collapse during drying and produces a more homogenous material.

The impact of material thickness on storage stability has a significant importance. It demonstrates how the same formulation can result in vastly different outcomes and explains how different freeze-drying protocols can affect storage stability. It also means that a suboptimal formulation with good encapsulation properties can outperform a perfected formulation with bad encapsulation. The material thickness has therefore become an important factor to consider when optimizing a downstream process. The material's encapsulating capacity is expected to reach an optimum point, beyond which a further increase in thickness does not enhance protection. Instead, additional thickness results in higher residual moisture. Exploring the optimal material thickness is an interesting topic for future work.

Future perspective

This thesis has demonstrated how material thickness plays an essential role in optimizing the stability of probiotics. The thickness can be modified in a controlled way by annealing. The material is anticipated to reach an optimum encapsulation capacity, after which further increase in thickness does not provide added protection. The annealing process not only affects the stability of the probiotics but also the increases the primary drying rate and decreases the secondary drying rate. Therefore, investigating the optimal material thickness is crucial for achieving maximum stability and process efficiency.

Examining the dynamics during annealing and freeze-drying processes is essential for optimizing the structure and enhancing the understanding of these processes. However, capturing these dynamics poses challenges. Lab-based µCT scans at the µm resolution require a scanning time of upwards of 3 hours, making dynamic monitoring impossible.

To decrease the scanning time significantly, a synchrotron facility (MAX IV ForMAX in Lund) was employed, capable of completing a 3D scan within 45 seconds and capturing images with good contrast between ice, freeze concentrate and air. This makes it possible to observe the dynamics during annealing and drying process. The results confirm the feasibility of monitoring freeze-drying with synchrotron-based µCT, offering new optimization opportunities.

References

Arsiccio, A., Sparavigna, A., Pisano, R., & Barresi, A. (2019). Measuring and predicting pore size distribution of freeze-dried solutions. *Drying Technology, 37*(4), 435-447.

Aschenbrenner, M., Foerst, P., & Kulozik, U. (2015). Freeze-drying of Probiotics. In P. Först & C. Santivarangkna (Eds.), *Advances in probiotic technology* (pp. 213-241). Boca Raton: CRC Press.

Assegehegn, G., Brito-de la Fuente, E., Franco, J. M., & Gallegos, C. (2019). The Importance of Understanding the Freezing Step and Its Impact on Freeze-Drying Process Performance. *Journal of pharmaceutical sciences, 108*(4), 1378-1395. doi:https://doi.org/10.1016/j.xphs.2018.11.039

Badal Tejedor, M., Fransson, J., & Millqvist-Fureby, A. (2020). Freeze-dried cake structural and physical heterogeneity in relation to freeze-drying cycle parameters. *International Journal of Pharmaceutics, 590*, 119891. doi:https://doi.org/10.1016/j.ijpharm.2020.119891

Bagad, M., Pande, R., Dubey, V., & Ghosh, A. R. (2017). Survivability of freeze-dried probiotic Pediococcus pentosaceus strains GS4, GS17 and Lactobacillus gasseri (ATCC 19992) during storage with commonly used pharmaceutical excipients within a period of 120 days. *Asian Pacific Journal of Tropical Biomedicine, 7*(10), 921-929. doi:https://doi.org/10.1016/j.apjtb.2017.09.005

Béal , C., & Fonseca, F. (2015). Freezing of Probiotic Bacteria. In P. Först & C. Santivarangkna (Eds.), *Advances in probiotic technology* (pp. 187-220). Boca Raton: CRC Press.

Bhugra, C., Rambhatla, S., Bakri, A., Duddu, S. P., Miller, D. P., Pikal, M. J., & Lechuga-Ballesteros, D. (2007). Prediction of the Onset of Crystallization of Amorphous Sucrose Below the Calorimetric Glass Transition Temperature from Correlations with Mobility. *Journal of pharmaceutical sciences, 96*(5), 1258-1269. doi:https://doi.org/10.1002/jps.20918

Brülls, M., & Rasmuson, A. (2002). Heat transfer in vial lyophilization. *International Journal of Pharmaceutics, 246*(1-2), 1-16.

Celik, O. F., & O'Sullivan, D. J. (2013). Factors influencing the stability of freeze-dried stress-resilient and stress-sensitive strains of bifidobacteria. *Journal of Dairy Science, 96*(6), 3506-3516. doi:https://doi.org/10.3168/jds.2012-6327

Champagne, C. P., Mondou, F., Raymond, Y., & Roy, D. (1996). Effect of polymers and storage temperature on the stability of freeze-dried lactic acid bacteria. *Food Research International, 29*(5), 555-562. doi:https://doi.org/10.1016/0963-9969(95)00050-X

Charoenrein, S., & Harnkarnsujarit, N. (2017). Chapter 2 - Food Freezing and Non-Equilibrium States. In B. Bhandari & Y. H. Roos (Eds.), *Non-Equilibrium States and Glass Transitions in Foods* (pp. 39-62): Woodhead Publishing.

Chen, B., Wang, X., Li, P., Feng, X., Mao, Z., Wei, J., Lin, X., Li, X., & Wang, L. (2023). Exploring the protective effects of freeze-dried Lactobacillus rhamnosus under optimized cryoprotectants formulation. *LWT, 173*, 114295. doi:https://doi.org/10.1016/j.lwt.2022.114295

Craig, D. Q., Royall, P. G., Kett, V. L., & Hopton, M. L. (1999). The relevance of the amorphous state to pharmaceutical dosage forms: glassy drugs and freeze dried systems. *Int J Pharm, 179*(2), 179-207. doi:10.1016/s0378-5173(98)00338-x

Daller, S., Friess, W., & Schroeder, R. (2020). Energy transfer in vials nested in a rack system during lyophilization. *Pharmaceutics, 12*(1), 61.

Dixit, M., Kulkarni, P., & Selvam, P. (2011). Review on: freeze drying as a crystallization technique. *Elixir Pharmacy, 41*, 5717-5730.

Duong, T., Barrangou, R., Russell, W. M., & Klaenhammer, T. R. (2006). Characterization of the tre locus and analysis of trehalose cryoprotection in Lactobacillus acidophilus NCFM. *Appl Environ Microbiol, 72*(2), 1218-1225. doi:10.1128/aem.72.2.1218-1225.2006

Ekdawi-Sever, N., Goentoro, L. A., & Pablo, J. J. D. (2003). Effects of Annealing on Freeze-Dried Lactobacillus acidophilus. *Journal of Food Science, 68*(8), 2504-2511. doi:10.1111/j.1365-2621.2003.tb07052.x

Erber, M., & Lee, G. (2015). Development of cryopelletization and formulation measures to improve stability of Echis carinatus venum protein for use in diagnostic rotational thromboelastometry. *Int J Pharm, 495*(2), 692-700. doi:10.1016/j.ijpharm.2015.09.038

Foerst, P., de Carvalho, T. M., Lechner, M., Kovacevic, T., Kim, S., Kirse, C., & Briesen, H. (2019a). Estimation of mass transfer rate and primary drying times during freeze-drying of frozen maltodextrin solutions based on x-ray µ-computed tomography measurements of pore size distributions. *Journal of Food Engineering, 260*, 50-57.

Foerst, P., Melo de Carvalho, T., Lechner, M., Kovacevic, T., Kim, S., Kirse, C., & Briesen, H. (2019b). Estimation of mass transfer rate and primary drying times during freeze-drying of frozen maltodextrin solutions based on x-ray µ-computed tomography measurements of pore size distributions. *Journal of Food Engineering, 260*, 50-57. doi:https://doi.org/10.1016/j.jfoodeng.2019.05.002

Fonseca, F., Cenard, S., & Passot, S. (2015). Freeze-Drying of Lactic Acid Bacteria. In W. F. Wolkers & H. Oldenhof (Eds.), *Cryopreservation and Freeze-Drying Protocols* (pp. 477-488). New York, NY: Springer New York.

Fonseca, F., Passot, S., Cunin, O., & Marin, M. (2004). Collapse Temperature of Freeze-Dried Lactobacillus bulgaricusSuspensions and Protective Media. *Biotechnology progress, 20*(1), 229-238. doi:https://doi.org/10.1021/bp034136n

Franks, F., & Auffret, T. (2008). *Freeze-drying of Pharmaceuticals and Biopharmaceuticals*: Royal Society of Chemistry.

Gaidhani, K. A., Harwalkar, M., Bhambere, D., & Nirgude, P. S. (2015). Lyophilization/freeze drying–a review. *World journal of pharmaceutical research, 4*(8), 516-543.

Gan, K. H., Bruttini, R., Crosser, O. K., & Liapis, A. I. (2005). Freeze-drying of pharmaceuticals in vials on trays: effects of drying chamber wall temperature and tray side on lyophilization performance. *International Journal of Heat and Mass Transfer, 48*(9), 1675-1687. doi:https://doi.org/10.1016/j.ijheatmasstransfer.2004.12.004

Ghorab, M. K., Toth, S. J., Simpson, G. J., Mauer, L. J., & Taylor, L. S. (2014). Water–solid interactions in amorphous maltodextrin-crystalline sucrose binary mixtures. *Pharmaceutical development and technology, 19*(2), 247-256. doi:10.3109/10837450.2013.775157

Giulio, B. D., Orlando, P., Barba, G., Coppola, R., Rosa, M. D., Sada, A., Prisco, P. P. D., & Nazzaro, F. (2005). Use of alginate and cryo-protective sugars to improve the viability of lactic acid bacteria after freezing and freeze-drying. *World Journal of Microbiology and Biotechnology, 21*(5), 739-746. doi:10.1007/s11274-004-4735-2

Gruber, S., Vorhauer-Huget, N., & Foerst, P. (2021). In situ micro-computed tomography to study microstructure and sublimation front during freeze-drying. *Food Structure, 29*, 100213.

Hancock, B. C., & Zografi, G. (1997). Characteristics and Significance of the Amorphous State in Pharmaceutical Systems. *Journal of pharmaceutical sciences, 86*(1), 1-12. doi:https://doi.org/10.1021/js9601896

Hansen, M. L. R., Petersen, M. A., Risbo, J., Hümmer, M., & Clausen, A. (2015). Implications of modifying membrane fatty acid composition on membrane oxidation, integrity, and storage viability of freeze-dried probiotic, Lactobacillus acidophilus La-5. *Biotechnology progress, 31*(3), 799-807.

Harnkarnsujarit, N., Charoenrein, S., & Roos, Y. H. (2012). Microstructure formation of maltodextrin and sugar matrices in freeze-dried systems. *Carbohydrate Polymers, 88*(2), 734-742. doi:https://doi.org/10.1016/j.carbpol.2012.01.028

Higl, B., Kurtmann, L., Carlsen, C. U., Ratjen, J., Först, P., Skibsted, L. H., Kulozik, U., & Risbo, J. (2007). Impact of water activity, temperature, and physical state on the storage stability of Lactobacillus paracasei ssp. paracasei freeze-dried in a lactose matrix. *Biotechnology progress, 23*(4), 794-800.

Hill, C., Guarner, F., Reid, G., Gibson, G. R., Merenstein, D. J., Pot, B., Morelli, L., Canani, R. B., Flint, H. J., Salminen, S., Calder, P. C., & Sanders, M. E. (2014). The International Scientific Association for Probiotics and Prebiotics consensus statement on the scope and appropriate use of the term probiotic. *Nature Reviews Gastroenterology & Hepatology, 11*(8), 506-514. doi:10.1038/nrgastro.2014.66

Hottot, A., Vessot, S., & Andrieu, J. (2004). A Direct Characterization Method of the Ice Morphology. Relationship Between Mean Crystals Size and Primary Drying Times of Freeze-Drying Processes. *Drying Technology, 22*(8), 2009-2021. doi:10.1081/DRT-200032717

Jackson, S. A., Schoeni, J. L., Vegge, C., Pane, M., Stahl, B., Bradley, M., Goldman, V. S., Burguière, P., Atwater, J. B., & Sanders, M. E. (2019). Improving End-User Trust in the Quality of Commercial Probiotic Products. *Frontiers in Microbiology, 10*. doi:10.3389/fmicb.2019.00739

Jameel, F., & Searles, J. (2010). Development and optimization of the freeze-drying processes. In F. Jameel & S. Hershenson (Eds.), *Formulation and process development strategies for manufacturing biopharmaceuticals.* (pp. 763-796). United States: John Wiley and Sons, Inc.

Kabalnov, A., Pertzov, A., & Shchukin, E. (1987a). Ostwald ripening in emulsions: I. Direct observations of Ostwald ripening in emulsions. *Journal of Colloid and Interface Science, 118*(2), 590-597.

Kabalnov, A. S., Pertzov, A. V., & Shchukin, E. D. (1987b). Ostwald ripening in emulsions: I. Direct observations of Ostwald ripening in emulsions. *Journal of Colloid and Interface Science, 118*(2), 590-597. doi:https://doi.org/10.1016/0021-9797(87)90492-9

Kharatyan, T., Gopireddy, S. R., Ogawa, T., Kodama, T., Nishimoto, N., Osada, S., Scherließ, R., & Urbanetz, N. A. (2022). Quantitative Analysis of Glassy State Relaxation and Ostwald Ripening during Annealing Using Freeze-Drying Microscopy. *Pharmaceutics, 14*(6). doi:10.3390/pharmaceutics14061176

Kiepś, J., & Dembczyński, R. (2022). Current Trends in the Production of Probiotic Formulations. *Foods, 11*(15), 2330. Retrieved from https://www.mdpi.com/2304-8158/11/15/2330

Konstantinidis, A. K., Kuu, W., Otten, L., Nail, S. L., & Sever, R. R. (2011). Controlled nucleation in freeze-drying: Effects on pore size in the dried product layer, mass transfer resistance, and primary drying rate. *Journal of pharmaceutical sciences, 100*(8), 3453-3470.

Kurtmann, L., Carlsen, C. U., Risbo, J., & Skibsted, L. H. (2009). Storage stability of freeze–dried Lactobacillus acidophilus (La-5) in relation to water activity and presence of oxygen and ascorbate. *Cryobiology, 58*(2), 175-180. doi:https://doi.org/10.1016/j.cryobiol.2008.12.001

Levi, G., & Karel, M. (1995). Volumetric shrinkage (collapse) in freeze-dried carbohydrates above their glass transition temperature. *Food Research International, 28*(2), 145-151. doi:https://doi.org/10.1016/0963-9969(95)90798-F

Lifshitz, I. M., & Slyozov, V. V. (1961). The kinetics of precipitation from supersaturated solid solutions. *Journal of Physics and Chemistry of Solids, 19*(1), 35-50. doi:https://doi.org/10.1016/0022-3697(61)90054-3

Liu, J. (2006). Physical characterization of pharmaceutical formulations in frozen and freeze-dried solid states: techniques and applications in freeze-drying development. *Pharmaceutical development and technology, 11*(1), 3-28.

Lundberg, L. (2023). *An exploratory journey into probiotic interactions : Bioactive properties of Limosilactobacillus reuteri and Bifidobacterium longum.* (PhD). Swedish University of Agricultural Sciences, Uppsala.

Mathlouthi, M. (1995). Amorphous sugar. In M. Mathlouthi & P. Reiser (Eds.), *Sucrose: Properties and applications* (pp. 75-100): Springer.

Mehta, M., Bhardwaj, S. P., & Suryanarayanan, R. (2013). Controlling the physical form of mannitol in freeze-dried systems. *European Journal of Pharmaceutics and Biopharmaceutics, 85*(2), 207-213. doi:https://doi.org/10.1016/j.ejpb.2013.04.010

Montel Mendoza, G., Pasteris, S. E., Otero, M. C., & Fatima Nader-Macías, M. E. (2014). Survival and beneficial properties of lactic acid bacteria from raniculture subjected to freeze-drying and storage. *J Appl Microbiol, 116*(1), 157-166. doi:10.1111/jam.12359

Mujat, M., Greco, K., Galbally-Kinney, K. L., Hammer, D. X., Ferguson, R. D., Iftimia, N., Mulhall, P., Sharma, P., Pikal, M. J., & Kessler, W. J. (2012). Optical coherence tomography-based freeze-drying microscopy. *Biomedical Optics Express, 3*(1), 55-63.

Nakagawa, K., Hottot, A., Vessot, S., & Andrieu, J. (2007). Modeling of freezing step during freeze-drying of drugs in vials. *AIChE Journal, 53*(5), 1362-1372. doi:https://doi.org/10.1002/aic.11147

Nakagawa, K., Tamiya, S., Sakamoto, S., Do, G., & Kono, S. (2018). Observation of microstructure formation during freeze-drying of dextrin solution by in-situ X-ray computed tomography. *Frontiers in Chemistry, 6*, 418.

Oddone, I., Barresi, A. A., & Pisano, R. (2017). Influence of controlled ice nucleation on the freeze-drying of pharmaceutical products: the secondary drying step. *International Journal of Pharmaceutics, 524*(1), 134-140. doi:https://doi.org/10.1016/j.ijpharm.2017.03.077

Oetjen, G. W., & Haseley, P. (2007). *Freeze-Drying:* (Vol. Second, Completely Revised and Extended Edition): John Wiley & Sons.

Olbrich, C., Plitzko, M., Luy, B., & Schneid, S. C. (2019). Method for the production of freeze-dried pellets comprising factor VIII. In: Google Patents.

Oluwatosin, S. O., Tai, S. L., & Fagan-Endres, M. A. (2022). Sucrose, maltodextrin and inulin efficacy as cryoprotectant, preservative and prebiotic - towards a freeze dried Lactobacillus plantarum topical probiotic. *Biotechnol Rep (Amst), 33*, e00696. doi:10.1016/j.btre.2021.e00696

Palmkron, S. B., Bergenståhl, B., Håkansson, S., Wahlgren, M., Fureby, A. M., & Larsson, E. (2023). Quantification of structures in freeze-dried materials using X-ray microtomography. *Colloids and Surfaces A: Physicochemical and Engineering Aspects, 658*, 130726. doi:https://doi.org/10.1016/j.colsurfa.2022.130726

Patel, S. M., Doen, T., & Pikal, M. J. (2010). Determination of end point of primary drying in freeze-drying process control. *AAPS PharmSciTech, 11*(1), 73-84. doi:10.1208/s12249-009-9362-7

Patel, S. M., & Pikal, M. J. (2011). Emerging freeze-drying process development and scale-up issues. *AAPS PharmSciTech, 12*(1), 372-378. doi:10.1208/s12249-011-9599-9

Pehkonen, K. S., Roos, Y. H., Miao, S., Ross, R. P., & Stanton, C. (2008). State transitions and physicochemical aspects of cryoprotection and stabilization in freeze-drying of Lactobacillus rhamnosus GG (LGG). *J Appl Microbiol, 104*(6), 1732-1743. doi:10.1111/j.1365-2672.2007.03719.x

Pikal, M. J., & Shah, S. (1990). The collapse temperature in freeze drying: Dependence on measurement methodology and rate of water removal from the glassy phase. *International Journal of Pharmaceutics, 62*(2), 165-186. doi:https://doi.org/10.1016/0378-5173(90)90231-R

Pikal, M. J., & Shah, S. (1997). Intravial distribution of moisture during the secondary drying stage of freeze drying. *PDA journal of pharmaceutical science and technology, 51*(1), 17-24.

Pikal, M. J., Shah, S., Roy, M. L., & Putman, R. (1990). The secondary drying stage of freeze drying: drying kinetics as a function of temperature and chamber pressure. *International Journal of Pharmaceutics, 60*(3), 203-207. doi:https://doi.org/10.1016/0378-5173(90)90074-E

Potts, M. (1994). Desiccation tolerance of prokaryotes. *Microbiological Reviews, 58*(4), 755-805. doi:10.1128/mr.58.4.755-805.1994

Prajapati, K., Bisani, K., Prajapati, H., Prajapati, S., Agrawal, D., Singh, S., Saraf, M., & Goswami, D. (2023). Advances in probiotics research: mechanisms of action, health benefits, and limitations in applications. *Systems Microbiology and Biomanufacturing*. doi:10.1007/s43393-023-00208-w

Qian, L., & Zhang, H. (2011). Controlled freezing and freeze drying: a versatile route for porous and micro-/nano-structured materials. *Journal of Chemical Technology & Biotechnology, 86*(2), 172-184.

Rambhatla, S., & Pikal, M. J. (2003). Heat and mass transfer scale-up issues during freeze-drying, I: atypical radiation and the edge vial effect. *AAPS PharmSciTech, 4*, 22-31.

Rao, N. S., Ermann Lundberg, L., Tomasson, J., Tullberg, C., Brink, D. P., Palmkron, S. B., van Niel, E. W. J., Håkansson, S., & Carlquist, M. (2023). Non-inhibitory levels of oxygen during cultivation increase freeze-drying stress tolerance in Limosilactobacillus reuteri DSM 17938. *Frontiers in Microbiology, 14*. doi:10.3389/fmicb.2023.1152389

Rao, N. S., Lundberg, L., Palmkron, S., Håkansson, S., Bergenståhl, B., & Carlquist, M. (2021). Flow cytometric analysis reveals culture condition dependent variations in phenotypic heterogeneity of Limosilactobacillus reuteri. *Scientific Reports, 11*(1), 23567. doi:10.1038/s41598-021-02919-3

Rascón, M., Huerta-Vera, K., Pascual-Pineda, L., Contreras-Oliva, A., Flores-Andrade, E., Castillo-Morales, M., Bonilla, E., & González-Morales, I. (2018). Osmotic dehydration assisted impregnation of Lactobacillus rhamnosus in banana and effect of water activity on the storage stability of probiotic in the freeze-dried product. *LWT, 92*, 490-496.

Rodríguez Furlán, L. T., Lecot, J., Pérez Padilla, A., Campderrós, M. E., & Zaritzky, N. (2011). Effect of saccharides on glass transition temperatures of frozen and freeze dried bovine plasma protein. *Journal of Food Engineering, 106*(1), 74-79. doi:https://doi.org/10.1016/j.jfoodeng.2011.04.010

Roe, K. D., & Labuza, T. P. (2005). Glass Transition and Crystallization of Amorphous Trehalose-sucrose Mixtures. *International Journal of Food Properties, 8*(3), 559-574. doi:10.1080/10942910500269824

Roos, Y. H. (1997). Frozen state transitions in relation to freeze drying. *Journal of thermal analysis, 48*(3), 535-544. doi:10.1007/BF01979500

Roos, Y. H., & Drusch, S. (2016a). Chapter 4 Water and phase transitions. In Y. H. Roos & S. Drusch (Eds.), *Phase transitions in foods* (pp. 79-113). San Diego: Academic Press.

Roos, Y. H., & Drusch, S. (2016b). Chapter 7 - Time-dependent phenomena. In Y. H. Roos & S. Drusch (Eds.), *Phase Transitions in Foods (Second Edition)* (pp. 215-273). San Diego: Academic Press.

Santivarangkna, C. (2015). Storage stability of probiotic powders. In P. Först & C. Santivarangkna (Eds.), *Advances in probiotic technology*. Boca Raton: CRC Press.

Santivarangkna, C., Aschenbrenner, M., Kulozik, U., & Först, P. (2011). Role of Glassy State on Stabilities of Freeze-Dried Probiotics. *Journal of Food Science, 76*, 152-156. doi:10.1111/j.1750-3841.2011.02347.x

Santivarangkna, C., Higl, B., & Foerst, P. (2008). Protection mechanisms of sugars during different stages of preparation process of dried lactic acid starter cultures. *Food Microbiol, 25*(3), 429-441. doi:10.1016/j.fm.2007.12.004

Searles, J. A., Carpenter, J. F., & Randolph, T. W. (2001). Annealing to optimize the primary drying rate, reduce freezing-induced drying rate heterogeneity, and determine T'g in pharmaceutical lyophilization. *Journal of pharmaceutical sciences, 90*(7), 872-887. doi:https://doi.org/10.1002/jps.1040

Seshagiri Rao, N. (2023). *Impact of Cultivation Parameters on Cell Physiology of Limosilactobacillus reuteri.* Lund University, Lund.

Tang, X., & Pikal, M. J. (2004). Design of Freeze-Drying Processes for Pharmaceuticals: Practical Advice. *Pharmaceutical Research, 21*(2), 191-200. doi:10.1023/B:PHAM.0000016234.73023.75

te Booy, M. P. W. M., de Ruiter, R. A., & de Meere, A. L. J. (1992). Evaluation of the Physical Stability of Freeze-Dried Sucrose-Containing Formulations by Differential Scanning Calorimetry. *Pharmaceutical Research, 9*(1), 109-114. doi:10.1023/A:1018944113914

Termont, S., Vandenbroucke, K., Iserentant, D., Neirynck, S., Steidler, L., Remaut, E., & Rottiers, P. (2006). Intracellular accumulation of trehalose protects Lactococcus lactis from freeze-drying damage and bile toxicity and increases gastric acid resistance. *Appl Environ Microbiol, 72*(12), 7694-7700. doi:10.1128/aem.01388-06

Thomik, M., Gruber, S., Foerst, P., Tsotsas, E., & Vorhauer-Huget, N. (2022). Determination of 3D pore network structure of freeze-dried maltodextrin. *Drying Technology, 40*(4), 748-766.

To, E. C., & Flink, J. M. (1978). 'Collapse', a structural transition in freeze dried carbohydrates: II. Effect of solute composition. *International Journal of Food Science & Technology, 13*(6), 567-581.

Trelea, I. C., Passot, S., Marin, M., & Fonseca, F. (2009). Model for Heat and Mass Transfer in Freeze-Drying of Pellets. *Journal of Biomechanical Engineering, 131*(7). doi:10.1115/1.3142975

Tymczyszyn, E. E., del Rosario Díaz, M., Gómez-Zavaglia, A., & Disalvo, E. A. (2007). Volume recovery, surface properties and membrane integrity of Lactobacillus delbrueckii subsp. bulgaricus dehydrated in the presence of trehalose or sucrose. *J Appl Microbiol, 103*(6), 2410-2419. doi:10.1111/j.1365-2672.2007.03482.x

Vali, G. (1994). Freezing rate due to heterogeneous nucleation. *Journal of Atmospheric Sciences, 51*(13), 1843-1856.

Vásárhelyi, L., Kónya, Z., Kukovecz, Á., & Vajtai, R. (2020). Microcomputed tomography–based characterization of advanced materials: a review. *Materials Today Advances, 8*, 100084.

Wang, H., Huang, T., Liu, K., Yu, J., Yao, G., Zhang, W., Zhang, H., & Sun, T. (2022). Protective effects of whey protein hydrolysate on Bifidobacterium animalis ssp. lactis Probio-M8 during freeze-drying and storage. *Journal of Dairy Science, 105*(9), 7308-7321. doi:https://doi.org/10.3168/jds.2021-21546

Wang, W. (2000). Lyophilization and development of solid protein pharmaceuticals. *International Journal of Pharmaceutics, 203*(1), 1-60. doi:https://doi.org/10.1016/S0378-5173(00)00423-3

Wegiel, L. A., Ferris, S. J., & Nail, S. L. (2018). Experimental Aspects of Measuring the Vial Heat Transfer Coefficient in Pharmaceutical Freeze-Drying. *AAPS PharmSciTech, 19*(4), 1810-1817. doi:10.1208/s12249-018-0998-z

Yde, B., Georgieva, T. I., Clausen, A., & Abrahamsen, S. (2018). Method for optimizing a process for freeze drying a bacteria-containing concentrate. In: Google Patents.

Zayed, G., & Roos, Y. H. (2004). Influence of trehalose and moisture content on survival of Lactobacillus salivarius subjected to freeze-drying and storage. *Process Biochemistry, 39*(9), 1081-1086.

Zhang, H., & Cooper, A. I. (2007). Aligned Porous Structures by Directional Freezing. *Advanced Materials, 19*(11), 1529-1533. doi:https://doi.org/10.1002/adma.200700154

Paper I

ORIGINAL RESEARCH ARTICLE

Temperature and Heat Transfer Control During Freeze Drying. Effect of Vial Holders and Influence of Pressure

Shuai Bai Palmkron[1] · Linnea Gustavsson[1,2] · Marie Wahlgren[1] · Björn Bergensthål[1] · Anna Millqvist Fureby[2]

Abstract

Objective A common issue of freeze drying is the inhomogeneity between samples, both in regards to water content and structure. The purpose of this study is to address this issue, and try to understand the cause of inhomogeneity in the heat transfer and sample temperature.

Methods The temperature and the heat transfer was measured using different setups, both with and without vial holders at various positions at different shelf temperature and chamber pressures. By comparing sublimation rate measurements (water sample) with temperature equilibrium measurements with a non-evaporating liquid (oil sample), the heat transfer contribution from radiation and conduction could be separated and investigated individually.

Results The oil sample temperature increases each time the pressure is decreased; the increase is highest at lower shelf temperatures. Using vial holder reduces the deviation between the samples but have limited effect on the temperature increase. The sublimation rate for water sample is pressure dependent and samples close to the walls have a higher sublimation rate than vials in the center. The sublimation rate increases slightly when using a vial holder but the deviation between vials becomes more random.

Conclusions The heat transfer consists of conduction through rectified vapor and radiation from surrounding walls, about 65–75% of the heat is transferred by conduction and 25–35% by radiation under normal operational conditions. As the vial holder is also influenced by the radiation, the vial inside the holder is indirectly affected by the surrounding radiation.

KEY WORDS freeze-frying · heat transfer · radiation · sublimation rate · vial holder

Introduction

In the pharmaceutical and biotechnology industries, freeze drying is commonly used to obtain products that have long-term stability. A successful freeze-drying process enables-gentle drying that results in a product with low water content, maintained structure and good rehydration properties. A key problem encountered in freeze-drying is the limited temperature and heat transfer control during the process caused by uneven heat transfer inside the freeze dryer, resulting in inhomogeneity between vials standing on different positions on the shelf during the drying process. This is an issue especially noticeable when freeze drying at low chamber pressures[1, 2]. The knowledge of how pressure influences heat transfer and sample temperature can be essential when designing a functional freeze-drying program.

Freeze-drying is conducted in three or four steps; freezing, (annealing), primary drying and secondary drying The quality of the freeze dried product is affected by the temperature in all steps but especially the temperature during the primary drying in correlation to material properties of the formulation.

The collapse temperature, T_c, is the maximum allowable temperature for an amorphous formulation to keep its macroscopic structure during freeze-drying to generate a porous cake. [3, 4] T_c is thus crucial when designing a freeze-drying program. Drying formulations with low T_c can be challenging as this requires a low sample temperature, usually obtained by a low shelf temperature and a low chamber pressure. The influence of low pressure and low

✉ Shuai Bai Palmkron
Shuai.bai@food.lth.se

1   Department of Food Technology, Engineering and Nutrition, Lunds Universitet, Institutionen För Livsmedelsteknik, Box 124, 221 00 Lund, Sweden

2   Chemical Process and Pharmaceutical Development, RISE, 114 28 Stockholm, Sweden

shelf temperatures on the heat transfer is unfortunately often overlooked, resulting in uneven heat transfer and loss of temperature control that can lead to inhomogeneous drying and loss of reproducibility. There are previous studies focusing on heat transfer during freeze-drying and how vial holders and radiation shields can help solve issues such as inhomogeneous drying [1, 5–7].

The heat transfer to the sample can occur in three different ways, direct contact conduction between the shelf and the vial, conduction or convection through the rarefied vapor, and by radiation. Direct contact conduction between shelf and vial transfers heat occurs by the molecular vibrations in the solid matter. As the surfaces of the vials and the shelves are not perfectly flat, the contact points of the solid vial and the shelves are almost negligibly small. The heat transfer *via* direct contact conduction is not affected by pressure and thus constant during freeze drying. Conduction or convection through the rarefied vapor over the thin gap between shelves and vial depends on the conditions determined by the distance of the gap, the temperature difference, and the pressure [5].Convective transfer occurs if the Rayleigh number (Ra, the ratio between the timescale of heat transport through diffusion and convection) is significant, Ra > 1800 [7]. Under typical conditions of the freeze-drying of vials, the characteristic distance is less than a millimeter, and Ra becomes around 1. Thus, the heat transport is clearly conductive under these conditions.

The conductive heat transport through a thin vapor layer can be described in relation to the Knudsen number (Kn, the ratio between the free path of a molecule and the characteristic dimension of the heat transfer). At Kn < 0.01, the gas may be treated as a continuum and can be described by the heat conductivity of the gas. The heat transfer is weakly dependent on temperature, independent of pressure, but dependent on the distance within the continuum regime. At Kn above 10, direct molecular collisions describe the conductivity. In this molecular regime, the conductivity is linearly dependent on the pressure but independent on the distance. At intermediate Kn (0.01 < Kn < 10), the conductivity is considered to be in a transition regime [5, 8, 9].

Radiation is the heat transfer by the emission and absorption balance of electromagnetic radiation. The thermal radiation comes from all available surfaces, thus not only from the temperature-controlled shelves. As the pressure inside the chamber is reduced, the heat transfer through radiation becomes more critical, and the radiation from the surrounding surfaces becomes more influential [1]. The vials on the perimeter of the shelf are more affected by the radiation from the door and walls than vials in the middle of the shelf, resulting in deviations in heat transfer between different positions.

The heat transfer from the freeze-dryer's chamber to the sample can be described as an apparent heat transfer coefficient, $K_{v,app}$. The coefficient is a sum of the three different

modes of heat transfer and defined as the ratio of heat flow to the temperature difference between a heat source and heat sink [10]. $K_{v,app}$ can be experimentally obtained by drying aqueous samples without solids by assuming a semi-constant temperature gradient in the sample and that all transferred heat can be considered consumed by sublimation [1, 2, 6–8, 13–15].

$$K_{v,app} = H_{sub} \Big/ (T_{shelf} - T_b) \tag{1}$$

where, T_{shelf}, is the shelf temperature, T_b is the temperature at the bottom of the sample, and H_{sub} is the heat flux consumed by the sublimation.

The $K_{v,app}$ has been calculated in several other studies. These authors have studied the heat transfer and sample temperature of sublimating formulations. These studies have focused on the total heat transfer, and have not separated the contribution of radiation from the conduction through the rarefied vapor, and therefor have not been able to determine the source to the inhomogeneous heat transfer. [1, 5, 11–15].

In this study we have compared sublimating with non-sublimating conditions with the objective to determine the radiative and conductive heat transfer contribution to vials in freeze drying. We also investigate how different set-ups influence the different heat transfer contributions and the vial-to-vial homogeneity in freeze drying. The results allow for a separation of the conductive heat transfer from radiative heat transfer. Thus, it has become possible to specifically follow the pressures influence on conductive heat transfer during freeze drying. The present study also aims to investigate the possibilities to improve the temperature control by using vial holder.

Material and Method

Freeze Dryer Setup

The experiment is conducted using an Epsilon 2-6D LSCplus freeze dryer (Martin Christ, Germany), operating under controlled pressure and shelf temperature. The lowest possible shelf temperature is -50 ± 1°C. The ice condenser is located in a second chamber, and the condenser temperature is kept constant at -88°C. The freeze dryer has four temperature sensors and three different pressure gauges Piezo, Capacitance, and Pirani. The vials used are 8 ml tubular glass vials with rubber stoppers (VCDIN8R SCHOTT, Germany), the outer diameter of the vial is 22 ± 0.2 mm.

Freeze Drying Program

For the oil sample temperature equilibrium experiment, the shelf is first cooled from 20°C to -45°C at a rate of 1°C/min and maintained at -45°C for 30 min. The shelf temperature

is then raised to either -40°C or -10°C depending on the experiment, the wide temperature range was chosen to clarify how shelf temperature affects the sample equilibrium temperature and heat transfer balance even though -40°C is rarely employed during primary drying. The pressure is then decreases to 200 Pa, and a sequence of pressure changes is started. The pressure is reduced by 50% every 2 h in 6 steps until the vacuum reaches 3.12 Pa (200, 100, 50, 25, 12.5, 6.25, and 3.12 Pa). The same freezing steps were used for the mass flux experiment. The heat transfer was determined batch-wise at the pressures 50, 25, 12.5, 6.25, and 3.12 Pa at -15°C shelf temperature. Pressures below 200 Pa were controlled using the capacitance vacuum gauge, and at pressures above 200 Pa, a Pirani vacuum gauge was used. The shift in pressure gauge caused some pressure fluctuations between 200 and 100 Pa.

Sample Temperature and Heat Transfer Experiments

The sample temperature was investigated by measuring the temperature of a non-sublimating sample using medium chain triglyceride oil, hereafter termed MCT oil (Miglyol 812, Caesar & Loretz, Germany) or a sublimating sample of pure water. Samples of oil were filled to 2 ml which is the typical fill volume for the vials used (around 1 cm depth),due to sublimation the water sample was filled to 4 ml to ensure that the temperature probes were in contact with the ice during the entire drying step. The sample temperature of three vials and the vial holder temperature were measured using the freeze dryer's temperature probes according to Fig. 1. The temperature was monitored for 2 h at each pressure. The average sample temperature of

each setup is presented with the standard deviation given as error bars.

For the heat transfer experiment, the sublimation flux, $\dot{m} = \frac{\Delta m}{\Delta t}$, was determined gravimetrically, assuming that the mass and heat transfer becomes stationary reasonably fast. The results are averages of 54 vials filled with 4 ml of water. The freeze-drying program was interrupted after each pressure step. The samples were weighted, water was refilled and, the program restarted by refreezing the sample at a rate of 1°C/min to -45°C, and the drying was resumed at the next pressure level.

The investigation of sample temperature and heat transfer was conducted using three different setups, as presented in Table I.

The vial holder used in setups was custom made in blank aluminum with 25 mm deep holes and 0,05 mm clearance between vial and holder. The holes are spaced at 8 mm between vials. The vial holder covers the entire freeze dryer shelf. See Fig. 1.

Results

Sample Temperature of the Non-Sublimating Sample

The temperature profiles for the experiments using MCT oil as samples are presented in Figs. 2, 3, 4. The experiment shows the temperature of the sample at different pressures under conditions when no mass and heat are removed by sublimation.

Fig. 1 Design of custom-made aluminum vial holder used in setups 2 and 3. The sample temperature is measured with a temperature probe inside the vials placed at positions marked blue. P1 is close to the door of the freeze dryer, and P3 is close to the condenser. The temperature probe can also be inserted into the vial holder (marked with red) to measure the temperature of the vial holder.
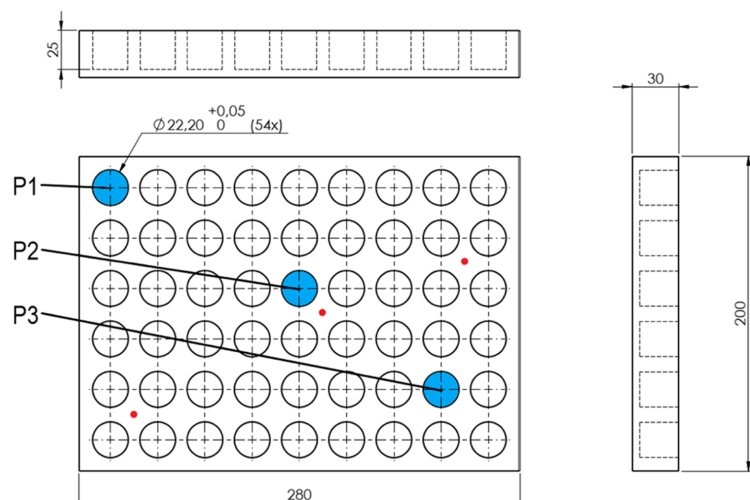
The change in the average temperature for samples containing oil using the setup vials standing on the shelf is presented in Fig. 2. The average sample temperature reaches an equilibrium value after a change in pressure. The temperature of the samples is always higher than the shelf temperature, and the difference between sample temperature and shelf temperature increases each time the pressure is decreased. At the pressure of 3.12 Pa, the average temperature difference between shelf and sample is 7°C when the shelf temperature is -10°C, and 14°C with a shelf temperature of -40°C. The difference is more pronounced for samples standing close to the door than for samples in the middle of the shelf and close to the condenser. The error bars show the between sample variation (n = 3). The individual sample temperatures are given in supplementary material Figure S1.

As described in Table I, two different methods to increase the contact between freeze drying shelf and vial using a vial holder were used. The results can be seen in Figs. 3 and 4. When the vials are inserted into a vial-holder, the temperature increase is reduced, and the deviations in sample temperature between sample positions are reduced, compared

Table I The Heat Transfer and Sample Temperature of the Sample Were Investigated Using these 3 Different Experimental Setups

Setup	Description
1. Only Vials	Vials are standing directly on the cooling shelf
2. With vial holder	Vials were placed inside an aluminum vial holder set on the cooling shelf
3. Vial holder with oil	MCT oil was added on the cooling shelf and inside the holes of the vial holder before inserting the vials

Fig. 2 The average sample temperature and the standard deviation between samples of oil using the conventional setup when vials are standing directly on the shelf. Figure A shows the sample temperature increase when pressure is lowered for samples standing on the -10°C shelf, and figure B show the sample temperature at the -40°C shelf temperature.

Fig. 3 The average sample temperature and its standard deviation of oil when vials are placed inside a vial holder. Figure A shows the sample temperature increase when pressure is lowered for samples standing on the -10°C shelf, and figure B show the sample temperature at the -40°C shelf temperature.
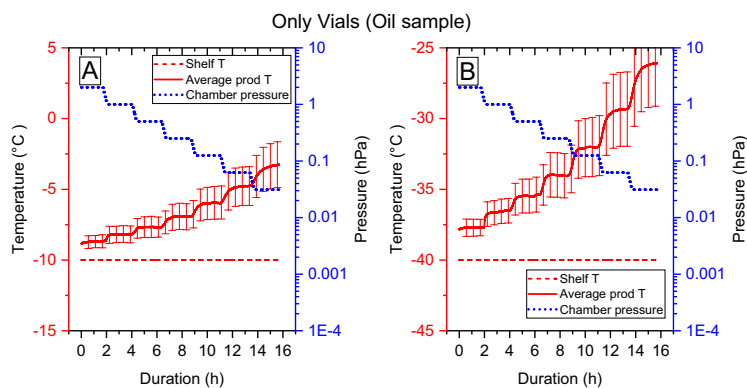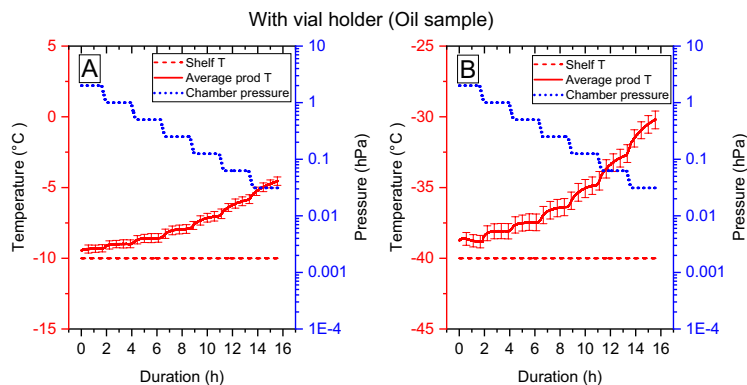
Fig. 4 The average sample temperature and its deviation of oil when vials are placed inside a vial holder with oil applied at the cooling shelf and between the vial and vial holder. Figure A shows the sample temperature increase when pressure is lowered for samples standing on the -10°C shelf, and figure B shows the sample temperature increase at the -40°C shelf temperature.
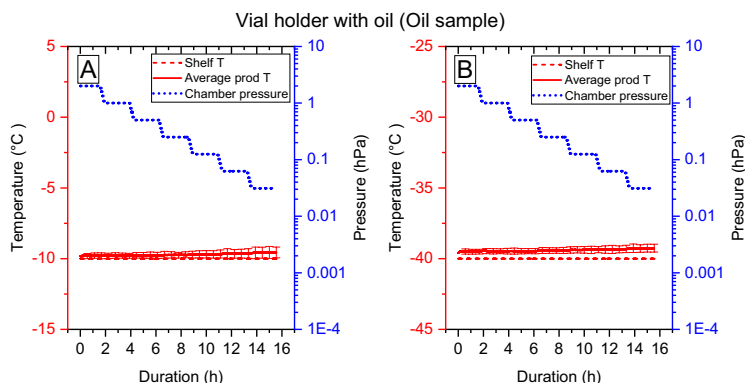
with the setup with vials on the shelf, see Fig. 3. At the pressure of 3.12 Pa the average temperature difference between shelf and sample is 5°C with a shelf temperature of -10°C, and 10°C with a shelf temperature of -40°C. The impact of vial position of individual vials and the effect of vial holders are shown in supplementary material Figure S1. However, the difference in temperature between samples and shelves is still large at low pressures.

The third set up, Fig. 4, is a conformation where the heat transfer between shelf and vial-holder as well as between vial and vial-holder is improved by filling the space with MCT oil. The temperature inside the aluminum vial-holder was unaffected by the decreasing pressure see supplementary material S2. The temperature of an oil sample standing on a -40°C shelf at 3.12 Pa pressure has a temperature increase of only 0.7°C. Also, the deviation between different vials in different positions becomes small. It was challenging to manage the experiment with this setup in a reproducible way, since air or vapor bubbles were a constant issue as even small air pockets will expand at low pressures resulting in loss of contact. The varying oil coverage between vials caused the largest deviations in the sublimation rate. Thus, reproducibility was lost, and no further evaluation could be performed. Thus, no results from this setup are further reported in this study.

The summary of the average temperature increases of the different setups is presented in supplementary material Figure S3. The magnitude of the temperature increase is higher at low pressures, and each measure to enhance contact between the vial and the shelf improves the temperature control.

Sublimation of Water as a Function of Pressure

Sublimation trials with free vials on the shelf and vials in vial-holder were performed. The results and the relative

standard deviation are presented in Fig. 5. It can be noted that the sublimation rate depends on the pressure, reaching a maximum at 25 Pa. A more pronounced pressure dependence is observed when using a vial holder rather than placing the vials directly on the shelf.

The variation in sublimation rate at the pressure of 12.5 Pa is shown in Fig. 6 and depends on the position on the shelf or in the vial holder. The experiment with the samples on the shelf displays a variation depending on the position, between 76 and 119 with an average of 92 µg/s. Samples close to the walls and in particular close to the door have a higher sublimation rate than the vials in the center. In setup 2 the variation (between 94 and 134 with an average of 109 µg/s) is more random. No noticeable wall effects can be seen. Vials on the shelf have higher variability than

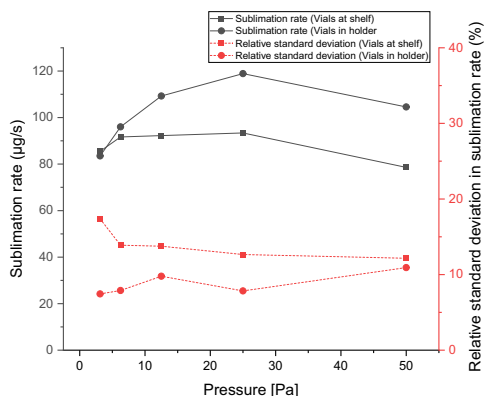**Fig. 5** Sublimation rate [µg/s ·vial] as a function of chamber pressure [Pa] and the relative standard deviation [%]. Results obtained with vials at the shelf are marked with squares, and vials in a vial-holder are marked with dots. The shelf temperature is -15°C. The result is an average of 54 vials measured over 2 h of drying time.

vials in the vial-holder. It can be observed that the variability between samples on the shelf is somewhat reduced at increasing drying pressure, while for samples in the vial-holder, it is slightly increasing with an increasing drying pressure.

Discussion

Heat transfer During Freeze-Drying Separated in Conduction and Radiation

The sublimation consumes heat. The heat is transferred from the shelves by conduction and by radiation from the surrounding walls and door. Thus, for the experiment with water, the heat balance can be written as:

$$\dot{H}_{sub,w} = \dot{H}_{cond,w} + \dot{H}_{rad,w} \tag{2}$$

In our experiment, the sublimation rate was measured gravimetrically. The sublimation heat flux is obtained by $\dot{H}_{sub,w} = \dot{m}_{sub,w} \cdot \Delta H_{sub}$ where $\dot{m}_{sub,w}$ is the sublimation flow, and ΔH_{sub} is the sublimation energy. ΔH_{sub} was determined to be 2840 kJ/kg from the vapor pressure curve using the Clausius-Clapeyrons equation for each condition. The data $T, \dot{m}_{sub,w}$ and $\dot{H}_{sub,w}$ are provided in the Table S5 in supplementary material. All the calculations of T are done in Kelvin and presented in Celsius.

In the absence of sublimation, the oil experiments are quite different from experiments with sublimating water. The temperature of the samples becomes higher than the shelf temperature, particularly when the pressure is low. The magnitude of temperature differences is prominent, up to 15°C at a shelf temperature of -40°C at 3 Pa. Thus, the heat transfer through contact between the shelf and the vials cools the sample. At the same time, heat is absorbed by radiation from other surfaces in the chamber. A stable

temperature is obtained when the heat flux through radiation from the surrounding surfaces becomes equal to the heat transfer by conduction.

$$\dot{H}_{cond,oil} = \dot{H}_{rad,oil} \tag{3}$$

The heat transferred by conduction is assumed to be described by an energy transferring constant, $K_{v,cond}$ and the temperature difference between shelf and the bottom of the material in the vial, $\Delta T_{b,ref}$. Ref refers to type of sample for the experiment (e. g. water or oil), which implies that K_v is independent of the content of the vial.

$$\dot{H}_{cond,ref} = \Delta T_{b,ref} \cdot K_{v,cond} \tag{4}$$

The temperature during sublimation of water is lowest at the sublimation front, T_{sf}, and highest at the shelf, T_{shelf}. We may divide the temperature drop into two parts, ΔT_{ice}, describing the temperature drop over the ice, and the temperature drop over the bottom of the vial over shelf, $\Delta T_{b,w}$:

$$T_{shelf} - T_{sf} = \Delta T_{ice} + \Delta T_{b,w} \tag{5}$$

The temperature drop over the ice layer is estimated assuming that the heat conductivity can be described by a single constant and that the thickness is constant over the experiment.

$$\Delta T_{ice} = \dot{H}_{sub,w} \Big/ \left(\lambda_{ice} \cdot \frac{A}{L} \right) \tag{6}$$

where λ_{ice} is the heat conductivity of ice, A is the cross-section area of the vial, and L is the thickness of the ice. However, the expression is an approximation, partly because the ice layer may be inhomogeneous, L changes over the experiment, and eventual heat conduction through the vial wall is neglected.

In the oil experiment, the temperature difference is obtained as:

Fig. 6 The sublimation rate of individual vials standing directly on the shelf, **A**, and vials standing in a vial-holder, **B**. The shelf temperature is -15°, **C** and the pressure is 12.5 Pa.
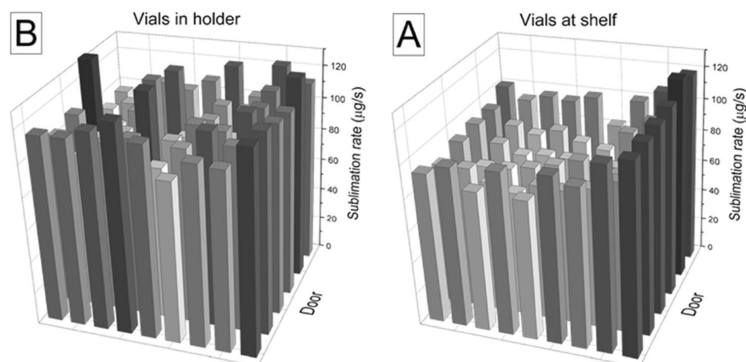
$$T_{oil} - T_{shelf} = \Delta T_{b,oil} \qquad (7)$$

where T_{oil} is the equilibrium temperature of the oil, $\Delta T_{b,oil}$ is the temperature difference over the bottom of the vial in the oil experiment. It is assumed that the temperature of the liquid oil in the samples are uniform. The heat transfer between the walls and the sample by radiation is assumed to be estimated by a system constant, c_{rad}:

$$\dot{H}_{rad,ref} = \left\{ T_{wall}^4 - T_{average,ref}^4 \right\} \bullet c_{rad} \qquad (8)$$

where the driving force for the radiation is an exponential difference between an assumed value for the walls (288 K), T_{wall} and a temperature average for the ice $T_{average,ref} = T_{sf} + \frac{\Delta T_{ice}}{2}$ have been used. For the oil experiments, it is assumed that the sample temperature can be used as a $T_{average}$. The constant c_{rad} includes geometrical features, absorption properties of the radiation as well as the universal radiation constant, and it is assumed to be equal in the experiment with water and with oil.

The $K_{v,cond}$ can be assumed to be equal to both oil and water experiment as this is the conductivity of surrounding materials. As for c_{rad} the emissivity of water and oil are different, but as the main radiation exchange is between the vial and the surroundings, the heat is then transferred from the vial to the sample *via* conduction. Thus we may assume that $c_{rad,oil}=c_{rad,w}$.

The system can be solved by combining Eqs. 2 with data from the water experiment and Eq. 3 with data from the oil experiments and using the relations for the temperatures (Eq. 5–7), the conduction (Eq. 4), and the radiation (Eq. 8). The interesting aspect is that the contribution from radiation and conduction can be separated. The derivation of the expressions for conductive heat transfer coefficient $K_{v,cond}$, and the radiative heat transfer constant, c_{rad}. Equation (9) and (10) is presented in the supplementary material S6.

$$K_{v,cond} = \frac{\dot{H}_{sub,w}}{\Delta T_w + \Delta T_{oil} \bullet \dfrac{\left\{ T_{wall}^4 - T_{average,w}^4 \right\}}{\left\{ T_{wall}^4 - T_{average,oil}^4 \right\}}} \qquad (9)$$

$$c_{rad} = \frac{\dot{H}_{sub,w} - K_{v,cond} \bullet \Delta T_{b,w}}{\left\{ T_{wall}^4 - T_{average,w}^4 \right\}} \qquad (10)$$

Using Eqs. 9, 10 and the data from the oil experiments in Fig. 2, 3, and the data from the drying of the water sample in supplementary material Table S5, the fraction of the heat flux originating from the conduction at the shelf and the radiation from the surrounding during the drying of water can be determined. The results are shown in Fig. 7.

The data is calculated based on an average of the values obtained from the oil experiment with -40°C and -10°C. The

differences in $K_{v,cond}$ were reasonably small (using Eq. 9) using data from both temperatures (3% for vials at shelf and 5% for vials in vial-holder).

The result shows that the heat flux from the radiation (H_{rad}) has an equal magnitude when the vial-holder is used and without it (Fig. 7). The limited shielding effect is primarily due to that the vial holder also receives radiation form the surrounding walls. As shown in Figure S2 in supplementary material, the vial-holder temperature increases with decreasing pressure in the same magnitude as the oil samples without vial-holder. This suggest that even if the vial holder is shielding the vials from direct radiation from the walls, the vials receives equal amount indirectly from the vial holder. The vial-holder adds to the conductive heat transfer that reaches a maximum at a pressure of 25 Pa. However, there is no dramatic difference using a vial-holder; the obtained increase in the conductive heat transfer is about 30%. The results also show that the heat flux by radiation is important and contributes to about 25% to 35% of the heat consumed by the sublimation process. It can be noted that the range of results obtained for vials on the shelf scatters between values 20% below and 20% above the average, and are highly dependent on the location of the sample, Fig. 6A, which agrees with an interpretation that an important part of the heat transfer is through radiation.

The conductive transfer coefficient, $K_{v,cond}$, and the radiation constant is shown as a function of the pressure in Fig. 8. It can be seen that that the transfer coefficient,
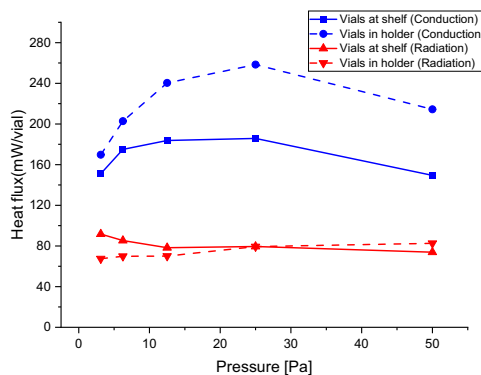
Fig. 7 Analyses of the heat flux when sublimating pure water distributed over a contribution from conduction from the shelves and radiation from the surrounding walls. A. Sublimation heat flux in absolute units [mW/vial] separated into heat transfer by conduction ($\dot{H}_{cond}$, blue), and heat transfer by radiation from the surrounding walls ($\dot{H}_{rad}$, red). The experiment using vials at the shelf is shown with a continuous line, and the experiment with a vial holder is shown with a dashed line. The data is obtained by solving Eqs. 2–10, using the results in Figs. 2 and 3. The values are an average of data from the -10 and -40°C shelf temperatures in Eq. 9.

$K_{v,cond}$, increases on increasing pressure and that it is higher with the vial holder. The curve shape (approaching a linear pressure dependence at very low pressures and showing a decreased gradient at higher pressure, theoretically tending towards a plateau value) agrees with an interpretation that the experiment is performed at a pressure when the heat transfer is in a transition region between conduction through direct molecular collisions (Kn > 10), and when the conduction can be estimated according to the continuum model from a heat transfer coefficient of the vapor (Kn < 0.1).). The Knudsen number in the experiment ranged from about < 1 for vials on the shelf at higher pressure to 10 with the low pressure and vial holder. The conduction through molecular collisions is expected to be linearly dependent on the pressure, while the conduction in the continuum model is independent of the pressure. The molecular collision model and the continuum model are usually combined into a transition model for intermediate Kn [16]. The heat transfer coefficient according to the transition model may be 3 mW/K and vial at low pressure (3 Pa) and around 15 mW/K at high pressure (50 Pa) for a vials on the shelf. The transfer coefficient at low pressure is lower than the experimental observation of 5 mW/K but in agreement at high pressure 18 mW/K (Fig. 8). Similar estimations for a vial holder would give around 5 mW/K at 3 Pa and 29 mW/K in good agreement with the experimental observations (Fig. 8). Also the sublimation rate was modelled and agreed well with the experimental data. For vials on the shelves a maximum sublimation heat flow of 150 mW/vial was observed at 20 Pa followed by a shallow decrease down to 140 mW/K at 50 Pa. For the vials in the vialholder a maximum sublimation heat flow of 220 mW/

vial was observed at 18 Pa followed by a shallow decrease down to 170 mW/K at 50 Pa. The transition equation and the results of the modelling of the heat transfer are displayed at S7 and of the sublimation heat flow at S8 in the supplementary material. However, these models demand a few parameters that are difficult to estimate. The free molecular model includes an accommodation parameter [16], and the continuum model is quite sensitive to the distances [5] Here we used 1 for the accommodation parameter and a comparable thin average distance of 0.25 mm. For the vial-holder the theoretical estimations are more complicated as there are two gaps to consider. However, the magnitude and the shape of the results seem to somewhat agree with what is expected from the theory.

The constant for the heat transfer through radiation, Fig. 8, appears slightly increasing with increasing pressure (if compared with the K_v). This observation supports that it is possible to estimate the two contributions of the energy transfer by using the simplified approximations in terms of the geometrical and surface temperature effects of the freeze dryer.

Control of the Temperature of Sublimating and Non-Sublimating Sample

The results show that the control of the sublimation is dependent on heat transfer by conduction (65–75%) and radiation (25–35%). It is expected that the conduction through the rarified vapor is relatively reproducible. However, the heat transfer through radiation to samples in free vials may vary.

The temperature during the primary drying is modeled by Eqs. 5–7. The temperatures are shown in Fig. 9 as a function of pressure for vials at the shelf and vials in vial-holders. It is clear that the drying pressure primarily determines the temperature. Although, if the shelf temperature is raised, the heat flux is expected to increase, and the vial bottom temperature differs more from the sublimation front temperature. The influence of radiation from door and walls affect the drying rate, resulting in deviation at the end of primary drying between various positions resulting in differences in water content in the final product, being a major issue for the industry [17].

In secondary drying, the drying flux is much lower. Thus, the sample temperature is expected to rise as the heat flux for vaporization gradually becomes smaller. As shown in the oil experiments, the temperature might be due to radiation rising above the shelf temperature.

The shelf temperature also influences the sample temperature increase. A lower shelf temperature means a larger difference in temperature between the walls/door and shelf (further from equilibrium) (Figs. 2 and 3). Therefore, a low shelf temperature results in larger relative temperature differences.
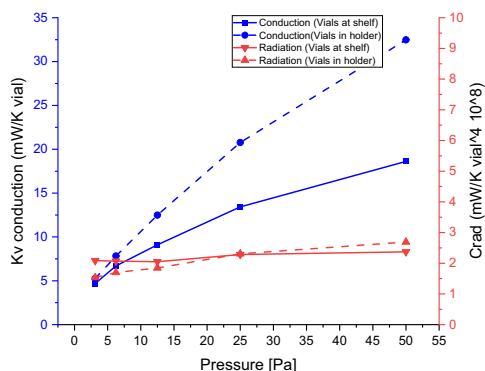
Fig. 8 Heat transfer coefficient for the heat conduction ($K_{v, cond}$) and the radiation heat transfer constant (C_{rad}) as a function of pressure. Continues curve represents experiments with vials at the shelf and dashed line experiments using a vial-holder. They were determined using Eqs. 9,10, and data from table 2 in supplementary material and Figs. 2 and 3. The values are an average of data from the -10 and -40°C shelf temperatures in Eq. 9.
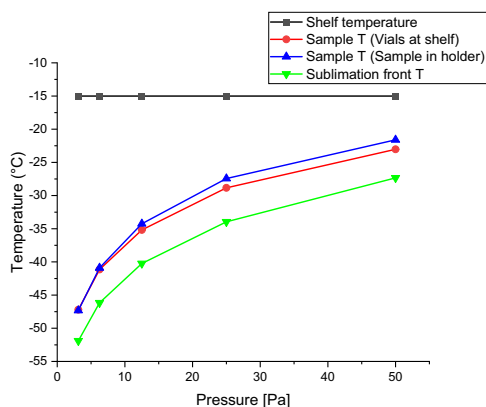
Fig. 9 The temperature at the shelf (black line), in the bottom of the sample (red line for vials at the shelf and blue line for vials in vial holder), and at the sublimation front (green line) given as a function of drying pressure. The results are estimated from the $K_{v, cond,}$ and c_{rad} determined in Fig. 8.

There are several purposes of having a vial holder: providing improved contact to the cooling shelf, keeping a homogenous temperature within the vial holder, and shielding the vials from radiation. However, this study shows that a vial holder neither maintains a very homogeneous temperature for non-sublimating samples, Fig. 3 nor a very homogeneous sublimation rate for sublimating samples, Figs. 5 and 6. Although, it can be noted from Fig. 5 that the variability is reduced by about 50% when the vial holders are used compared to without them.

This deviation for vials at the shelf is mainly caused by the difference between vials close to the door or walls and in the center of the shelf (Fig. 6). The variation between samples increases as the pressure decreases (Fig. 5). When pressure is low, the heat transfer from radiation becomes relatively more important and affects the results stronger (Fig. 7) in agreement with an increase in variation between samples.

However, for a sublimating sample in the vial-holder, the deviations in sublimation rate are more random, and no obvious pattern can be observed. The variation is observed to be increasing with increasing pressure (Fig. 8). As the samples are mostly isolated from the surroundings by the vial holder, it is safe to assume that the heat transfer is affected mainly by variations in the contact between vial and vial holder, as there is a strong correlation between snug fitting vials and high sublimation rate. This interpretation agrees with the smaller contribution (in relative terms) of the radiation to the total heat transfer (Fig. 7). It was also noticed that even the smallest amount of moisture between contact surfaces enhanced the sublimation rate significantly, most likely as

this would increase the heat transfer by conduction. At low pressures, the molecular transfer mechanism dominates, making the distance dependence smaller and thereby the fitting issue smaller, explaining the reduced variation at very low pressures.

Conclusions

The study shows that temperature control and heat transfer control are challenging tasks in freeze-drying. Temperature control is vital for preventing sample collapse during freeze-drying. Heat transfer management is crucial to ensure homogenous drying conditions where all samples end up with the same water content at the end of secondary drying.

The heat transfer consists of both a conduction contribution through a thin layer of rarified vapor as well as a radiation contribution from surrounding walls.

By comparing sublimation rate measurements with temperature equilibrium measurements for a non-evaporating liquid, it was possible to separate the heat transfer through conduction from the heat transfer from radiation. The total heat transfer was higher when using the vial holder, and the increase was due to improved conduction. The results showed that about 65–75% of the heat is transferred by conduction and 25–35% by radiation under normal operational conditions. The ratio showed a limited dependence on the investigated pressure range (3–50 Pa). This shows how big influence radiation have on freeze drying, and can be especially relevant when freeze drying samples with bad contact to the shelf such as with syringes [12] and pellets. The knowledge gained from this study can influence new ways to solve issues with radiation or utilizing radiation in freeze drying such as in freeze drying pellets.

When vials are standing on the shelf, the radiation from the surrounding surfaces that keep a higher temperature becomes more influential for the vials standing close to the perimeter of the shelf. These vials become warmer and dry faster than the samples in the center of the shelf. This effect is more pronounced at low pressures (< 10 Pa) than at higher pressures (10–100 Pa) due the relatively more important radiation at low pressures and at lower shelf temperatures. Important observation is that the vials standing in the middle of the shelf have a homogenous sublimation under all conditions. This suggest that to obtain a homogenous freeze drying, vials should be avoided to be placed close to the walls and door and avoid freeze drying at very low pressures and temperatures.

When vial holders are used, the samples remain exposed to the radiation but *via* the vial holder instead, and the conduction efficiency increases. Thus, the vial-to-vial variation is reduced. However, an inhomogeneous contact between

the vial and vial-holder due to uneven vial surfaces and contamination may lead to quite variable sublimation even when using a vial-holder.

When oil was applied between surfaces, the contact and temperature control were further improved. However, the issue of the variable vial to vial-holder contact was also further amplified, and the final deviation in sublimation rate was further increased. The inhomogeneous results also resulted in a loss of reproducibility between experiments.

Declarations

Conflict of Interest All authors declare that they have no conflict of interest.

References

1. Rambhatla S, Pikal MJ. Heat and mass transfer scale-up issues during freeze-drying, I: atypical radiation and the edge vial effect. AAPS PharmSciTech. 2003;4(2):E14. https://doi.org/10.1208/pt040214

2. Wegiel LA, Ferris SJ, Nail SL. Experimental aspects of measuring the vial heat transfer coefficient in pharmaceutical freeze-drying. AAPS PharmSciTech. 2018;19(4):1810–7. https://doi.org/10.1208/s12249-018-0998-z

3. Roos YH, Drusch S. Chapter 4 - water and phase transitions. In: Roos YH, Drusch S, editors. Phase Transitions in Foods. 2nd ed. San Diego: Academic Press; 2016. p. 79–113.

4. Mujat M, Greco K, Galbally K, Hammer D, Ferguson D, Iftimia N, *et al*. Optical coherence tomography-based freeze-drying microscopy. Biomed Opt Express. 2012;3:55–63. https://doi.org/10.1364/BOE.3.000055

5. Brülls M, Rasmuson A. Heat transfer in vial lyophilization. Int J Pharm. 2002;246(1–2):1–16. https://doi.org/10.1016/s0378-5173(02)00353-8

6. Pikal MJ, Pande P, Bogner R, Sane P, Mudhivarthi V, Sharma P. Impact of natural variations in freeze-drying parameters on product temperature history: application of quasi steady-state heat and mass transfer and simple statistics. AAPS PharmSciTech. 2018;19(7):2828–42. https://doi.org/10.1208/s12249-018-1155-4

7. Goshayeshi B, Di Staso G, Toschi F, Clercx HJH. Numerical study of heat transfer in Rayleigh-B\'enard convection under rarefied gas conditions. Phys Rev E. 2020;102(1): 013102. https://doi.org/10.1103/PhysRevE.102.013102

8. Ganguly A, Nail SL, Alexeenko A. Experimental determination of the key heat transfer mechanisms in pharmaceutical freeze-drying. J Pharm Sci. 2013;102(5):1610–25. https://doi.org/10.1002/jps.23514

9. Nail SL. The effect of chamber pressure on heat transfer in the freeze drying of parenteral solutions. PDA J Pharm Sci Technol. 1980;34(5):358

10. Pikal MJ, Roy ML, Shah S. Mass and heat transfer in vial freeze-drying of pharmaceuticals: Role of the vial. J Pharm Sci. 1984;73(9):1224–37. https://doi.org/10.1002/jps.2600730910

11. Patel SM, Pikal MJ. Freeze-Drying in Novel Container System: Characterization of Heat and Mass Transfer in Glass Syringes. J Pharm Sci. 2010;99(7):3188–204. https://doi.org/10.1002/jps.22086

12. Korpus C, Friess W. Evaluation of Different Holder Devices for Freeze-Drying in Dual-Chamber Cartridges With a Focus on Energy Transfer. J Pharm Sci. 2017;106(4):1092–101. https://doi.org/10.1016/j.xphs.2016.12.016

13. Tang X, Pikal MJ. Design of Freeze-Drying Processes for Pharmaceuticals: Practical Advice. Pharm Res. 2004;21(2):191–200. https://doi.org/10.1023/B:PHAM.0000016234.73023.75

14. Tang X, Nail SL, Pikal MJ. Evaluation of manometric temperature measurement, a process analytical technology tool for freeze-drying: part I, product temperature measurement. AAPS PharmSciTech. 2006;7(1):E14-E. https://doi.org/10.1208/pt070114

15. Fissore D, Pisano R, Barresi AA. Advanced approach to build the design space for the primary drying of a pharmaceutical freeze-drying process. J Pharm Sci. 2011;100(11):4922–33. https://doi.org/10.1002/jps.22668

16. Nakhosteen CB, Jousten K. Handbook of vacuum technology. John Wiley & Sons; 2016.

17. Patel SM, Doen T, Pikal MJ. Determination of end point of primary drying in freeze-drying process control. AAPS PharmSciTech. 2010;11(1):73–84. https://doi.org/10.1208/s12249-009-9362-7

Publisher's Note Springer Nature remains neutral with regard to jurisdictional claims in published maps and institutional affiliations.

Paper II

Check for updates

Quantification of structures in freeze-dried materials using X-ray microtomography

Shuai Bai Palmkron [a,*], Björn Bergenståhl [a], Sebastian Håkansson [b,c], Marie Wahlgren [a], Anna Millqvist Fureby [d], Emanuel Larsson [e]

[a] Department of Food Technology, Engineering and Nutrition, Lund university, SE-221 00 Lund, Sweden,
[b] Division of Applied Microbiology, Department of Chemistry, Lund University, Lund, Sweden
[c] BioGaia AB, 241 38 Eslöv, Sweden
[d] Chemical process and pharmaceutical development, RISE Research Institutes of Sweden, Stockholm, Sweden
[e] Division of Solid Mechanics and LUNARC, Department of Construction Sciences, Lund University, Lund 22100, Sweden

HIGHLIGHTS

- Wall thickness of freeze dried material can be a relevant factor when large biological bodies needs to be encapsulated.
- It is possible to use X-ray μCT for characterizing and quantifying the wall thickness of freeze-dried materials.
- The annealing procedure provides a structure with larger chambers and thicker wall material.
- The wall thickness can be determined both by the measured wall thickness and re-estimated based on the chamber size.
- The thickness of the materials are similar despite the very different drying conditions.

GRAPHICAL ABSTRACT
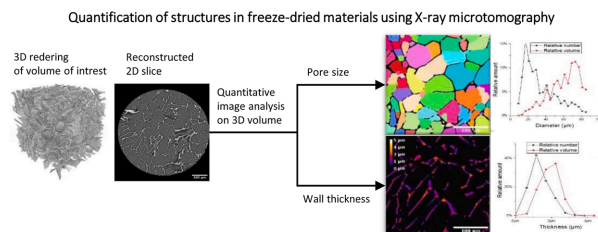
Quantification of structures in freeze-dried materials using X-ray microtomography

ARTICLE INFO

ABSTRACT

The structure of a freeze-dried material is essential for its ability to preserve and protect biologics such as proteins, cells and other sensitive structures. The structure of a typical freeze-dried matrix can be described as pores surrounded by thin walls where the walls are the encapsulating material (for e.g. cells).

The objective of this investigation is to evaluate X-ray microtomography (μCT) as a characterization method to quantifying the matrix of a freeze dried material, and compare it to scanning electron microscopy (SEM). The material consists of maltodextrin, freeze-dried below or above the glass transition temperature of the maximal freeze concentration (T_g') and after applying annealing.

The SEM images have high resolution and provide an excellent view of the sample. However, it is challenging to perform any image analysis and to ensure that a representative section is presented. The μCT images provide a rather uniform contrast between material and void, allowing for a simple grey-level thresholding when separating structure from the background. A robust image analysis procedure allows the results extracted from a representative sample volume to be evaluated. Further image analysis has been focused on understanding the

thickness of the encapsulating structures by estimations of volume-weighted averages of inscribed spheres within the walls.

The results show two types of structures: A large pore structure of around 20–100 μm separated by thin walls around 2–3 μm thick, and a finer structure consisting of smaller pockets of air (< 10 μm) packed in a honeycomb like structure. The structures of the samples dried below and above T_g' have smaller and thinner structures, while material dried after annealing has larger and thicker structures. The structures display comparably small differences between the different drying protocols despite the quite different drying conditions.

1. Introduction

Freeze-drying, or lyophilization, is commonly used to stabilize biopharmaceuticals such as proteins [1,2] and high value foods [3,4] for long-term storage. It is also the most common way to ensure the viability of probiotics by encapsulating the dried cells in a protective matrix [5–7]. It has also been shown that the freeze-drying process as well as the composition of the freeze-dried product strongly affects the long-term stability of probiotics [6,8]. While freeze-drying is a well-established technique, the factors impacting the structure of the freeze-dried cake, such as pore size and wall thickness are still not sufficiently well understood. One of the problems has been the lack of quantitative methods to study the complex structure obtained after freeze-drying.

X-ray microtomography (μCT) is a powerful technique to study and quantify morphology and structure of advanced materials. For porous materials, Vásárhelyi, L. et al. [9] recommend a combination of scanning electron microscopy (SEM) and X-ray microtomography (μCT) to obtain a complete picture. The main advantage of μCT is that it is a nondestructive method, that combined with advanced image analysis can provide a quantitative measurement of the 3D-structure of a sample. However, there are limitations to μCT. A high-resolution scan leads to a long scanning time in la bench top instrument, which can compromise the integrity of the sample, especially for soft samples and if the delivered dose becomes too high [10]. Compared to SEM the resolution of the processed images has so far been slightly lower, and for freeze-dried material the smallest pixel size using bench top μCT has been 1 μm [11,12] for the wall material studies. Using synchrotron-based X-ray microtomography (SRμCT) with a parallel and monochromatic beam, the resolution can be increased. There are previous studies that have used μCT to investigate freeze-dried structures for traditional freeze-drying in vials [11–16] as well as spin freeze-drying [15,17]. It can thus be a complementary method to more qualitative methods, such as SEM. μCT has been used to evaluate pore size linked to mass transfer [12,15,18,19], collapse temperature of the pharmaceutical formulation [13], tracking the sublimation front [11,15,16], and quantitative evaluation of cake integrity [14] and even looking at the finer structures and comparing the morphology obtained with μCT with SEM [18]. However, these articles have not been focused on quantifying the finer structure of the cake or the wall thickness but rather on giving an overview of the cake structure and to improving the understanding of the freeze drying process.

There has been a limited focus on the encapsulation capacity of freeze-dried materials in the pharmaceutical industry, mainly because the structure per se has not been a primary topic of concern as the active pharmaceutical ingredient is generally much smaller than the dimensions of the freeze-dried material. The focus has instead been directed towards developing the most suitable formulation and process for lowering the stress on the API [1,2] and reproducibility, robustness and efficiency of the process [12]. Thus, the approach in pharmaceutical industry is to freeze-dry at a low sample temperature to obtain an elegant, freeze dried cake, without visible collapse and with good rehydration properties. This approach has influenced freeze-drying processes for probiotics in industrial process development, as well as in academic research. The question is whether such a conservative freeze-drying process results in an optimal structure to achieve the

encapsulation needed for stability for larger entities such as bacterial cells. It has been observed that there is a positive correlation between some degree of material collapse of the freeze drying cake and prolonged shelf life of probiotic [20]. One reason for this could be that collapse will lead to a thicker wall material. A hypothesis could be that wall thickness plays an essential role in the viability of bacteria during storage. This as the encapsulating capacity of the material in terms of how well the bacteria can be embedded inside the wall would be affected by wall thickness. The wall thickness could therefore be an essential factor to consider when designing a suitable freeze drying protocol and matrix for e.g. probiotics. However, there is also some drawbacks of thick walls such as prolonged secondary drying time, and higher residual moisture. The latter has been shown to have adverse effect on shelf life of probiotics [21].

Methods that can determinate the wall thickness would be of importance when evaluating and optimizing freeze drying for bacterial cells. The wall thickness can either be estimated directly or evaluated based on pore size. To our knowledge there is no golden standard on how to directly measure wall thickness in freeze dried material and μCT could be a viable method if high enough resolution can be obtained. The pore size is correlated to the wall thickness, as smaller and more abundant pores have a larger surface area leading to a thinner freeze-dried material. Quantitative image analysis of μCT data sets can be used to quantify the pore size and wall thickness and thus be used to directly compare various samples with each other.

The structure formed for a freeze-dried product is a combination between formulation and freeze-drying program. One important aspect is that the formulation needs to be amorphous to efficiently encapsulate and stabilize the probiotics. In this work we used maltodextrins as the freeze-drying formulation. It forms amorphous structures and has been seen to have good physicochemical properties for formulations of probiotic products, preserving the viability of a probiotic strain [22].

The freeze-drying process consists of three main steps: freezing, primary drying and secondary drying. In some cases, an additional step of annealing is added in the freezing. The annealing step involves increasing the sample temperature above the T_g', but below the melting point of the freeze concentrate. At these temperatures Oswald ripening occurs and promotes ice crystal growth [23]. Larger ice crystals are expected to give a freeze-dried cake with larger pore size. The purpose of annealing is dual – to increase ice crystal size and to generate better uniformity within and across the vials in a freeze-drying batch. Previous research has shown that annealing enables a shorter primary drying process [1,2] and thus, a more cost-efficient process. The formulation dictates the critical temperature parameters during processing and for storage the final dried material. One critical parameter in this context is the glass transition of the maximally freeze-concentrated material, T_g', and another is the glass transition temperature, T_g of the freeze-dried material. The T_g' is indicative of the physical stability of the freeze concentrate that surrounds the ice crystals in the frozen formulation and is thus important for maintaining structural stability during the drying process. The T_g is indicative of the physical stability of the final dried amorphous formulation. Bjeloševič et al. [24] have shown that aggressive freeze-drying, i.e. at product temperatures above T_g', resulted in collapse on the micro level, but not at the macro level. Haeuser et al. [25] used different additives in sucrose to successfully freeze-dry an antibody at temperatures above T_g', thus obtaining elegant freeze-dried

Table 1
Freeze-drying protocols.

	Low Temp.	High Temp.	Annealed
Freezing	Cooling rate: 1 °C/min from 20 to − 45°C	Cooling rate: 1 °C/min from 20 to − 45°C	Cooling rate: 1 °C/min from 20 to − 45°C
	Holding: − 45 °C for 2 h	Holding: − 45 °C for 2 h	Holding: − 45 °C for 2 h
Annealing	No annealing	No annealing	Annealing 6 h − 5 °C
Primary drying	Shelf T: − 30°C	Shelf T − 7°C	Shelf T − 7°C
	Pressure: 8 Pa	Pressure: 100 Pa	Pressure: 100 Pa
Secondary drying	Shelf T: 20°C	Shelf T 20°C	Shelf T 20°C
	Heating rate 0.1 C/min	Heating rate 0.1 C/min	Heating rate 0.1 C/min
	Holding: 20 °C for 24h	Holding: 20 °C for 24h	Holding: 20 °C for 24h
	Pressure: 8 Pa	Pressure: 8 Pa	Pressure: 8 Pa

cakes, with microstructural collapse as determined by μCT. However, whether the drying step influences the freeze-drying structure when the sample temperature is below the T_g' is a topic of debate [24].

Previous research has shown the applicability of μCT for 3D investigations of whole freeze-dried cakes, which is difficult to capture using other imaging techniques. In this study we investigate the potential of μCT for investigation and quantification of the microstructure in freeze-dried materials, and compare results obtained using SEM. The main focus is on quantifying the wall thickness, as this is a parameter that is difficult to obtain using other methods and of importance for encapsulation of live probiotics. Further, μCT and SEM are used to investigate effects of primary drying parameters and annealing on the 3D structure of freeze-dried maltodextrin materials.

2. Material and methods

2.1. Material

The maltodextrin used was Glucidex 9 (hydrolyzed potato starch, dextrose equivalent 8–10, obtained from Roquette, France). The vials used were 8 ml tubular glass vials with rubber stoppers (VCDIN8R SCHOTT, Germany), with an outer diameter of the 22 ± 0.2 mm.

2.2. Determination of T_g'

10% (w/w) maltodextrin samples in MilliQ water were analyzed using Differential Scanning Calorimeter – DSC (DSC 1, Mettler Toledo, Switzerland). Triplicate of 10 mg sample solution were placed in a 40 μl aluminum pan and hermetically sealed. The measurements were conducted at a cooling rate of 10 °C/min starting from 30 °C followed by equilibration for 5 min at − 70 °C and uniform heating step (10 °C/min) followed by equilibration for 5 min at 30 °C. An empty aluminum pan was used as a reference and calibration was performed using indium. The measured T_g' was used to design the freeze-drying protocols.

2.3. Freeze-drying

Formulations containing 10% maltodextrin in MilliQ water were prepared and 2 ml of this solution was filled in 8 ml tubular glass vials with rubber stoppers. The fill height is around 8 mm. One batch of each protocol was produced. The freeze-drying was conducted using an Epsilon 2–6D LSC plus (Martin Christ, Germany), with three temperature probes for the sample temperature and three different pressure gauges: piezoelectric pressure sensor, capacitance sensor, and Pirani sensor (heat conductivity). The pressure during the freeze drying was determined by the capacitance sensor. The vials were inserted into custom made aluminum vial holders, to ensure reproducibility amongst the vials at various positions [26]. Three different freeze-drying protocols were used to induce differences in the material, where the protocols differed with regards to implementation of annealing and the level of primary drying temperature, while the freezing step and the secondary drying step were kept the same. The sample temperature is

determined by the shelf temperature and the chamber pressure, therefore both the shelf temperature and the chamber pressure was adapted to obtain the intended sample temperature. The sample temperature was kept below the T_g' for the samples that underwent the low temperature protocol, while the sample temperature was kept slightly above the T_g' for samples that dried with the high temperature protocols.

The effect of annealing was investigated in the last protocol and dried the same way as high temperature protocol. The freeze-drying protocols are presented in Table 1. The end of the primary drying was defined/determined by when the Pirani and capacitance sensors had the same pressure readings, after which the secondary drying step was initiated automatically.

2.4. SEM

A sharp metal tube was used to cut a 5 mm cylindrical sample part through the entire freeze-dried cake approximately 8 mm in height, and then cut in half in the vertical direction using a scalpel. The sample was sputter-coated with gold-palladium (at a ratio of 60:40) with expected film thickness of 9 nm and investigated using a JEOL JSM-6700 F SEM microscope (Tokyo, Japan). The samples were investigated at the top, middle and bottom section of the cross-section with a magnification of 200X and 600X. A cylindrical sample from three different vials from each freeze-drying protocol were investigated. The pore size and wall thickness were visually evaluated using a ruler and counting every pore in the 600x magnification images.

2.5. X-ray microtomography (μCT)

One new sample from each freeze-drying protocol were cut into 5 mm cylindrical using a sharp metal tube through the entire sample height (approximately 8 mm) and placed in a glass cylinder. The cylinder was then capped with a lid to avoid adsorption of moisture. A local μCT scan of the middle and inner part of the samples were carried out using a Zeiss Xradia Versa 520 (Zeiss, Heidelberg, Germany) at the 4D Imaging Lab (Lund University, Lund, Sweden), with the following scanning parameters; FOV (Field-of-View): 665×665 μm2; Source-voltage: 65 kV; Source Power: 5 W; Exposure time per projection: 12 s; number of projections: 2401; effective pixel size: 0.657 μm; total scan time: 9 h; Magnification objective: 4X; Binning: 2×2; Filter: Air; Source to sample distance: 11 mm; Sample to detector distance: 103 mm. The reconstruction was performed using the Zeiss reconstruction software, which provided 16-bit image volumes of the linear attenuation coefficient (LAC) with cubic voxels size of 0.657 μm.

2.6. Image processing and analysis

The size of the volume of interest (VOI) was determined to 300 μm x 300 μm x 300 μm, following a prior representative volume of interest (RVI) test[27,28]. One representative VOI per sample was used to quantify the pore size and wall thickness.

The grey scale images of the VOIs were then median filtered

(size=3x3x3) and segmented using standard grey-level thresholding. The porosity was calculated in Python by counting the number of voxels related to the air part in the segmented mask (binarized volume) and dividing with the total number of voxels made up the pore by the chosen VOI. Quantitative image analysis on the binary images was conducted using the following Python software packages; SciPy (scipy.org), Scikit-image (Scikit-image.org) with the function 'regionprops' to quantify the equivalent pore diameters, following prior water shedding. This function fills each pore with a 'blob' (a space filling body in 3D resembling a spheroid), which is then used to calculate the maximum and minimum diameter, which can be used to calculate an isotropy value or sphericity of the pore. The actually volume making up the pore is also used to calculate an equivalent diameter. The package PoreSpy (porespy.org) was used for calculating the wall thickness (local thickness) of the freeze-dried material structure. In PoreSpy the 'local thickness procedure' is generating a count of the number of inscribed spheres (in 3D) that can be packed with a diameter equal to the thickness of a continuous material structure. The counts are given as frequencies of number of spheres as a function of their diameter.

The image analysis of the pore size produces a number weighted average that is described in Eq. 1.

$$d_{number} = \frac{\sum d_{i \bullet} f_i}{\sum f_i} \qquad (1)$$

Where d_i refers to the pore diameter (based on a sphere) of class i and f_i to the frequency of objects of class i.

However, the pore structure is polydisperse and the number weighted distribution is dominated by the smaller objects, usually the smallest objects determined by the applied method. The focus of this study is to know where the material is distributed rather than the number of objects. A common approach to this is to convert the number weighted distribution of objects into a volume weighted distribution and a corresponding volume weighted average (d(4.3)):

$$d_{vol} = \frac{\Sigma f_i d_i^4}{\Sigma f_i d_i^3} \qquad (2)$$

The precision of the data averages can be estimated from the standard error of mean of the observations. However, the observations are skewed in favor of the smaller pores, to compensate for that, the standard error of mean of d(0.1) and d(4.3) are estimated n equal to two times the number of observations above the actual average.

A wall thickness can be estimated from the pore size assuming that the material is uniformly distributed. A wall between two pores is formed by the material expelled from the ice-crystal creating the two pores during the sublimation. The average material thickness of such a layer can be estimated by comparing the volume fraction of material as the difference between the volume of the pore and the wall and just the pore.

$$\varphi_S = \frac{V(d_c + \Delta) - V(d_c)}{V(d_c)} = \frac{\left(\frac{\pi(d_c+\Delta)^3}{6} - \frac{\pi(d_c)^3}{6} \right)}{\left(\frac{\pi(d_c+\Delta)^3}{6} \right)} = \frac{3d_c^2\Delta + 3d_c\Delta^2 + \Delta^3}{(d_c + \Delta)^3} \qquad (3)$$

Where φ_S is the volume fraction of the solids Δ is the wall thickness, d_c is the inner pore diameter and $V(d)$ is a function giving the volume of a sphere as a function of the diameter d.

Eq. 3 does not have a simple analytical solution, and thus it is solved numerically using Maple (version 2020.1) to obtain $\Delta = f(d_c, \varphi_S)$.

The volume fraction solid material is obtained from the mass fraction of solids and the density of the solids in the glassy state.

$$\varphi_s = \frac{\left(\frac{m_s}{\rho_s} \right)}{\left(\frac{m_w}{\rho_w} \right) + \left(\frac{m_s}{\rho_s} \right)} \qquad (4)$$

Where m_s is the mass fraction of solids, m_w is the mass fraction of water, ρ_s is the density of the solids in the glassy state and ρ_w is the

density of water. 1.5 g/ml is used as the density of maltodextrin in the glassy state [29]. The standard error of the wall thickness estimated from the solution of Eq. 3 is assumed to be proportional to the relative standard error of pore size estimations.

The wall thickness obtained directly from the tomographic images using the 'PoreSpy' package are obtained as a function of the frequency and the diameter of the inscribed spheres. From the distribution of the spheres the number and volume weighted wall thicknesses averages were calculated as:

$$\Delta_{number} = \frac{\sum f_i \Delta_i}{\sum f_i} \qquad (5)$$

$$\Delta_{vol} = \frac{\sum f_i \Delta_i^4}{\sum f_i \Delta_i^3} \qquad (6)$$

Where Δ_i is the wall thickness as described by the diameter of inscribed spheres of class i and f_i is the frequency of inscribed spheres of class i.

The precision of the data averages is estimated from the standard error of mean of the observations. However, the number of 'spheres' is very large (about 10^7) and display a large covariance. Thus, we assume that the evaluated pores size provides a better picture of the variation of the observations than the number of inscribed spheres. Thus, n, in the standard error of mean estimation is taken from the pore size evaluation.

3. Results

3.1. DSC

The onset T_g' of 10% maltodextrin was measured to be $-9.8\ °C$. The DSC thermogram is presented in Supplementary material Fig. 1. The state diagram of the maltodextrin-water system was constructed based on the measured T_g', the T_g curve for maltodextrin derived from literature [30] and the more precise data on the T_g for the dry material from van Sleuwen [29], and the assumption that Cg' is at a mass fraction of about 0.8, see Fig. 1.

3.2. Freeze-drying

For the low temperature protocol the sample temperature during drying was measured to be $-30\ °C$ at the bottom of the vial using a
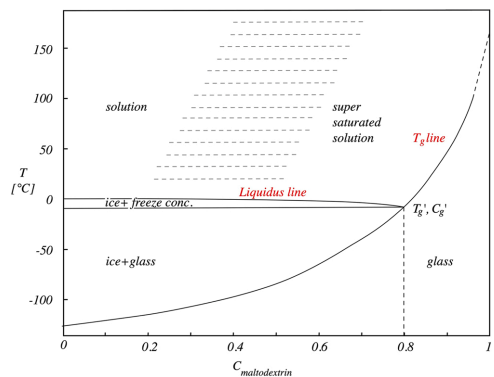

Fig. 1. State diagram of the maltodextrin-water system based on the T_g' measurement, T_g of dry glassy state from van Sleeuwen et al. [29] and principal structure from Roos and Karel [30]. The dashed lines between the solution and the supersaturated solution indicates that the boundary depends on the chain length distribution of the maltodextrin.

temperature probe. Freeze-drying using the high temperature protocol gave sample temperature readings at around −10 °C. The annealing protocol showed similar temperatures readings as the high temperature protocol. The most noticeable difference between the different drying protocols is the primary drying time as the sample dried with low temperature protocol had 3.5 times longer primary drying time, 42 h compared to 12 h for the samples dried using high temperature protocol. Visual examination of the samples after freeze-drying showed that the freeze-dried cakes had an elegant appearance, with no sign of macroscopic collapse and only a minimal change in volume, see Fig. 2.

3.3. SEM

SEM images were taken of the top, middle and bottom of the freeze-dried sample and representative pictures from the three freeze-drying programs are shown in Fig. 3. A summary of the morphology and size of the structures is presented in Table 2. The cut plane may contain some minor debris created during the cutting procedure.

Two types of structures can be observed. The first is a cell like structure of pores separated by thin walls. This is the dominating structure in all samples. The pores have a polyhedric shape. The pore size distribution is large, ranging from 10 to 150 µm. The pores are interconnected to each other by round large connecting pores (5–30 µm) through the walls, most likely making the air in the freeze-dried cake completely continuous. The connecting pores are round with smooth edges and show no signs of bursting or fracturing. Most of the connecting pores are localized in the middle of a separating wall between two pores. Pores, walls and connecting pores are marked in Fig. 3. The average pore size seems to be similar between the low and high temperature protocols, while they appear to become larger (fewer small pores) when the sample has undergone annealing. There is also a trend that the pores are smaller at the bottom of the sample, but no noticeable difference is detected between the middle and top of the sample. Six out of nine sample had smaller pores at the bottom of the sample, while the rest of the samples had approximately the same pore size over the entire depth. A visual assessment suggests that the pores are isotropic, the visual assessment of pore size and shape is therefore independent of the samples cutting plane (further assessment is done with µCT). The walls are on average 1–3 µm thick in samples processed following the low temperature and the high temperature freeze-drying procedure. The wall thickness of the annealed samples is larger (1–5 µm) and there seem to be more traces of thin and protruding wall material in samples that have not undergone annealing. Slightly thicker material can be observed in the corners when the walls of three or more pores meet, marked in Fig. 3. This structure is also more pronounced in the annealed sample. Thinnest walls are observed around the connecting pores.

The second type of structure can be observed inside the pores of samples processed at the low temperature and high temperature protocols. There are well-defined and uniform honeycomb like structures with small pockets with low size distribution and a diameter of approximately 5–10 µm. These structures are always clustered together
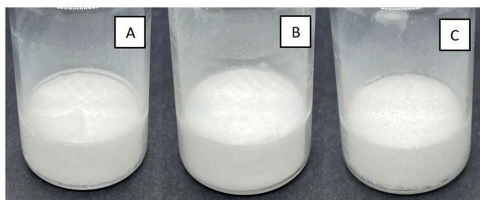

Fig. 2. Freeze-dried cake from each of the freeze-drying protocols, Where A: Low temperature B: High temperature C: Annealed + high temperature. None of the samples shows any sign of macroscopic collapse.

and are distinctly different from the pore structures, see highlighted features in Fig. 3. In one of the samples dried with the low temperature protocol, needle-like structures can be observed, see Supplementary material Fig. 3. These structures have similar thickness as the honeycomb structures but are elongated to several hundred micrometers. The presence of honeycomb structures depended on the freeze-drying conditions. In samples that were freeze-dried with the low temperature protocol, all samples showed the presence of the honeycomb structure, and two samples had a high amount of honeycomb structure, while one only had traces of this structure. For samples freeze-dried following the high temperature protocol the honeycomb structures were less frequent, and two out of three samples displayed honeycomb structures. No difference in prevalence of honeycomb structure was detected across the height of the freeze-dried cake. The annealing procedure seems to have eliminated the honeycomb structure completely.

3.4. X-ray microtomography (µCT)

Reconstructed 2D slices from the inner part of the freeze-dried cakes are presented in Fig. 4. A good contrast-to-noise ratio between air and the freeze-dried matrix is noted.

The structure appears as pores separated by thin walls. The honeycomb structures found in SEM images can also be observed in the 2D µCT slices as well, see Fig. 4. Under certain conditions connecting pores can be difficult to identify in the 2D µCT slices due to the direction of the resulting cut plane. The walls between the pores are clearly visible. The thick corner structure is difficult to distinguish from walls with a plane parallel to the image. Walls parallel to the 2D slice appears as white blurs and should not be interpret as thick walls. The pore morphology is rather uniform in the annealed sample compared to the un-annealed samples, see Fig. 4. Looking at the different orthogonal view of 2D slices of all samples no difference in pattern can be observed, suggesting that the material is isotropic on the scale of the field of view. Walls thinner than pixel size will lead to so called partial volume effects [31], with grey scale values between the air and material structure, which might hamper further image segmentation. Walls thinner than the resolution, approximately double the size of the pixel size as a general rule, i.e. 1.3 µm can therefore not be clearly resolved and appear as interrupted lines in Fig. 4. The 2D slices were assembled into 3D rendering of the material, see Fig. 5. By utilizing external lighting options causing shadows – as offered in advanced rendering software, e.g. by using the Dragonfly software (ORS – Object Research Systems, Montréal, Quebec, Canada), 3D renderings can often be improved thereby aiding visual inspection of certain material structures, see Fig. 5.

3.4.1. Equivalent pore diameter

The 3D images were evaluated using image analysis to quantify the size of the pores. All procedures were performed on the VOI (Volume Of Interest) and involves segmentation and the creation of a binarized volume, see Fig. 4, where the pores can be separated with a 3D water shedding procedure, see Fig. 6. The illustrating figures are displayed in 2D, while all image processing procedures were applied in 3D manner. Challenging aspects of the thresholding are related to the inability to select very thin walls, below the pixel size and resolution limit, which will introduce a cut off in the lower width of the structures during this operation. Thin and non-segmented walls can often be recreated using water shedding, as shown in Fig. 6. The observed porosity for the low temperature procedure was 89%, while it was 88% for the high temperature procedure and 93% for the annealed procedure. The compositional porosity is around 93%.

The equivalent diameter of the pores was quantified on the water shed images, see Fig. 6. Individual pores are marked in different pseudo colors. The relative number weighted and the relative volume weighted size distributions of the pores are plotted in Fig. 7. Since the detection of thin walls is limited in µCT, the calculated pore sizes will be larger than those detected by SEM imaging, which provides higher resolution
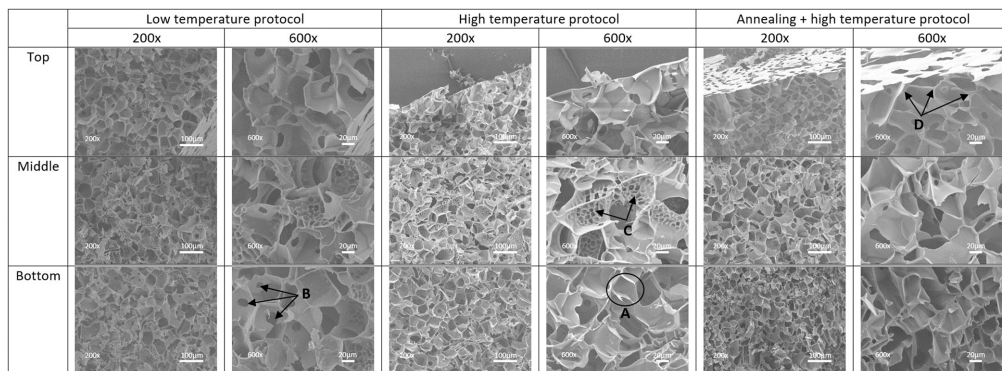
Fig. 3. SEM images from one sample of each freeze-drying protocols in 200x and 600x. The different types to structures are marked in the images. A: Pores 10–150 μm surrounded by wall material. Difference in shape and size. B: Round smooth connecting pores interconnect pores with each other. C: Honeycomb structures of 5–10 μm, which are similar in shape and size. D: Accumulation of wall material at the corners, where several pores meet.

Table 2
Summary of SEM image characteristics based on visual examination.

Freeze-drying protocol	Morphology	Pore size	Wall thickness
Low Temp.	- Pores separated by thin walls, - Plenty of thin wall fragments- Plenty of honeycomb structures present	- Range 10–80 μm- Plenty of small pores around 10 μm- Typical pore size around 20 μm	- Range < 1–3 μm - Typical thickness is 1 μm - Very thin around the connecting pores
High Temp.	- Pores separated by thin walls, - Plenty of thin walls fragments- Honeycomb structures are present in few samples	- Range 10–100 μm- Plenty of small pores around 10 μm- Typical pore size is around 20 μm	- Range < 1–3 μm- Typical thickness is 1 μm - Very thin around the connecting pores
Annealed	- Pores separated by thin walls.- Fewer thin wall fragments compared to the other protocols.- Honeycomb structures are not observed	- Range 10–150 μm- Few small pores, less than 20 μm- Typical pore size is around 30 μm	- Range < 1–5 μm- Typical thickness is 1–2 μm - Very thin around the connecting pores

images. The total number of pores inside the VOI (300 μm x 300 μm x 300 μm) and the number and volume weighted average were calculated for each of the samples and are presented in Table 3. The number weighted size distribution shows that there are only minor differences in pore size between freeze-drying with low and high temperature protocol, both distributions have a mode value with 12% of the pores being around 70 μm. The sample freeze-dried with low temperature protocol has a higher abundance of small pores, most noticeable for pores around 20 μm. Few pores less than 10 μm (roughly the size of honeycomb structures) was detected in low temperature protocol sample. The similarities between low temperature and high temperature protocol are also evident when looking at the amount of pores in the VOI as well as the number and volume-weighted averages. The annealed sample differs from the other protocols, as the sample has much less of pores smaller than 20 μm, no structures below 10 μm and overall a lower frequency of pores smaller than 40 μm. Therefore the annealed sample has a higher number and volume weighted average for the pore size compared to the other protocols.

3.4.2. Wall thickness

The wall thickness of the samples was quantified from the segmented 3D binary image, as described under Section 2.6 Image processing and analysis. Slices visualizing the 3D quantified wall thickness have been color coded and shown in Fig. 8. A range of wall structures with a thickness from around 1 μm to around 4.5 μm can be observed. Wall structures partly being parallel with the image plane and partly thick corners can also be distinguished.

The number and volume weighted distribution of the inscribed spheres has been calculated and plotted in Fig. 9. The volume weighted distribution is the most relevant parameter to examine, as this highlights

how the volume of the encapsulated material is distributed. It has been noted that the limited resolution does not allow us to observe the finer structures, this leads to an uncertainty of detecting material below roughly 1.3 μm. The volume weighted distribution functions in Fig. 9 have maxima of 2–3 μm, well above the resolution limit for all three tomographic data sets.

Looking at the volume weighted distribution, the mode value of the wall thickness is around 2.5 μm for all three samples. The wall thickness gradually increases in range, when going from low temperature to high temperature and finally to the annealed sample. The annealed sample has a higher frequency of a wall thickness which is 2 μm above, compared to the other samples. The walls are thickest in the corners where several pores intersect, see Fig. 8.

The number and volume weighted average of wall thickness obtained from Eqs. 5 and 6 is presented in Table 4. The average wall thickness can also be calculated based on the volume weighted average pore size and using Eqs. 3 and 4. This estimation is assuming that the shape is spherical and that the wall thickness is even. The pore-size based average wall thickness is about 60% of the volume weighted average showing that the unevenness of the distribution of the structure is important when evaluating the encapsulating power of the structure.

4. Discussion

In this study X-ray μCT and SEM were used to investigate the structure of the freeze-dried cakes of maltodextrin samples, which were dried using three different freeze-drying protocols. SEM is widely used to study structures of freeze-dried samples, but it has limitations in providing quantitative data [32–35]. 3D tomographic imaging showing the potential of providing quantitative data for this type of samples has
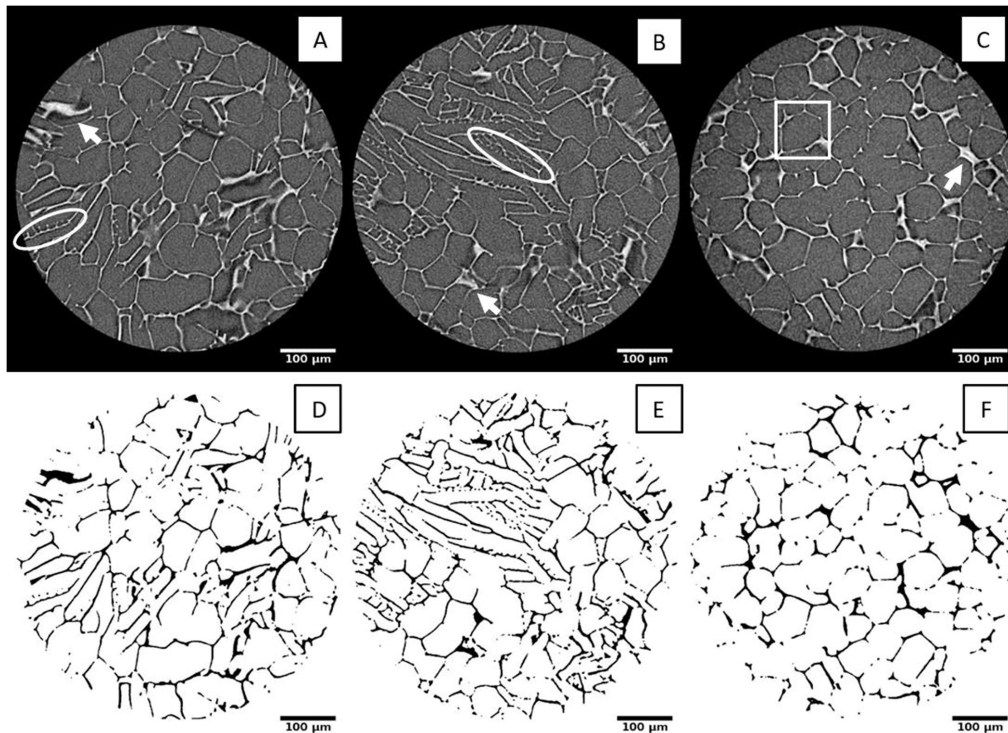
Fig. 4. A, B, C) Filtered 2D µCT slices and D, E, F) corresponding binarized images. Where A, D) Low temperature B, E) High temperature C, F) Annealed + high temperature. Structures corresponding to pores are marked with a square, and structures that correspond well to honeycomb structures are marked with an ellipse. Walls parallel to the 2D slice appear blurry and are highlighted with arrows.
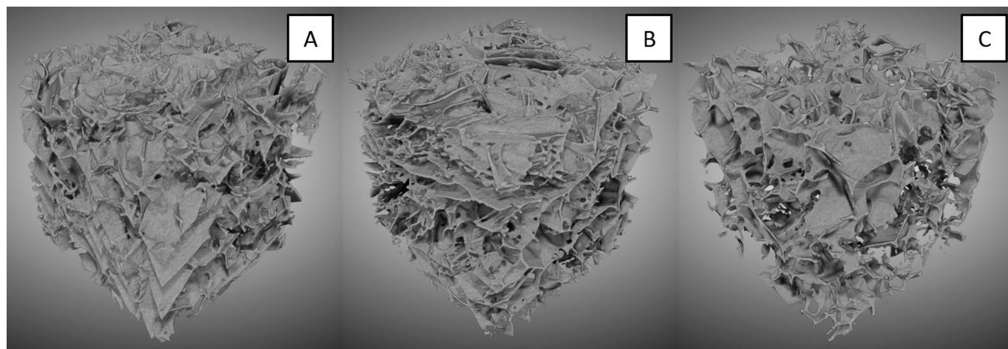
Fig. 5. 3D rendering of VOIs using shadowing effects. The dimensions of the rendered VOIs are 300 µm x 300 µm x 300 µm. A: Low temperature B: High temperature C: Annealed+ high temperature.

only been produced by a few other authors [11,12,16]. One of the purposes of this study is to evaluate the suitability of tomography to provide information on the structure of freeze-dried maltodextrin samples.

Characteristics of particular interest are the pore size and the wall thickness. When comparing this study to previous work [11, 12, 16, 34–36] the focus is mainly on wall thickness, rather than the pore size. This focus is chosen as it can be expected to be critical for the function of
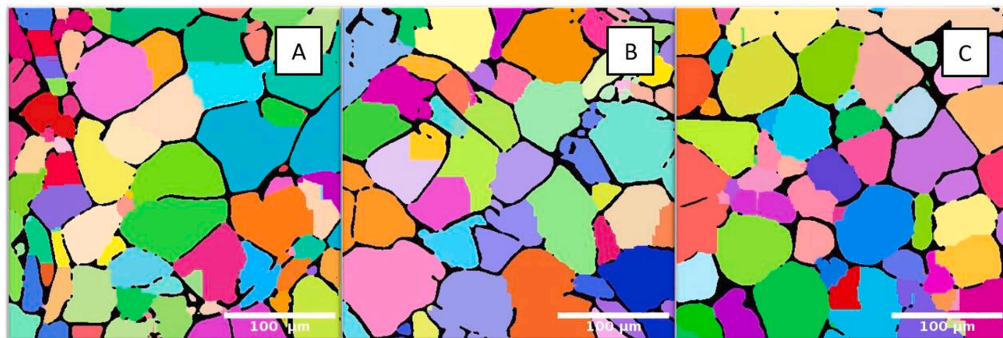
Fig. 6. 2D μCT slices after 'region props' and 'water shedding' carried out in 3D using the Scikit-image Python package. Each equally colored domain corresponds to a 'blob' in the image analyses and is interpreted as an individual pore. Thinner wall or missing wall structures can be detected using the water shedding procedure, and pores can be separated. A: Low temperature B: High temperature C: Annealed + high temperature.
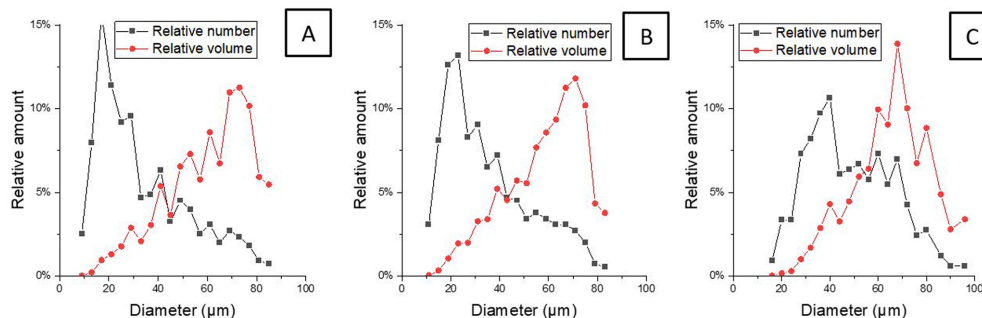
Fig. 7. Plotted number and volume weighted distribution of the pore size as quantified on the obtained water shedding images, where A: Low temperature B: High temperature C: Annealed + high temperature.

Table 3
The total number of pores in a VOI (300×300×300 μm) and the number and volume weighted average pore diameter.

	Low Temp.	High Temp.	Annealed
Total number of pores in VOI	554	555	330
Pore diameter. Number weighted average diameter (μm) using Eq. 2. and standard error of mean	35.6 ± 0.8	34.1 ± 0.8	46.6 ± 0.8
Pore diameter. Volume-weighted average diameter (μm) using Eq. 3. and standard error of mean	58.4 ± 1.3	60.8 ± 1.5	63.1 ± 1.4

the freeze-dried product when it comes to protecting larger biologics, such as virus or bacteria, for which interactions with the pore surface could be expected to be detrimental.

X-ray μCT generates a 3D map of the linear attenuation coefficient of X-rays interaction with matter. The advantage of using tomography to study structure is that the data sets provide volumes with a contrast suitable for quantitative evaluations. The distributions can then be translated between different types of averages for example number weighted and volume weighted dimensions. The drawback of this method is the relatively low resolution in relation the finest dimensions in the freeze dried cake structure.

SEM however is a qualitative method that provides topographic images with higher resolution and being closer to a visual image of a non-transparent macroscopic object. However, cross-sections of certain

structures can only be visualized with respect to the physically induced cutting planes, which in turn impedes wall thickness quantification from SEM images. Thus, it is more challenging to derive quantitative information from SEM images than the tomographic images, although this was attempted by e.g. Arsiccio, A. et al. [37].

The results of the pore size obtained from the tomographic images, show a skewed number distribution, where the mode is dominated by pores around 20–30 μm, where the number then decreases for larger pores up until 80–100 μm, see Table 3 and Fig. 7. This corresponds well to the typical pore size observed in SEM images (Table 2 and Fig. 3). Small wall protrusions around 5–8 μm apart can be observed in the tomographic slices, which correspond well to the honeycomb structures seen in SEM. However, there are relatively few pores smaller than 10 μm in the data, thus suggesting that the fine honeycomb structures were not
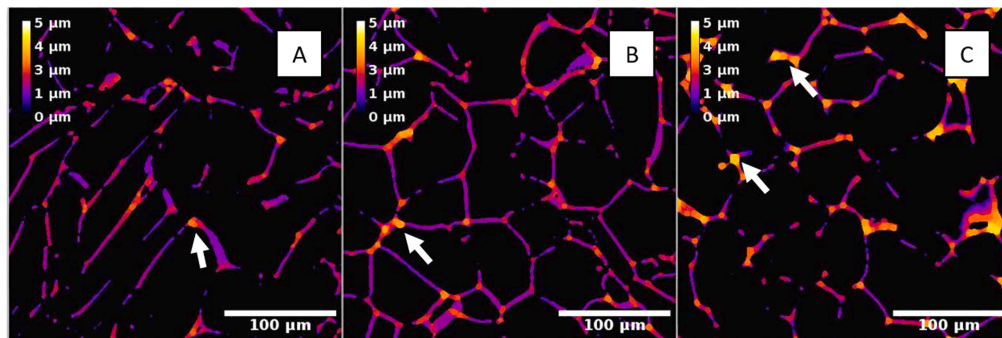
Fig. 8. 2D slice of the color coded wall thickness after image analyses carried out in 3D using PoreSpy using the 'local thickness procedure'. The measured thickness are colored according to size. Dark purple represents thinner wall material structures and bright yellow color represents thicker wall material. The thickest wall material accumulates in the crossroads, where several pores meet, as highlighted by the white arrowhead. The thickest material structure can be found in the annealed sample as shown in C). A: Low temperature B: High temperature C: Annealed + high temperature.
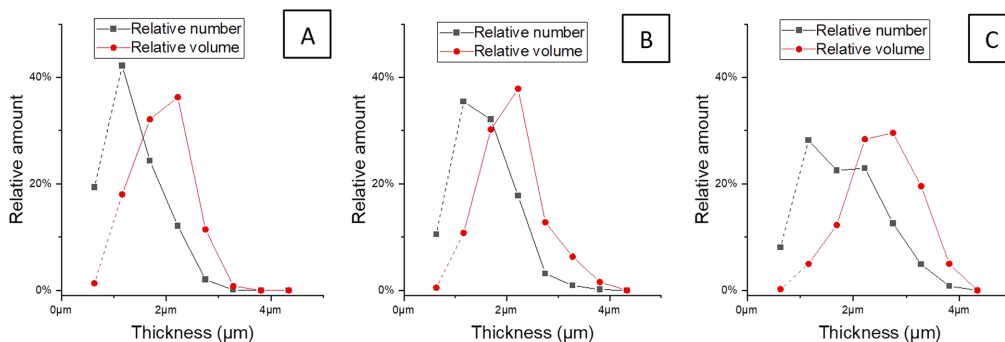

Fig. 9. The relative number and volume weighted size distribution of wall material thickness obtained from the amount of inscribed spheres from local thickness (PoreSpy). Uncertainties in detecting the thinnest wall material < 1.3 µm is visualized with dotted line also note that there is a cut-off at 0.64 µm. A: Low temperature B: High temperature C: Annealed + high temperature.

Table 4

Number and volume weighted average wall thickness obtained from the 3D rendered tomographic images. The wall thickness estimated based on volume weighted average pore size.

Wall thickness methods	Low Temp.	High Temp.	Annealed
Number weighted average diameter (µm) and standard error of mean using Eq. 5 based on wall thickness	1.50 ± 0.024	1.67 ± 0.027	1.91 ± 0.042
Volume weighted average diameter (µm) and standard error of meanusing Eq. 6 based on wall thickness	2.00 ± 0.041	2.21 ± 0.051	2.65 ± 0.059
Volume weighted average diameter (µm) and standard error of mean using Eqs. 3 and 4 and the volume pore distribution from Table 3.	1.41 ± 0.031	1.47 ± 0.036	1.52 ± 0.033

well detected using the water-shedding method. Looking at the width of the size distribution in Fig. 7 all three protocols seem to be very similar, but due to a lower frequency of small pores and higher frequency of larger pores in annealed sample, the annealed sample appears to have a more uniform structure, see Fig. 4.

There are different factors that influence the final pore size of the material, the size distribution of the ice crystals in the frozen phase, and the amount of collapse induces during drying. The collapse can then be divided into two different types, the microscopic collapse and the macroscopic collapse. The microscopic collapse means that finer structure elements (for instance the honey comb structures) are lost while

macroscopic collapse means that the volume of the cake is lost.

The most challenging characteristic data to obtain from this study is the wall thickness. The limited amount of broken or cracked wall material allowing for measurements of thickness in the SEM images gives a somewhat limited insight so that the dimensions of the structures can only be roughly estimated. Using the obtained tomographic data sets, the wall thickness can be determined directly in a 3D manner. The distribution obtained is a number distribution of virtually inscribed spheres. The distribution can be converted to a more physically relevant volume weighted distribution (Table 4), as the focus is on how the matrix material may protect and encapsulate the active material The

wall thickness obtained from tomography could be compared to complementary SEM images that give a wall thickness of around 1–3 μm for un-annealed samples and 1–5 μm for annealed samples. The high value obtained using Eq. 6 based on wall thickness is likely due to the presence of the thick corners observed in all the material, which is more pronounced after the annealing process. These features are clearly visualized in the 2D cut slices in Fig. 8. Further, the thinner walls (<1.3 μm) are not well-resolved with μCT at the given scanning geometry and resolution.

In this investigation the wall thickness has also been estimated assuming that the walls are formed from the freeze concentrate surrounding the pore-forming ice crystals. The model assumes a spherical pore geometry, and that the walls are even. The resulting wall thickness is about 60% of the volume average-based wall thickness (Table 4), suggesting that the uneven distribution of material (e. g. thick corners) is important to create conditions for encapsulation.

Even though tomography is a powerful and non-destructive tool to quantify material structural details, certain details such as honeycombs and shape of connecting pores can be difficult to visualise and analyse using a bench top instrument due to the limited resolution. Honeycomb structure can be observed in the reconstructed 2D μCT slices before binarization of the images but are difficult to quantify, due to the very thin structures. It is challenging to characterize finer details as the voxel length is limited to 0.657 μm, finer structures less than 1.3 μm might be unable to be depicted, which is evident in the wall thickness data (Fig. 9). One consequence of excluding the thinner walls is that the average wall thickness is overestimated as the walls thinner than 1 μm are excluded from the thickness distribution. However, looking at the volume weighted distribution of wall thickness in Fig. 9 leads to the conclusion that most of the detected wall material resides in walls thicker than 1.5 μm. Therefore, the lack of resolution does not play a crucial role in relation to investigation of the encapsulating volume of the material. Other consequences in the structure analysis are that the pore size is overestimated as thinner parts of the walls are missing in the reconstruction, so that two or more actual pores are detected as one pore. This also makes further connectivity analysis irrelevant as non-existent paths are created where the walls are missing. These may lead to a slight overestimation of wall thickness using 3D tomographic imaging in combination with image analysis.

The resolution in the X-ray μCT can be increased at the cost of obtaining longer scanning times for each sample, thereby increasing the risk of damaging the sample due to extended irradiation, especially for soft samples, which in turn can lead to movement artefacts in the reconstructed image (No dose related damages could be observed in our samples with total scan time of 9 h). A higher resolution is therefore unsuitable for a bench top tomography and hence SRμCT would be the next step. When this article is written, the highest tomographic pixel size obtained on freeze-dried material was 1 μm [11,12,16,38]. Investigating the SEM images it becomes clear that there are two size levels of structures in the un-annealed samples, where honeycomb structures are < 10 μm in size and pores that typically are > 20 μm in size. The existence of these two kinds of structures raises the question of how they originate. The honeycomb and needle-like structures correspond well to the shape and size of ice crystals in frozen sugar solutions [11,16,39] and are believed to originate from the freezing step, while the larger pores are primarily formed as a consequence of Ostwald ripening and glassy state relaxation [16,23], occurring during the freeze-drying process. Interconnecting pores in the walls are round and have smooth edges suggesting that no bursting has occurred and that the pores are created under rubbery conditions (temperature and water content just above the T_g line in the state diagram, see Fig. 1).

In our experiment, the low temperature protocol kept the material well below the T_g' for the system during the complete process, while for the high temperature protocol the shelf temperature was raised above T_g' during the drying and according to the annealing protocol the sample

were kept above T_g' during the annealing. Thus, it is surprising that despite these differences in the freeze-drying protocols, the characteristics of the freeze-dried material structures are so similar. Examining the result from SEM images and tomographic data sets there is no large difference in pore structure between freeze-drying with high or low temperature protocols. However, a more noticeable difference can be observed for the samples that have undergone annealing. In this case the pores are slightly larger with less thin wall residues protruding, and a noticeably thicker corners and walls. The biggest difference between annealed and un-annealed sample as seen by SEM is the lack of honeycomb structures for the annealed sample. Looking at the tomographic data sets in terms of pore size, the samples from low temperature and high temperature are almost identical in both number of pores and the size distribution. The annealed sample shows fewer and larger pores compared to previous protocol, which is a consequence of letting the ice crystals grow larger during the annealing step. Nakagawa et al. [16] showed that an annealed sample using maltodextrin with similar dextrose equivalent as the one used in this study can grow the ice crystals from < 10 μm to > 50 μm using the same annealing process, which is in accordance with our results. Kharatyan et al. [23] proposed Ostwald ripening as the mechanism of the crystal growth in freeze-drying, as observed by microscopy, during the annealing procedure. This is likely the reason why no honeycomb structures were observed in the annealed sample. The reason for the small difference in structure might be due to the high viscosity of maltodextrin in the freeze-concentrate and that the sample temperature obtained with high temperature protocol remains too close to the T_g' during drying. A more noticeable difference can be seen in other low molecular sugar solutions with lower viscosity [40,41]. Even if the structures do not seem to differ notably between protocols the primary drying time differs significantly, as the sample dried with low temperature protocol had 3.5 times longer primary drying time. The main reason for the slow drying rate at lower temperatures is due to the lower heat and mass transfer at lower pressures [26].

For the purpose of encapsulating and drying e.g. bacterial cells, the wall thickness of the freeze dried material is of relevance as thicker walls would have a higher capacity to fully embed the cells within the walls. In the case of fully amorphous wall materials, the cells can become well encapsulated in the walls while in thin walls the cells are expelled from the matrix [21]. However, for materials with crystalline character, the walls are very differently constructed so that the crystalline structures dominate and appear coated with an amorphous layer, see e.g. Badal Tejedor et al.[42]. Such structures are not likely to be able to support the integrity of relatively large and complex structures such as bacterial cells. However, combined crystalline and amorphous formulations are well suited for proteins, which are orders of magnitudes smaller than cells [43]. The pore structure on the other hand, appears less important for the encapsulation of the cells, but plays a role for the freeze-drying process and in particular the duration of the primary drying phase, as established in several publications[11,12,15,19,44]. Large pores, however, inevitably implies thicker walls (Eq. 3), providing that the freeze-dried cake does not change its overall dimensions. If the cake shrinks, and hence macroscopic collapse occurs, the direct link between pore size and wall thickness is lost. Potentially, controlled micro- and even macro-collapse may be beneficial for the encapsulation of cells as the wall thickness and encapsulation capacity increase.

5. Conclusions

This study has shown that it is possible to use X-ray μCT for characterizing the morphology of freeze-dried materials, in combination with complimentary and visual examination of SEM images. The SEM provides a images with topographic character. The resolution is high allowing for observations of fine details (thin walls, connecting pores and honeycomb structures).

X-ray μCT makes it possible to obtain a full 3D map of the linear attenuation coefficient of a sample. However, inspecting the reconstructed 2D cut slices can often be more useful, in order to detect certain structures. The tomographic images provide contrast suitable for image analysis and quantitative evaluations. However, μCT requires a long analysis time, and the detection of structures on the limit of the pixel size and resolution, might lead to challenges when selecting an appropriate threshold for segmentation. Investigating the fine details (observed in SEM) with tomography is challenging as the resolution is an issue with bench top μCT. However, the majority of the structure forming material could be quantitatively analyzed.

The structures of the materials obtained using the different drying protocols are similar despite the very different drying conditions. The results show that there is a fine structure (honeycomb structures) in the freeze-dried matrix when dried with low temperature protocol. The presence of these structures is reduced when the sample is dried at higher temperature and eliminated if the sample is annealed above T_g'. The annealing procedure provides a structure with larger pores as seen in both SEM images and reconstructed 2D tomographic slices. The μCT and image analyses showed that the average wall thickness becomes larger in the annealed samples. It can be assumed that thicker structures provide a better encapsulating capacity for biological objects such as probiotic bacteria. The close relation between average wall thickness of the structure and the pore size means that the wall thickness could be both determined by the measured wall thickness and re-estimated based on the pore size.

CRediT authorship contribution statement

Shuai Bai Palmkron: Methodology, Formal analysis, Writing – original draft, Writing – review & editing, Investigation. **Björn Bergenståhl:** Conceptualization, Formal analysis, Writing – review & editing, Funding acquisition. **Sebastian Håkansson:** Conceptualization, Writing – review & editing, Supervision. **Marie Wahlgren:** Conceptualization, Methodology, Writing – review & editing, Funding acquisition. **Anna Millqvist Fureby:** Conceptualization, Methodology, Writing – review & editing, Funding acquisition. **Emanuel Larsson:** Conceptualization, Methodology, Formal analysis, Writing – original draft, Writing – review & editing.

Declaration of Competing Interest

The authors declare the following financial interests/personal relationships which may be considered as potential competing interests: Shuai Bai Palmkron reports financial support was provided by BioGaia AB. Shuai Bai Palmkron reports financial support was provided by Sweden's Innovation Agency.

Data Availability

Data will be made available on request.

References

[1] W. Wang, Lyophilization and development of solid protein pharmaceuticals, Int. J. Pharm. 203 (2000) 1–60.

[2] X. Tang, M.J. Pikal, Design of freeze-drying processes for pharmaceuticals: practical advice, Pharm. Res. 21 (2004) 191–200.

[3] C. Ratti, Hot air and freeze-drying of high-value foods: a review, J. Food Eng. 49 (2001) 311–319.

[4] D. Nowak, E. Jakubczyk, The freeze-drying of foods—the characteristic of the process course and the effect of its parameters on the physical properties of food materials, Foods 9 (2020).

[5] S. Kandasamy, R. Naveen, A review on the encapsulation of bioactive components using spray-drying and freeze-drying techniques, J. Food Process Eng. 45 (2022).

[6] K.C. Baral, R. Bajracharya, S.H. Lee, H.K. Han, Advancements in the pharmaceutical applications of probiotics: dosage forms and formulation technology, Int. J. Nanomed. 16 (2021) 7535–7556.

[7] G. Broeckx, D. Vandenheuvel, I.J. Claes, S. Lebeer, F. Kiekens, Drying techniques of probiotic bacteria as an important step towards the development of novel pharmabiotics, Int J. Pharm. 505 (2016) 303–318.

[8] F. Fonseca, S. Cenard, S. Passot, Freeze-drying of lactic acid bacteria, in: W. F. Wolkers, H. Oldenhof (Eds.), Cryopreservation and Freeze-Drying Protocols, Springer New York, New York, NY, 2015, pp. 477–488.

[9] L. Vásárhelyi, Z. Kónya, Á. Kukovecz, R. Vajtai, Microcomputed tomography–based characterization of advanced materials: a review, Mater. Today Adv. 8 (2020).

[10] E. Maire, P.J. Withers, Quantitative X-ray tomography, Int. Mater. Rev. 59 (2014) 1–43.

[11] S. Gruber, N. Vorhauer-Huget, P. Foerst, In situ micro-computed tomography to study microstructure and sublimation front during freeze-drying, Food, Structure 29 (2021).

[12] P. Foerst, T. Melo de Carvalho, M. Lechner, T. Kovacevic, S. Kim, C. Kirse, H. Briesen, Estimation of mass transfer rate and primary drying times during freeze-drying of frozen maltodextrin solutions based on x-ray μ-computed tomography measurements of pore size distributions, J. Food Eng. 260 (2019) 50–57.

[13] K. Greco, M. Mujat, K.L. Galbally-kinney, D.X. Hammer, R.D. Ferguson, N. Iftimia, P. Mulhall, P. Sharma, W.J. Kessler, M.J. Pikal, Accurate prediction of collapse temperature using optical coherence tomography-based freeze-drying microscopy, J. Pharm. Sci. 102 (2013) 1773–1785.

[14] C. Haeuser, P. Goldbach, J. Huwyler, W. Friess, A. Allmendinger, Imaging techniques to characterize cake appearance of freeze-dried products, J. Pharm. Sci. 107 (2018) 2810–2822.

[15] B. Vanbillemont, J. Lammens, W. Goethals, C. Vervaet, M.N. Boone, T. De Beer, 4D micro-computed x-ray tomography as a tool to determine critical process and product information of spin freeze-dried unit doses, Pharmaceutics 12 (2020).

[16] K. Nakagawa, S. Tamiya, S. Sakamoto, G. Do, S. Kono, Observation of microstructure formation during freeze-drying of dextrin solution by in-situ x-ray computed tomography, Front. Chem. 6 (2018).

[17] R. Mousavi, T. Miri, P.W. Cox, P.J. Fryer, A novel technique for ice crystal visualization in frozen solids using X-ray micro-computed tomography, J. Food Sci. 70 (2005) e437–e442.

[18] K.I. Izutsu, E. Yonemochi, C. Yomota, Y. Goda, H. Okuda, Studying the morphology of lyophilized protein solids using X-ray micro-CT: Effect of post-freeze annealing and controlled nucleation, AAPS PharmSciTech 15 (2014) 1181–1188.

[19] R. Pisano, A.A. Barresi, L.C. Capozzi, G. Novajra, I. Oddone, C. Vitale-Brovarone, Characterization of the mass transfer of lyophilized products based on X-ray micro-computed tomography images, Dry. Technol. 35 (2017) 933–938.

[20] T.I.G. Birgitte Yde, Anders Clausen, Susanne Abrahamsen, Method for optimizing a process for freeze drying a bacteria-containing concentrate, JustiaUS, 2013.

[21] N. Ekdawi-Sever, L.A. Goentoro, J.J.D. Pablo, Effects of annealing on freeze-dried lactobacillus acidophilus, J. Food Sci. 68 (2003) 2504–2511.

[22] H.W. Tang, S. Abbasiliasi, P. Murugan, Y.J. Tan, H.S. Ng, J.S. Tan, Influence of freeze-drying and spray-drying preservation methods on survivability rate of different types of protectants encapsulated Lactobacillus acidophilus FTDC 3081, Biosci. Biotechnol. Biochem. 84 (2020) 1913–1920.

[23] T. Kharatyan, S.R. Gopireddy, T. Ogawa, T. Kodama, N. Nishimoto, S. Osada, R. Scherließ, N.A. Urbanetz, Quantitative analysis of glassy state relaxation and ostwald ripening during annealing using freeze-drying microscopy, Pharmaceutics 14 (2022).

[24] M. Bjelošević, K.B. Seljak, U. Trstenjak, M. Logar, B. Brus, P. Ahlin Grabnar, Aggressive conditions during primary drying as a contemporary approach to optimise freeze-drying cycles of biopharmaceuticals, Eur. J. Pharm. Sci. 122 (2018) 292–302.

[25] C. Haeuser, P. Goldbach, J. Huwyler, W. Friess, A. Allmendinger, Be aggressive! amorphous excipients enabling single-step freeze-drying of monoclonal antibody formulations, Pharmaceutics 11 (2019).

[26] S.B. Palmkron, L. Gustavsson, M. Wahlgren, B. Bergensthål, A.M. Fureby, Temperature and heat transfer control during freeze drying. effect of vial holders and influence of pressure, Pharm. Res (2022).

[27] M. Martínez-Sanz, E. Larsson, K.B. Filli, C. Loupiac, A. Assifaoui, A. López-Rubio, P. Lopez-Sanchez, Nano-/microstructure of extruded Spirulina/starch foams in relation to their textural properties, Food Hydrocoll. 103 (2020), 105697.

[28] E. Larsson, D. Gürsoy, F. De Carlo, E.T. Lilleodden, M. Storm, F. Wilde, K. Hu, M. Müller, I. Greving, Nanoporous gold: a hierarchical and multiscale 3D test pattern for characterizing X-ray nano-tomography systems, J. Synchrotron Radiat. 26 (2019) 194–204.

[29] R. van Sleeuwen, S. Zhang, V. Normand, Spatial glass transition temperature variations in polymer glass: application to a maltodextrin-water system, Biomacromolecules 13 (2012) 787–797.

[30] Y. Roos, M. Karel, Water and molecular weight effects on glass transitions in amorphous carbohydrates and carbohydrate solutions, J. Food Sci. 56 (1991) 1676–1681.

[31] J.F. Barrett, N. Keat, Artifacts in CT: recognition and avoidance, RadioGraphics 24 (2004) 1679–1691.

[32] J.-Y. Her, M.S. Kim, K.-G. Lee, Preparation of probiotic powder by the spray freeze-drying method, J. Food Eng. 150 (2015) 70–74.

[33] K.S. Pehkonen, Y. Roos, S. Miao, R.P. Ross, C. Stanton, State transition ad physicochemical aspects of cryoprotection and stabilization in freeze-drying of L, rhamnosus GG (LGG) (2008).

[34] G. Thakur, A. Mitra, A. Basak, D. Sheet, Characterization and scanning electron microscopic investigation of crosslinked freeze dried gelatin matrices for study of drug diffusivity and release kinetics, Micron 43 (2012) 311–320.

[35] N. Harnkarnsujarit, S. Charoenrein, Y.H. Roos, Microstructure formation of maltodextrin and sugar matrices in freeze-dried systems, Carbohydr. Polym. 88 (2012) 734–742.

[36] M. Thomik, S. Gruber, P. Foerst, E. Tsotsas, N. Vorhauer-Huget, Determination of 3D pore network structure of freeze-dried maltodextrin, Dry. Technol. 40 (2022) 748–766.

[37] A. Arsiccio, A.C. Sparavigna, R. Pisano, A.A. Barresi, Measuring and predicting pore size distribution of freeze-dried solutions, Dry. Technol. 37 (2019) 435–447.

[38] K. Nakagawa, S. Tamiya, G. Do, S. Kono, T. Ochiai, Observation of glassy state relaxation during annealing of frozen sugar solutions by X-ray computed tomography, Eur. J. Pharm. Biopharm. 127 (2018) 279–287.

[39] P. Klinmalai, M. Shibata, T. Hagiwara, Recrystallization of ice crystals in trehalose solution at isothermal condition, Food Biophys. 12 (2017).

[40] Y. Zhao, P. Takhar, Freezing of foods: mathematical and experimental aspects, Food Eng. Rev. 9 (2017).

[41] D.Q. Craig, P.G. Royall, V.L. Kett, M.L. Hopton, The relevance of the amorphous state to pharmaceutical dosage forms: glassy drugs and freeze dried systems, Int J. Pharm. 179 (1999) 179–207.

[42] M. Badal Tejedor, J. Fransson, A. Millqvist-Fureby, Freeze-dried cake structural and physical heterogeneity in relation to freeze-drying cycle parameters, Int. J. Pharm. 590 (2020), 119891.

[43] R.E. Johnson, C.F. Kirchhoff, H.T. Gaud, Mannitol–sucrose mixtures—versatile formulations for protein lyophilization, J. Pharm. Sci. 91 (2002) 914–922.

[44] M. Hilmer, J. Peters, M. Schulz, S. Gruber, N. Vorhauer, E. Tsotsas, P. Foerst, Development of an experimental setup for in situ visualization of lyophilization using neutron radiography and computed tomography, Rev. Sci. Instrum. 91 (2020).

Paper III

Quantification of structures in quenched annealed and nonannealed freeze-dried pellets using X-ray microtomography

Shuai Bai Palmkron[1]*, Björn Bergenståhl[1], Stephen Hall[6,7], Sebastian Håkansson[2,3], Marie Wahlgren[1], Emanuel Larsson[5,6], Anna Millqvist Fureby[1,4]

[1] Department of Process and Life Science Engineering, Division of Food and Pharma Lund University, 221 00 Lund, Sweden

[2] Division of Applied Microbiology, Department of Chemistry, Lund University, 221 00 Lund, Sweden

[3] BioGaia AB, 241 38 Eslöv, Sweden

[4] Chemical process and pharmaceutical development, RISE Research Institutes of Sweden, Stockholm, Sweden

[5] Department of Experimental Medical Science, Lund University, 221 00 Lund, Sweden

[6] LUNARC, Lund University, Box 118, 221 00 Lund, Sweden

[7] Division of Solid Mechanics, Department of Construction Sciences, Lund University, Lund, 22100, Sweden

* Corresponding author

Abstract

Freeze drying in the pellet format is a common method to enhance the storage stability of probiotics. This study evaluates the structural changes of the freeze-dried material influenced by annealing and solute concentrations of pellets quenched in liquid nitrogen. The pore size and material thickness are quantified and evaluated using Scanning Electron Microscopy (SEM) and X-ray microtomography (µCT). Quantifying the material thickness can be especially useful for evaluating the encapsulation properties in the freeze-dried material. The formulation consists of maltodextrin and probiotic cells (*Limosilactobacillus reuteri*) with a concentration of solids between 10% to 30%. The results reveal a broad range in both the pore size and material thickness. Non-annealed samples exhibit a very thin material with an elongated structure, these samples could not be investigated quantitatively using µCT due to the limitation in resolution. The annealing changed the structure significantly, resulting in a coarser material that can be quantitatively analysed using µCT. The annealed sample displayed a material with a thickness ranging from 2 to 5 µm and pores measuring between 20 and 30 µm. Material thickness increases with prolonged annealing time and higher solute concentration. The impact of annealing observed on pellets is notably more pronounced than the effects observed previously in vial freeze-drying. Local collapse is also observed, leading to increased material thickness around the collapse.

Introduction

Freeze-drying is the most common method to dry biological material, i.e., proteins, nucleotides, and probiotic cells. While protein drugs are mostly freeze-dried in vials, probiotics are often dried as pellets. In the latter case, pellets are formed by quenching the formulation in liquid nitrogen, resulting in a rapid freezing of the material. The pellets are then freeze-dried in trays (Ekdawi-Sever et al., 2003; Trelea et al., 2009). Similar types of pellets can also be used for the formulation of diagnostics (Erber & Lee, 2015) and in some cases for proteins (Olbrich et al., 2017). Pellet freeze-drying holds an advantage over vials in terms of both more rapid freezing of the material (Kasper & Friess, 2011) and a faster freeze-drying process.

While structural properties of the freeze-dried cake in vials have been previously examined (Bai Palmkron et al., 2023; Foerst et al., 2019; Izutsu et al., 2014; Pisano et al., 2017; Vanbillemont et al., 2020). It can be characterized as a matrix of pores separated by thin materials. There are only a few studies on the structures of pellet (Ekdawi-Sever et al., 2003). The obtained structure in a freeze-dried product will be affected by the formulation, freezing, annealing, and drying procedures. Rapid freezing normally results in the formation of small ice crystals. Thus, small pores

and thin materials are expected. To obtain larger ice crystals, the material can be annealed before drying, which can lead to faster primary drying (Tang & Pikal, 2004; Wang, 2000) and thicker material structures (Bai Palmkron et al., 2023). Although, in the pellet study by Ekdawi-Sever et al., smaller and more uniform pores were observed, as a consequence of the annealing time (Ekdawi-Sever et al., 2003).

In vial freeze-drying, the predominant heat transfer occurs through conduction from the shelf to the vial bottom (approximately 60-70%) (Bai Palmkron *et al.*, 2023). Conversely, pellet freeze-drying relies solely on radiation. Pellet formulations feature a significantly higher surface area per volume exposed to the vacuum, promoting effective mass transfer. For larger pellets, in the mm scale, as typically encountered in the drying of probiotics, the sublimation occurs simultaneously for all individual pellets in the tray (Trelea et al., 2009). The absence of conductive heat transfer allows for an increase in shelf temperature, while the temperature at the sublimation front remains controlled by the pressure, preventing collapse during drying and enhancing overall drying efficiency.

The structural stability during the freeze-drying process is linked to the glass transition temperature of the maximally freeze-concentrated material (Tg') and the collapse temperature (Tc) (Fonseca et al., 2021; Fonseca et al., 2004; Pikal & Shah, 1990). For amorphous materials, the drying should be performed below the Tc. Drying above this temperature leads to viscous flow in the sample, changes in the pore structure and eventually collapse (Liapis & Bruttini, 2009). The Tc is often a few degrees above Tg' (Fonseca et al., 2021; Pikal & Shah, 1990), but for formulations containing bacteria it can be as much as 10°C higher (Fonseca et al., 2004). Drying above Tc may lead to two types of collapse 1) a small microscopic collapse, where the material undergoes a viscous flow leading to larger pores, but without any visual change in the volume or shape of the sample, and 2) macroscopic collapse referring to large changes in the structure thus leading to changes in sample volume and shape (Bjelošević et al., 2018).

X-ray microtomography (µCT) has been used in several different applications to study freeze-dried structures during the last years (Chitu et al., 2015; Foerst et al., 2019; Hilmer et al., 2020; Izutsu et al., 2014; Pisano et al., 2017; Trelea et al., 2009; Vanbillemont et al., 2020) focusing on evaluating the pore structure of in freeze-dried materials. However, concerning the storage stability of bacteria, the material thickness may be a more relevant parameter to investigate, since the bacteria are similar in size to the freeze-dried material thickness. An increase in material thickness can lead to a better encapsulation of the bacteria. There is yet only one study about the material thickness of the freeze-dried material quantified using µCT (Bai Palmkron et al., 2023)

It is well known that the freeze-drying protocol affects the survivability of microorganisms. The hypothesis is that the material thickness of the freeze-dried

material plays a major role in the encapsulation capacity and the stability of probiotics. This article aims to investigate how the structure of frozen pellets is affected by the concentration and annealing of the freeze-dried formulation (maltodextrin and *Limosilactobacillus reuteri* cells). The structure is studied using both scanning electron microscopy (SEM) and µCT as previously shown in (Bai Palmkron et al., 2023).

Materials and methods

Material of the pellets and the determination of $T_g{}'$

To produce the pellets, maltodextrin Glucidex 9 (hydrolyzed potato starch, dextrose equivalent 8-10, from Roquette, France) was used. The $T_g{}'$ of the maltodextrin was analyzed using a Differential Scanning Calorimeter (DSC) (Mettler Toledo, Switzerland). Triplicates of 10 mg sample solution containing 10% (w/w) maltodextrin in MilliQ were placed in a 40 µl aluminum pan and hermetically sealed. The measurements were conducted at a cooling rate of 10°C/min starting from 20°C to -70°C with an equilibration step for 5 min at -70°C followed by a heating step (10°C/min) to 30°C. An empty aluminium pan was used as a reference and calibration was performed using indium. The Tg' were determined in STARe Software by ISO standard (ISO 11357–2:1999). The measurement results were used to design the annealing method.

Pellets production method

Limosilactobacillus reuteri DSM 17938 (previously named *Lactobacillus reuteri* DSM 179382) was obtained as freeze-dried powder provided by BioGaia AB (Sweden) containing $2 \cdot 10^{11}$ CFU/g powder and 0.289g dry weight of cell/g powder. The cells were washed with MQ water and centrifuged. The washed cells were then re-suspended in a solution consisting of maltodextrin to obtain the desired concentration of 10, 20, and 30% dry weight corresponding to $2 \cdot 10^{11}$ CFU/g dry matter. A detailed description of the formulations can be seen in *Table 1*.

The pellets were produced by quench-freezing the solution dropwise into liquid nitrogen, using a syringe pump at approximately 160 drops/min. The approximate drop diameter was 4 mm. The frozen pellets were stored at -80°C until further processed.

Table 1: Formulation recipes for pellets investigated. *Including water originating from the cell suspension

Total dry matter in the formulation [%]	Cell mass (dry matter) [g]	Maltodextrin [g]	Total amount of water (g)*
10	1.4	3.6	45
20	2.8	7.2	40
30	4.2	10.8	35

*Including water originating from the cell suspension

Freeze drying and annealing.

The pellets were distributed in aluminum cups, forming 2-3 layers of pellets. The cups were suspended about 2 cm above the shelf, which created an environment where the heat transfer during the freeze drying originates from radiation. The pellets that required annealing were placed in the precooled freeze-dryer at the annealing temperature of -7°C for 1h and 4h respectively. After the annealing step was finished, the freeze dryer was cooled down to -40°C, and the non-annealed pellet was placed in the freeze dryer. Thereafter, all the pellets were freeze-dried according to the freeze-drying protocol.

The freeze-drying was performed using an Epsilon 2-6D LSC plus (Martin Christ, Germany), with three different pressure gauges: piezoelectric pressure sensor, capacitance sensor, and Pirani sensor. The chamber pressure was first decreased to 30 Pascal (equivalent to -32°C sublimation temperature of the ice). The shelf temperature was then increased from -40°C to 30°C at a rate of 4.6°C/min. The pressures and temperatures were selected to keep the sample temperature below the collapse temperature, which is determined by the sublimation rate and the heat transfer balance (Bai Palmkron *et al.*, 2023). The same chamber pressure and shelf temperature were used in both primary and secondary drying. The end of the primary drying was set to when the Pirani and capacitance sensors had the same pressure readings, after which the program automatically started the secondary drying step which lasted for 24 hours.

Scanning electron microscopy

SEM images of the inner structures of the pellets were investigated by splitting a pellet in half using a razor blade. The sample was then attached to a sample holder and sputter-coated with gold-palladium (at a ratio of 60:40) and investigated using a JEOL JSM-6700F SEM microscope (Tokyo, Japan). The sample structures were investigated at 50x, 200X, and 800X magnification. 2000x magnification was used to examine how cells were embedded in the material.

X-ray microtomography

Two pellets from each protocol were cut into quarters (wedge-shaped) using a razor. The sample was wedged into a 200 µl pipette tip acting as a sample holder in the tomograph. The pipette tips were sealed with parafilm to avoid absorption of moisture. An overview and a local µCT scan of the upper half wedge were carried out using a Zeiss Xradia Versa 520 (Zeiss, Heidelberg, Germany). The local scan had a volume of interest (VOI) measuring 390 µm x 390 µm x 390 µm. The scanning parameters are presented in *Table 2*. The reconstruction was performed using the Zeiss reconstruction software and provided 16-bit image volumes of the linear attenuation coefficient (LAC).

Table 2: µCT Scanning parameters for the overview and local scan.

	Overview scan	Local scan
Source voltage	80 kV	80 kV
Source current	87uA	87uA
Source power	7W	7W
Exposure time per projection	0.3 s	3.0 s
Number of projections	1601	3201
Zoom (Lens)	4x	20x
Source to sample distance	9.03mm	9.03mm
Sample to detector distance	21.4mm	9.81mm
Effective pixel size	2.00µm	0.64µm

Image processing and analysis

A median filter with a size of 4x4x4 pixels was applied to the grey-scale images and a standard grey-level thresholding was used to segment the images. For quantitative image analysis, Python software packages SciPy and Scikit-image were used. The 'regionprops' and water shedding function from the Scikit-image package were used to measure the equivalent pore volume, pore diameter, and equivalent sphere volume. The PoreSpy package was used to calculate the material thickness (referred to as local thickness) in the freeze-dried material. In PoreSpy, the local thickness procedure presents the number of 'blobs' with a specific width in the material. The counts were presented as a frequency distribution, indicating the number of blobs at various diameters.

The objective of the study is to understand the distribution of the material rather than the quantity of objects. To accomplish this, the distribution of objects based on

their number can be transformed into a distribution that takes the volume they occupy into account. This results in a volume-weighted distribution and a corresponding volume-weighted average d(4.3). The volume-weighted average of the pore size was calculated from the diameter of all pores and the volume-weighted material thickness was calculated from the volume-weighted average of the inscribed 'blobs'.

$$d_i(4,3) = \frac{\sum_{i=1}^{N} d_i^4}{\sum_{i=1}^{N} d_i^3} \qquad\qquad [1]$$

$$h_{vol} = \frac{\int_0^V h \, dV}{\int_0^V dV} \approx \frac{\sum_{j=1}^{J} d_j V_j}{\sum_{j=1}^{J} V_j} \qquad\qquad [2]$$

where d_i is the diameter of pore i and h is the thickness of the material. N is the number of pores counted. The volume-weighted average thickness is obtained from the volume-weighted average of the blobs in each class j counted over J classes. V_j is the total volume of all particles in class j.

The mode value of the volume-weighted pore size distribution is obtained from the midpoint of a horizontal line at 2/3 of the height of the peak.

Results

Glass transition temperature.

The onset Tg' of 10% maltodextrin in MQ water was measured to be -9.8°C.

Freeze-drying

A representative freeze-drying cycle is given in *Figure S2* under *Supplementary Information*. The primary drying of the pellets took approximately 12 hours. Images of the freeze-dried pellets can be seen in *Figure 1*. There are no signs of macroscopic collapse after freeze-drying. There are no visual differences in size or colour between the frozen pellets, but the appearance changes after freeze-drying. The 10% and 20% pellets that have undergone annealing have a more yellowish hue and are less shiny on the surface than the other pellets. These changes indicate a coarsening of the structures in the pellets. All 10% pellets have a fragile structure, and they are difficult to handle without disintegrating, which is especially true for pellets that have been annealed for 4h, which deformed during packaging. The pellets become less fragile as the maltodextrin concentration is increased.

Annealing time

0h   1h   4h

10%

20%

30%
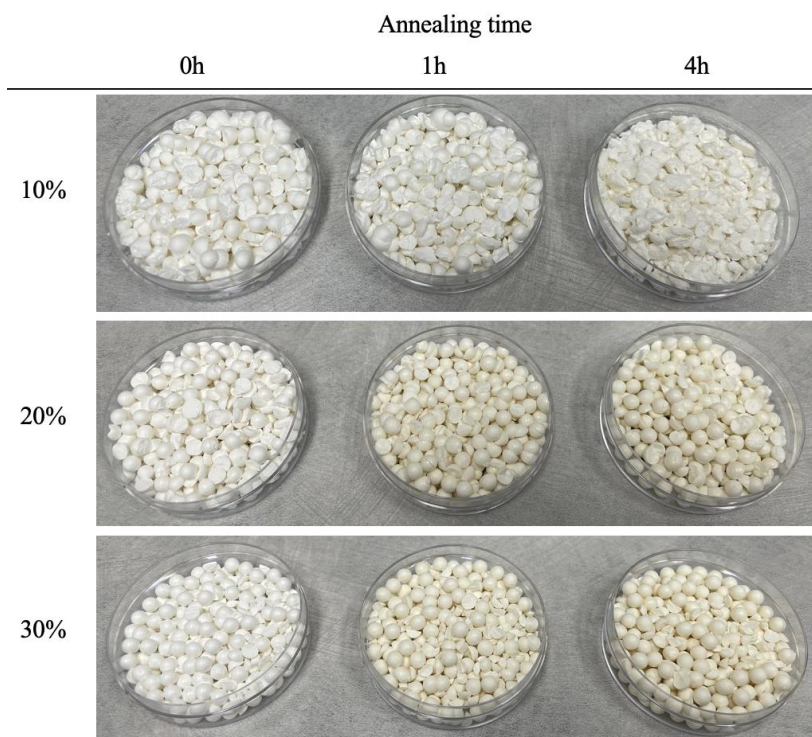
Figure 1: Photographs of freeze-dried pellet directly after freeze-drying.

Water activity

The water activity of the pellets is given in *Table 3*. Overall, the water activity is very low in all pellet formulations. As can be seen, the water activity increases with the annealing time and decreases with increasing amounts of dry matter. The water activity is lowest for the 30% pellets. However, it is quite similar for all samples varying between 0.7 and 2.3 %. As all samples have the same composition in the dry matter, it can be assumed that the water content will follow the same trends as the water activity.

Table 3: The water activity of freeze-dried pellets.

Total dry matter[a] in solution before drying [%]	Annealing time [h]	Water activity
10	0	0.0139
10	1	0.0157
10	4	0.0235
20	0	0.0065
20	1	0.0098
20	4	0.0100
30	0	0.0025
30	1	0.0081
30	4	0.0070

[a] The dry matter consists of 28% cell material and 72% maltodextrin.

Structure of the freeze-dried pellets using SEM

The SEM images of pellet structure at 50X, 200X, and 800X are shown in *Figure 2* and *Figure 3*. The orientation of the overall structure of the pellets is radially oriented from the centre of the pellets, as can be seen from the overview pictures (50X) in *Figure 2*. The clear orientation of the freeze-dried material makes it anisotropic. For the non-annealed pellets with 10% dry matter, the structure is very fine without any large pores or evidence of collapse. Increasing the dry matter content gives an increase in the degree of coarseness of the structure. This is especially evident for the 30% dry matter pellets. Upon annealing the porosity increases. The structure of 10% pellets is especially affected, where the entire pellet seems to have collapsed, while there is no sign of major collapse in the 20% pellets. In the 30% pellet, a microscopic collapse is observed in all the samples, in the form of larger pores.

Figure 2. Overview of SEM images of microspheres at 50X magnification. The panels show pellets with a dry-matter content of 10%, 20%, and 30% respectively.

Figure 3 illustrates the structure at higher resolutions. The non-annealed pellets have a very fine lamella-like structure. The lamellar structures overlap with each other, displaying some visual similarity to fish scales. There is a short ridge-like orthogonal protrusion at one side of each lamellar sheet. As the pellets undergo an annealing process the structures are substantially changed, and the structures become increasingly coarser the longer annealing time pellets undergo. The lamellae also become thicker, and pore-like structures appear. The pore structures dominate at the higher concentrations, where the matrix turns into more spherical pores. The pore-like structures of 30% dry matter annealed for 4 h are similar to the common structure in freeze-drying in vials (Bai Palmkron *et al.*, 2023). It is also observed that the pores are more spherical in the centre and more elongated closer to the surface.
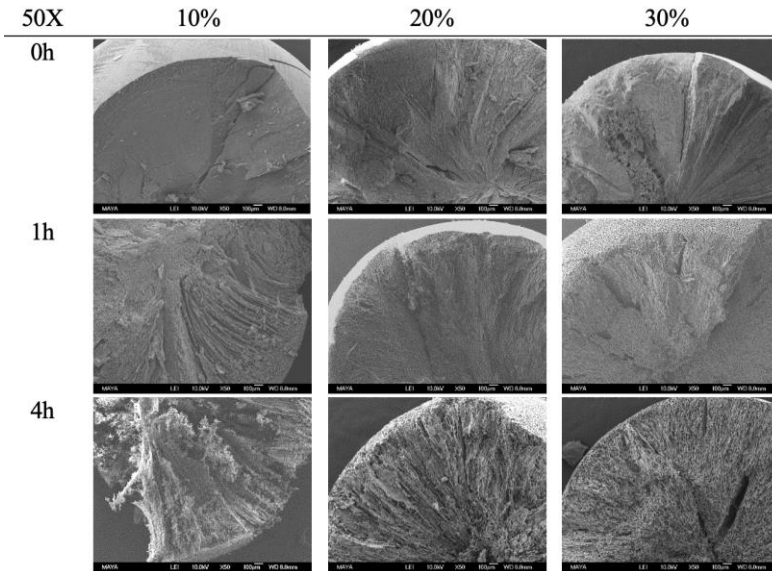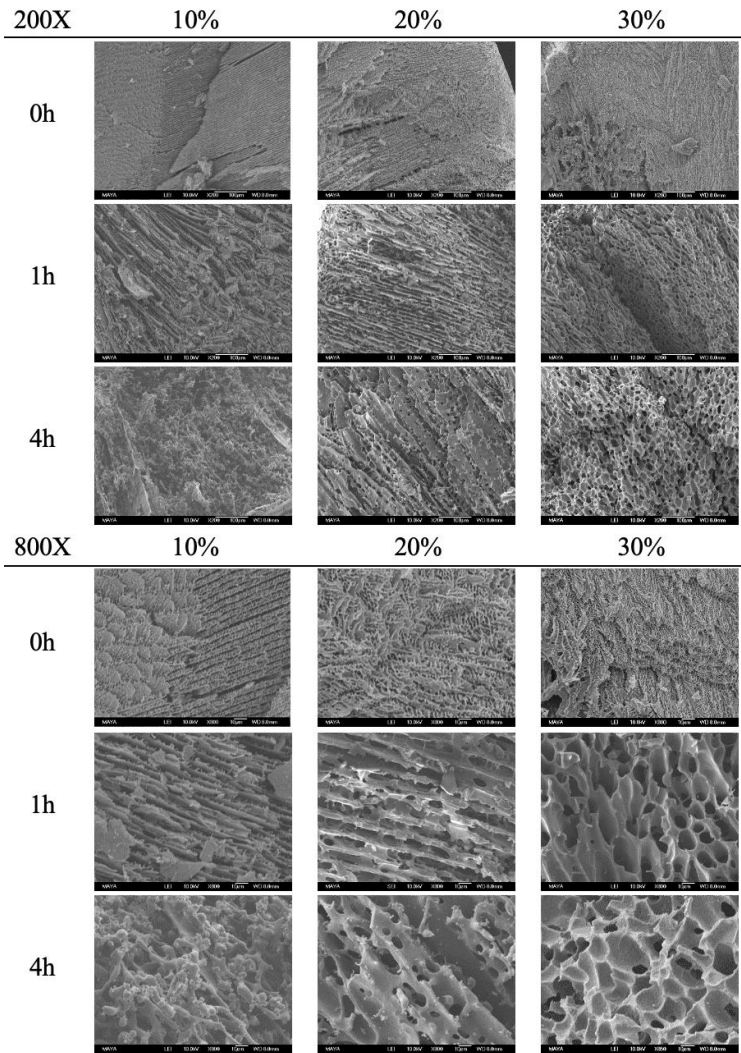
Figure 3. Detailed SEM images of pellets at 200X and 800X magnification. The panels show pellets with a dry-matter content of 10%, 20%, and 30% respectively.
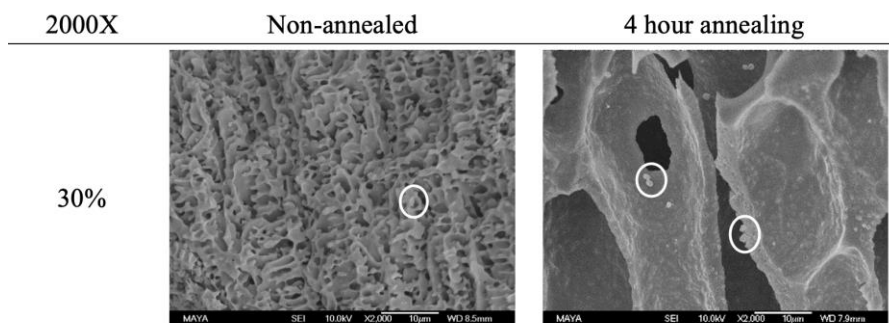
Figure 4. SEM 2000X of freeze-dried pellets. Circles show structures that are likely to be probiotic cells.

The thickness of the structures is relatively constant throughout the pellet, although the material surrounding collapsed domains can exhibit significantly thicker material. The 10% 4h pellets have undergone extensive collapse where the entire lamellar structure is replaced by beads of melted and solidified material, although the overall spherical pellet shape is retained. The 20% 4h shows a more local collapse and pellets with 30% dry matter have a locally collapsed structure regardless of the annealing time. The annealed pellets also show less anisotropy with increasing concentration and annealing time.

The location of the probiotic cells in the freeze-dried materials at a magnification of 2000X is shown in Figure 4. Most of the cells are embedded into the freeze-dried materials, and it can be hard to distinguish between cells within the material and protruding material for the non-annealed pellets. Although some structures appear to be cells based on their dimensions and shape. The cells are more easily located for the annealed samples, where the materials are thicker and the embedded cells can be identified at the fracture surface, especially for samples with higher dry-matter concentration.

X-ray microtomography

µCT was carried out on all the samples. The 10% maltodextrin samples were, however, too fragile and fell apart during the preparation, thus, only the 20 % and 30% samples could be scanned. Non-annealed samples of all formulations, with mainly submicron structures could not be further analysed due to resolution and contrast limitations. All annealed samples at 20% and 30% dry matter gave images that appeared useful for further quantitative image analysis. *Figure 5* shows reconstructed tomography slices. There is a clear contrast between the air and the freeze-dried material, with a good contrast-to-noise ratio. The structures seen are in good agreement with the SEM images revealing a more elongated pore formation

for the 20% pellets than for the 30% ones. This is also evident in the images after water-shedding has been applied, as shown in *Figure S2*.

Figure 6 shows the µCT slices with colour-coded material thickness. The thickness of the material is colour-coded where a more yellowish hue represents thicker material structures, and purple colour represents thinner material structures. It can also be seen that thicker material structures are concentrated around the micro-collapses and at the junctions between different pores.
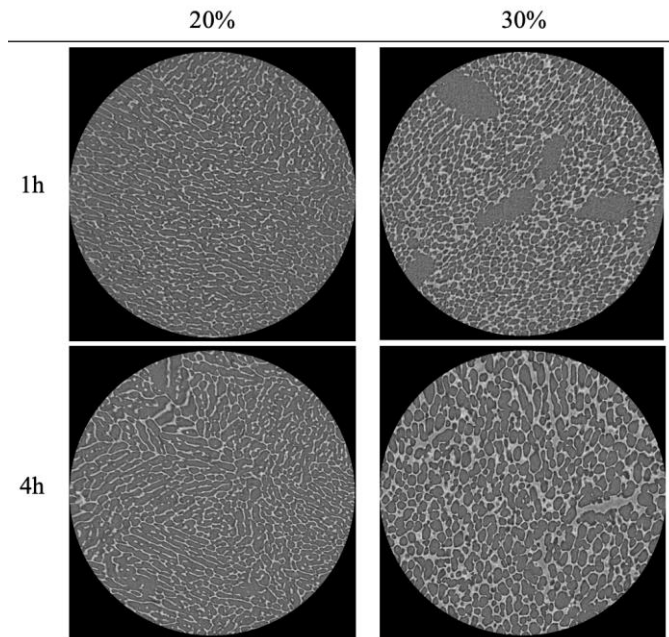
Figure 5. Reconstructed µCT slices for pellets with 20% and 30% dry matter annealed for 1 and 4h.
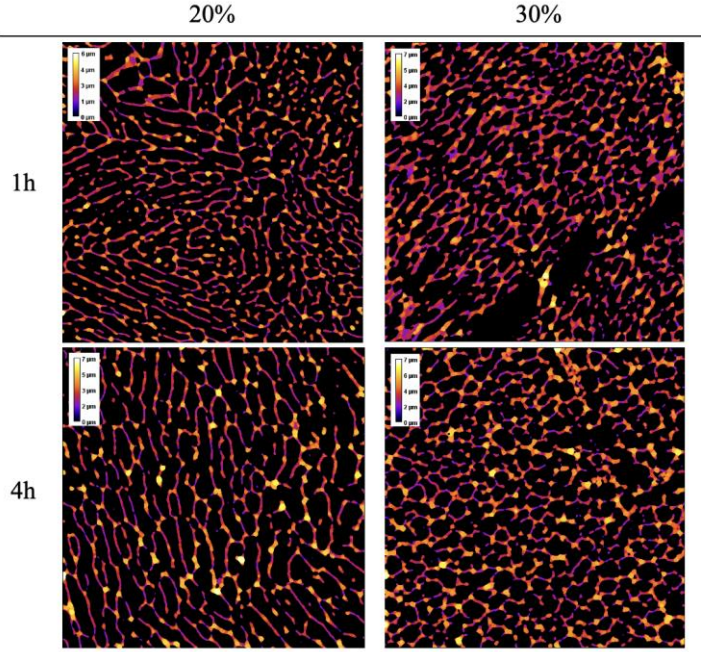
Figure 6. Cropped µCT slices colour-coded with respect to the material thickness using 'local thickness' image analysis carried out in 3D. The materials are coloured according to thickness. Purple colour represents thinner material structures and bright yellow color represents thicker material structures.

The volume distribution of the material thickness is shown in *Figure 7*. The material thickness of each condition displays a symmetric distribution around a mode value. Increasing annealing time as well as increasing dry-matter concentration leads to a thicker material.

14
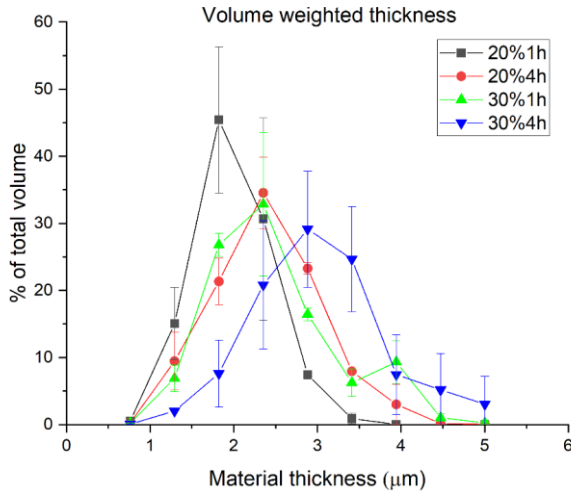
Figure 7. The relative volume-weighted size distribution of the material thickness. 20% 1h (black line) 20% 4h (red line) 30% 1h (Green line) 30% 4h (Blue line) The data set is distributed over 9 size classes with equal width. The curves represent the average of the two replicates and the error bars are the standard deviations between the replicates at each material thickness position.

The average volume-weighted material thickness (Table 4) increases from 2 µm for sample 20% 1h, to 3 µm for sample 30% 4h. The percentage of material that is above 2.5 µm is also presented in table 4, which can be used as an indicator on how well a probiotic cell (1-3 µm) is encapsulated in this material, while sample 20% 1h only have around 8% above 2.5 µm, the thickest sample 30% 4h have around 70% of its material above 2.5 µm.

Table 4. Averages and mode values of the volume-weighted distributions (eq. 2) of pore diameter and material thickness in annealed pellets. The results are an average of the two batches given the standard deviation between them.

	20% 1h	20% 4h	30% 1h	30% 4h
Average pore diameter d (4,3)	23.4 ± 0.9µm	28.2 ± 0.7 µm	32.4 ± 6.4 µm	26.2 ± 0.7 µm
Mode value of pore size. (figure 7)	22.6 ± 0.1 µm	28.0 ± 0.0 µm	19.5 ± 0.1 µm	26.5 ± 0.1 µm
volume in pores above 40 µm	2.5 ± 1.5%	8.0 ± 0.3%	23.0 ± 8.9%	4.5 ± 1.2%
Volume-weighted average material thickness	2.0 ± 0.1 µm	2.4 ± 0.1 µm	2.5 ± 0.1 µm	3.0 ± 0.3 µm
Mode value of thickness	1.8 µm	2.4 µm	2.4 µm	2.9 µm
volume with material thickness above 2.5 µm	8.4% ± 1.0%	34.4% ± 1.7%	33.3% ± 5.0%	69.5% ± 10.0%
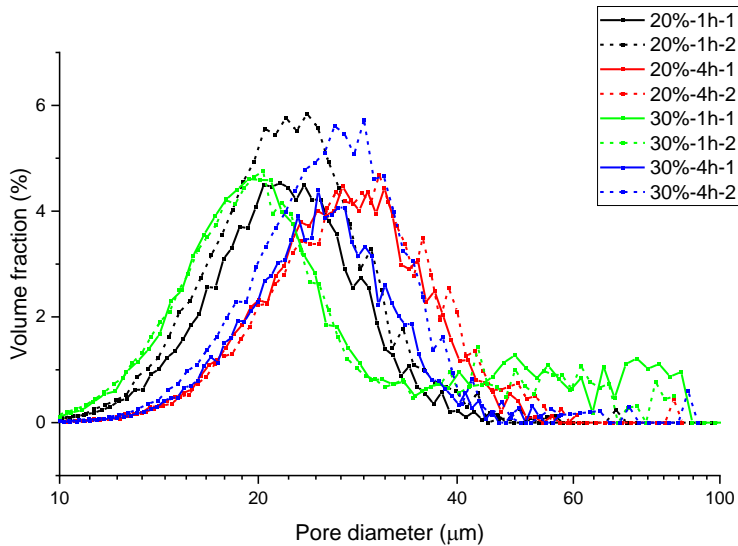
Figure 8. Volume-weighted distribution of the pore diameter as quantified from water-shedding. Batch 1 is represented as solid lines, batch 2 dashed lines. 20%1h (black lines) 20%4h (red lines) 30%1h (Green lines) 30%4h (Blue lines). The volume fractions are distributed over 50 size classes. The width of each class is scaled logarithmically.

The pore size distribution of the pellets is shown in Figure 8. It can be seen that all samples are characterized by a rather symmetric and sharp peak in a range between 20 and 30 µm. The 30% 1h pellet has the smallest pores and a narrow pore size distribution, followed by the 20% 1h sample. The two 4-hour annealed samples have slightly larger pore sizes and a broader pore size distribution.

It can further be observed that the 1h annealing, 30% sample has a tailing of quite large pores (up to 100 µm) indicating the micro-collapse in these samples, the average pore diameter (d 4,3) presented in Table 4 shows that these sample is comparably large compared to the other samples which also indicates the high frequency of collapse. The mode values demonstrate that the most prevalent pore size remains unaffected by micro-collapse.

16

Discussion

The expected trajectory of the frozen formulation containing maltodextrin and water through the state diagram is illustrated in Figure 9 The rapid cooling is expected to lead to very fine structures with smaller pores compared to freeze-drying in vials, typically around 50 µm (Bai Palmkron et al., 2023). The rapid freezing method gives rise to initially small ice crystals due to the fast freezing and also prevents water to diffuse from the freeze-concentrate to the ice crystals and leads to incomplete freezing of the available water before the temperature drops below the Tg (Roos & Drusch, 2016). The pellets were stored at -80°C after the initial freezing. During this storage time, it can be expected that the frozen liquid adapts to the Tg line leading to the growth of the initial ice crystals extracting the water from the freeze-concentrate (moving from E to F in Figure 9). This process is termed relaxation following the nomenclature and interpretations by Nakagawa et al (Nakagawa et al., 2018). The extent of the relaxation process is expected to develop further when the non-annealed pellets are transferred to the pre-cooled freeze dryer at -40°C and the freeze-drying conducted at the drying temperature to about -32°C (30 Pa vapour pressure).

The annealing process occurs by maintaining the temperature of the sample between Tg' and Tm', this allows for movement of material and structural changes. The process encourages larger ice crystals to grow while the small crystals shrink and disappear, this process is driven by Ostwald ripening, and is heavily dependent on particle size, with the ice-crystal growth rate being proportional to d^{-3} (Kharatyan *et al.*, 2022; Lifshitz & Slyozov, 1961) Therefore the effects of annealing is more evident in samples with small ice crystals such as quenched pellet compared to samples with large ice crystals such as samples frozen slowly. The Ostwald ripening has no net increase in ice content and should be distinct from the relaxation process.

Due to the temperature gradient formed when the pellet is dripped into liquid nitrogen (directional cooling) the crystallization of ice will occur in the direction towards the centre and form a radial structure that is characteristic of the quenched frozen pellets. Similar radial structures have been observed in sprayed quench frozen samples (Osanlóo *et al.*, 2022).
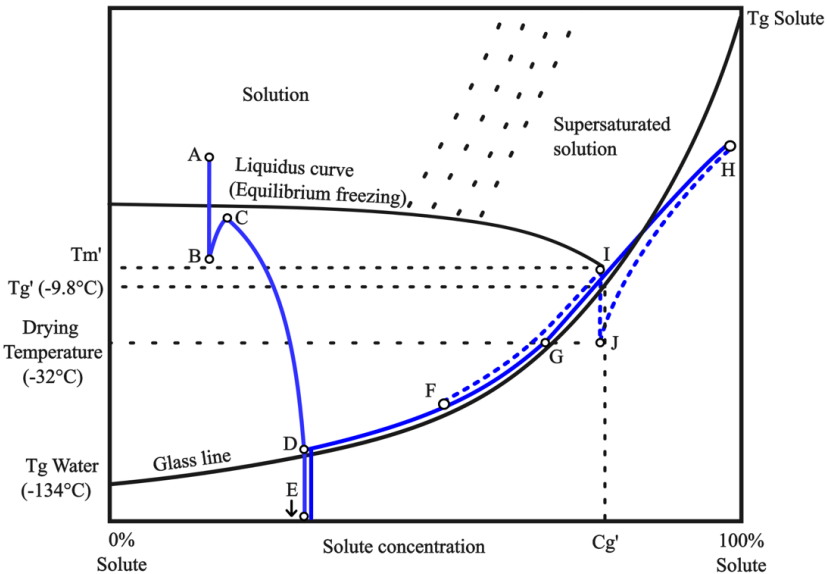
Figure 9. State diagram of maltodextrin and water. Modified after Palmkron et al (6). The pellet freezing and freeze-drying trajectory is shown in a blue solid line, the dotted line depicts the trajectory of annealed pellets. The pellet is created by placing a liquid sample (A) in contact with liquid nitrogen. The pellet undergoes undercooled freezing (B), where ice nucleation/crystallization creates a two-phase system composed of ice crystals and freeze concentrate. the nucleation releases heat and the local temperature rises to C. All heat is rapidly consumed by the liquid nitrogen and further crystallization concentrates the freeze concentrate while it is rapidly cooled down to position D when the remaining freeze-concentrate converts into a stable glassy state and further ice formation is stopped. The final temperature is reached at point E. Subsequently, the samples are stored at -80°C, allowing the freeze concentrate to undergo relaxation, releasing water to ice crystals until reaching equilibrium at point F. Annealing is performed (at the position I) resulting in a composition of the glassy state corresponding to Cg'. The freeze-drying occurs at -32°C, potentially leading to additional relaxation to point G for the non-annealed pellets. Notice the difference in the drying starting position between annealed(J) and non-annealed pellets (G). After the ice has been evaporated, the sample is further dried to the stable position H.

The structure of a freeze-dried material is to a large extent determined by the ice structure in the frozen formulation before the drying (Nakagawa *et al.*, 2018). For the non-annealed pellets, the dimensions of the pores are around 1-5 µm with a material thickness of <1 µm. Unfortunately, these structures were not possible to characterize quantitatively using lab-based µCT. The changes in the ice crystal structure during annealing are reflected in the dried pellets. The shape of the pores changes from lamella-like thin structures to more spherical structures. The size of the pores increases to 20-30 µm and material thickness to 2-3 µm.

There are different reasons for and types of collapses. The extensive collapse for non-annealed freeze-dried pellets shown in the work by Ekdawi-Sever et al is due to insufficient relaxation (Ekdawi-Sever *et al.*, 2003), a non-relaxed quenched pellet has small ice crystals and a high proportion of freeze concentrate with low Tg. This results in an unstable material that causes a global and extensive collapse during drying. Other reasons for collapse are due to high mass transport resistance, which

18

can occur for samples with small pores leading to high tortuosity, for samples with high solute concentration, or a combination of both. The high mass transfer resistance leads to an increase in temperature due to the increased pressure at the sublimation front. The increase in temperature can cause the material to reach a softer rubber state that may have insufficient mechanical strength to keep the structures stable (Bjelošević *et al.*, 2018) . This is evident in all samples at 30% solute concentrations. Collapse can also occur due to extensive annealing of samples with low solute concentration, where there is not enough material to maintain a continuous network, leading to breakdown of the pellet structure. This is shown in the 10%4h sample, where a global collapse is evident.

Conclusions

This paper shows how the microstructure formed after freeze-drying in quench frozen pellets can be efficiently evaluated using tomography. The effects of solute concentration and annealing processes have been assessed. The results show that freeze-drying of quench frozen pellets may lead to very thin material structures with the thickness dimension, around 1 µm, comparable to the dimensions of bacterial cells. Annealing at a temperature just above Tg' results in a uniform pore structure and thicker material structures where bacterial cells can be well encapsulated. It is also shown that the material thickness increases with increasing solute concentration and annealing time.

Collapse was observed for samples with low solute concentrations and long annealing time (10%, 4h) and all samples with high solute concentrations (30%). Samples with a solute concentration of 20% showed a uniform, intact structure at all annealing conditions. The ability to obtain freeze-dried material with different material thicknesses presents future possibilities to assess the impact of material thickness on the stability of freeze-dried probiotic products.

References

Bai Palmkron, S., Bergenståhl, B., Håkansson, S., Wahlgren, M., Fureby, A. M., & Larsson, E. (2023). Quantification of structures in freeze-dried materials using X-ray microtomography. *Colloids and Surfaces A: Physicochemical and Engineering Aspects, 658*. doi:10.1016/j.colsurfa.2022.130726

Bjelošević, M., Seljak, K. B., Trstenjak, U., Logar, M., Brus, B., & Ahlin Grabnar, P. (2018). Aggressive conditions during primary drying as a contemporary approach to optimise freeze-drying cycles of biopharmaceuticals. *European Journal of Pharmaceutical Sciences, 122*, 292-302. doi:https://doi.org/10.1016/j.ejps.2018.07.016

Chitu, T., Vessot, S., Peczalski, R., Andrieu, J., Woinet, B., & Françon, A. (2015). Influence of Operating Conditions on the Freeze-Drying of Frozen Particles in a Fixed Bed and Modeling Data. *Drying Technology, 33*(15-16), 1892-1898. doi:10.1080/07373937.2015.1066386

Ekdawi-Sever, N., Goentoro, L. A., & Pablo, J. J. D. (2003). Effects of Annealing on Freeze-Dried Lactobacillus acidophilus. *Journal of Food Science, 68*(8), 2504-2511. doi:10.1111/j.1365-2621.2003.tb07052.x

Erber, M., & Lee, G. (2015). Development of cryopelletization and formulation measures to improve stability of Echis carinatus venum protein for use in diagnostic rotational thromboelastometry. *Int J Pharm, 495*(2), 692-700. doi:10.1016/j.ijpharm.2015.09.038

Foerst, P., Melo de Carvalho, T., Lechner, M., Kovacevic, T., Kim, S., Kirse, C., & Briesen, H. (2019). Estimation of mass transfer rate and primary drying times during freeze-drying of frozen maltodextrin solutions based on x-ray μ-computed tomography measurements of pore size distributions. *Journal of Food Engineering, 260*, 50-57. doi:https://doi.org/10.1016/j.jfoodeng.2019.05.002

Fonseca, F., Girardeau, A., & Passot, S. (2021). Freeze-Drying of Lactic Acid Bacteria: A Stepwise Approach for Developing a Freeze-Drying Protocol Based on Physical Properties. *Methods Mol Biol, 2180*, 703-719. doi:10.1007/978-1-0716-0783-1_38

Fonseca, F., Passot, S., Lieben, P., & Marin, M. (2004). Collapse temperature of bacterial suspensions: the effect of cell type and concentration. *Cryo Letters, 25*(6), 425-434.

Hilmer, M., Gruber, S., & Foerst, P. (2020). Development of a Freeze-Drying Stage for In-Situ μ-CT Measurements. *Processes, 8*(7). doi:10.3390/pr8070869

Izutsu, K. I., Yonemochi, E., Yomota, C., Goda, Y., & Okuda, H. (2014). Studying the morphology of lyophilized protein solids using X-ray micro-CT: Effect of post-freeze annealing and controlled nucleation. *AAPS PharmSciTech, 15*(5), 1181-1188.

Kasper, J. C., & Friess, W. (2011). The freezing step in lyophilization: physico-chemical fundamentals, freezing methods and consequences on process performance and quality attributes of biopharmaceuticals. *Eur J Pharm Biopharm, 78*(2), 248-263. doi:10.1016/j.ejpb.2011.03.010

Kharatyan, T., Gopireddy, S. R., Ogawa, T., Kodama, T., Nishimoto, N., Osada, S., Scherließ, R., & Urbanetz, N. A. (2022). Quantitative Analysis of Glassy State Relaxation and Ostwald Ripening during Annealing Using Freeze-Drying Microscopy. *Pharmaceutics, 14*(6). doi:10.3390/pharmaceutics14061176

Liapis, A. I., & Bruttini, R. (2009). A mathematical model for the spray freeze drying process: The drying of frozen particles in trays and in vials on trays. *International Journal of Heat and Mass Transfer, 52*(1), 100-111. doi:https://doi.org/10.1016/j.ijheatmasstransfer.2008.06.026

Lifshitz, I. M., & Slyozov, V. V. (1961). The kinetics of precipitation from supersaturated solid solutions. *Journal of Physics and Chemistry of Solids, 19*(1), 35-50. doi:https://doi.org/10.1016/0022-3697(61)90054-3

Nakagawa, K., Tamiya, S., Sakamoto, S., Do, G., & Kono, S. (2018). Observation of Microstructure Formation During Freeze-Drying of Dextrin Solution by in-situ X-ray Computed Tomography. *Front Chem, 6*, 418. doi:10.3389/fchem.2018.00418

Olbrich, C., Plitzko, M., Luy, B., & Schneid, S. C. T. (2017). World Intellectual Property Organization Patent No.

Osanlóo, D. T., Fransson, J., Bergenståhl, B., & Millqvist-Fureby, A. (2022). Effects of drying methods on physical properties and morphology of trehalose/mannitol mixtures. *Drying Technology, 41*(4), 503-522. doi:10.1080/07373937.2022.2103564

Pikal, M. J., & Shah, S. (1990). The collapse temperature in freeze drying: Dependence on measurement methodology and rate of water removal from the glassy phase. *International Journal of Pharmaceutics, 62*(2), 165-186. doi:https://doi.org/10.1016/0378-5173(90)90231-R

Pisano, R., Barresi, A. A., Capozzi, L. C., Novajra, G., Oddone, I., & Vitale-Brovarone, C. (2017). Characterization of the mass transfer of lyophilized products based on X-ray micro-computed tomography images. *Drying Technology, 35*(8), 933-938. doi:10.1080/07373937.2016.1222540

Roos, Y. H., & Drusch, S. (2016). *Phase Transitions in Foods: Second Edition*. San Diego: Academic Press.

Tang, X., & Pikal, M. J. (2004). Design of Freeze-Drying Processes for Pharmaceuticals: Practical Advice. *Pharmaceutical Research, 21*(2), 191-200. doi:10.1023/B:PHAM.0000016234.73023.75

Trelea, I. C., Passot, S., Marin, M., & Fonseca, F. (2009). Model for Heat and Mass Transfer in Freeze-Drying of Pellets. *Journal of Biomechanical Engineering, 131*(7). doi:10.1115/1.3142975

Vanbillemont, B., Lammens, J., Goethals, W., Vervaet, C., Boone, M. N., & De Beer, T. (2020). 4D micro-computed x-ray tomography as a tool to determine critical process and product information of spin freeze-dried unit doses. *Pharmaceutics, 12*(5).

Wang, W. (2000). Lyophilization and development of solid protein pharmaceuticals. *International Journal of Pharmaceutics, 203*(1), 1-60. doi:https://doi.org/10.1016/S0378-5173(00)00423-3

Supplementary Information
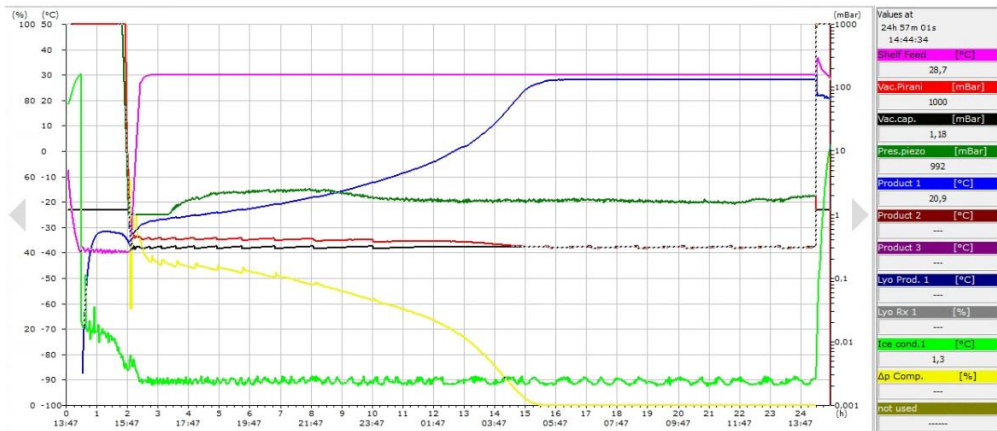
Figure S1. Freeze-drying cycle
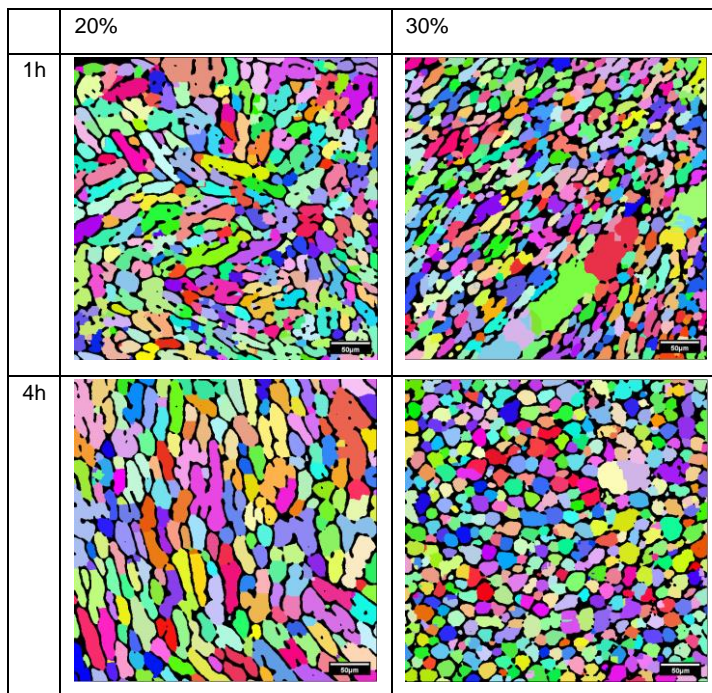
Figure S2. µCT slices after 'water shedding' was carried out in 3D using the Scikit-image Python package. Each coloured domain corresponds to a detected pore and will be used in image analysis pipeline for quantifying a set of pore parameters. Thinner material or missing material structures can be detected using the water-shedding procedure, and pores can be separated.

Paper IV

The impact of annealing methods on the encapsulating structure and storage-stability of freeze-dried pellets of probiotic bacteria

Shuai Bai Palmkron[1]*, Björn Bergenståhl[1], Stephen Hall[6,7], Sebastian Håkansson[2,3], Marie Wahlgren[1], Emanuel Larsson[5,6], Anna Millqvist Fureby[1,4]

[1] Department of Process and Life Science Engineering, Division of Food and Pharma Lund University, 221 00 Lund, Sweden

[2] Division of Applied Microbiology, Department of Chemistry, Lund University, 221 00 Lund, Sweden

[3] BioGaia AB, 241 38 Eslöv, Sweden

[4] Chemical process and pharmaceutical development, RISE Research Institutes of Sweden, Stockholm, Sweden

[5] Department of Experimental Medical Science, Lund University, 221 00 Lund, Sweden

[6] LUNARC, Lund University, Box 118, 221 00 Lund, Sweden

[7] Division of Solid Mechanics, Department of Construction Sciences, Lund University, Lund, 22100, Sweden

* Corresponding author

Abstract

This paper aims to evaluate the importance of the material thickness of freeze-dried pellets on the storage stability of the encapsulated bacteria, focusing on the influence of annealing on structure and storage stability. The structure was investigated using SEM and quantified using X-ray microtomography. The different annealing protocols give rise to a range of material thicknesses, where more extensive annealing results in a thicker material. The storage stability showed a strong correlation with the material thickness, where thicker material due to annealing or collapse resulted in greater storage stability. Different degrees of relaxation for the non-annealed pellets resulted in large deviations in structure and storage stability and demonstrated the impracticality of avoiding annealing for quenched samples. The benefits of applying extensive annealing are therefore both to increase the storage stability of the probiotic product and to gain control of the freeze-drying process to ensure a homogenous and reproducible product.

Introduction

Pellets are one of the most used formats of industrial freeze-drying for probiotics. However, most scientific studies on the freeze-drying of probiotics are carried out using vials or trays (Badal Tejedor *et al.*, 2020; Bagad *et al.*, 2017; Béal & Fonseca, 2015; Champagne *et al.*, 1996; Fonseca *et al.*, 2015; Giulio *et al.*, 2005). There are important differences, between the freeze-drying of pellets and vials, in freeze-drying performance, as well as in the structure of the freeze-dried material (Bai Palmkron *et al.*, 2023a). One principal aspect is that the quenching of pellets in liquid nitrogen results in small ice crystals with a fine structure and non-equilibrium freezing that results in a freeze concentrate with low T_g (Bai Palmkron *et al.*, 2023b), while the comparably slow cooling inside a freezer or freeze-dryer results in a much coarser structure (Bai Palmkron *et al.*, 2023a). The different freezing methods also exert very different kinds of stress on the bacteria (Béal & Fonseca, 2015). The structure of ice crystals in the frozen pellet affects the final structure of the freeze-dried product. One way of modifying the ice structure in a sample is to expose the sample to a temperature between the glass transition temperature and the freezing point, a so-called annealing process. Annealing allows larger ice crystals to grow while the smaller crystals shrink and disappear, the process is usually termed Ostwald ripening. Factors that increase the rate of annealing are short distances between ice crystals, large surface area from which the water molecule can diffuse, and high Laplace pressure (Kharatyan *et al.*, 2022). A sample with small ice crystals has a short distance between each other, a large surface, and high Laplace pressure. The Ostwald ripening is therefore especially efficient for quenched pellets with small ice crystals. However, the effects of annealing are more

limited in vial freezing as the ice crystals after crystallization already are comparatively large, and thus the kinetics of the process are slow (Bai Palmkron *et al.*, 2023a; Ekdawi-Sever *et al.*, 2003).

The heat transfer in vial freeze-drying primarily originates from the heat conduction from the shelf through the bottom of the vial (about 60-70 %) (Bai Palmkron *et al.*, 2022), while the heat transfer for pellets is solely through radiation. A pellet formulation also has a significant increase in surface area per volume exposed to the vacuum, which facilitates mass transfer. The lack of conductive heat transfer allows for a significant increase in the shelf temperature, while the temperature at the sublimation front remains controlled by the pressure (which prevents collapse during drying) and results in more efficient drying. After freeze-drying, the cells are encapsulated in a protective material often consisting of an amorphous non-reducing sugar, that protects the cell membrane integrity (Santivarangkna *et al.*, 2008), and a longer oligomer/polymer such as maltodextrin to increase the stability during storage. The hypothesis for this paper is that the thickness of the encapsulating material has an impact on protecting the cells from oxidative stress (Bai Palmkron *et al.*, 2023b). This is based on that sugars in a glassy state provide a good barrier towards oxygen and act as a buffering material for the humidity (Roos & Drusch, 2016; Santivarangkna *et al.*, 2011). A thicker protective material is also expected to be less sensitive to structural movements during storage. Thus, we expect to observe that thicker material structures provide better protection of the cells and provide a slower loss of viability during storage. The material thickness was measured using X-ray microtomography (µCT) and scanning electron microscope (SEM).

To evaluate the storage stability of bacteria in formulations that have different structures, three different protocols were designed;1) anneal the sample under "aggressive and fast" conditions, 2) anneal under mild and slow conditions, and 3) compared with a reference condition without annealing. To compare the impact of oxygen on storage stability, the pellets were stored in plastic canisters permeable to oxygen and containing a desiccant and in aluminum vacuum bags that act as an oxygen barrier.

Materials and methods

Fermentation

The fermentation of *Limosilactobacillus reuteri* DSM 17938 was performed in two 1L Multifors-bioreactors (Infors HT, Switzerland) and monitored using eve® software (Infors HT, Switzerland). The bioreactors were cooled down to 10°C and inoculated with 10 ml preculture provided by BioGaia (Eslöv, Sweden), the temperature was then ramped up to 37 °C. MRS broth (GranuCult, Millipore) was

used as a growth medium, and the pH was maintained stable at 5.5 using 3M KOH. The base consumption was used to monitor the growth of the cells and the program was stopped when the pH became stable (after approx. 9h). The fermentation was performed without aeration and a stirrer speed of 250 RPM.

Formulation and production of pellets

The content of the two reactors was pooled after fermentation and the number of viable cells was counted using a flow cytometer CytoFLEX (Beckman Coulter, US). It resulted in a final concentration of $1.9 \cdot 10^9$ cells/ml. The number of viable cells was used to obtain the desired viable cell concentration in the formulations. Further, the sample was centrifuged and washed with phosphate buffer saline solution. A formulation was created with a total dry matter of 20 % (w/w) consisting of 2/3 sucrose (for molecular biology, Sigma-Aldrich) and 1/3 maltodextrin 9 (hydrolyzed potato starch, dextrose equivalent 8-10, from Roquette, France). The formulation was mixed with the cells to obtain a final concentration of $2 \cdot 10^{11}$ cells/ml. The suspension was then pumped using a peristaltic pump at 20 ml/min and quenched by dripping it into liquid nitrogen. The pellets were spherical and ranged from 4-5 mm in diameter. The time between mixing the formulation with the cells and the freezing was kept short (less than 15 minutes). The obtained pellets were directly transferred and stored in a -80°C freezer. For the annealing process, the pellets were divided into three equal parts; whereas one underwent an annealing process at -20 ± 0.5°C in a freezer for a week (to emulate an industrial storage situation), another part underwent a quick annealing process at -9°C for 2h, and the last part remained at -80°C and did not undergo any annealing process (referred to as non-annealed). After the different annealing processes, all the pellets were stored in a -80°C freezer until freeze-drying.

Freeze-drying of pellets

Both batches of prepared frozen pellets were loaded into aluminum cups and suspended inside an Epsilon 2-6D LSC plus Freeze dryer from Martin Christ equipped with Pirani, piezo, and capacitance pressure sensors (Germany) that had been pre-cooled to -30°C. The loading of the pellets into the freeze dryer from the -80° C freezer took approximately 10-15 min per batch and as a result, Batch 1 of the pellet was subjected to -30°C for a longer time compared to Batch 2. Once the pellets were loaded, the pressure inside the chamber was decreased to 30 Pa. When the desired pressure was reached, the shelf temperature was increased to 20°C at a rate of 4.5°C/min. There was no distinction between the primary and secondary steps. Instead, the entire drying process was performed under the same conditions. The end of the drying process was determined to be at 18h after the time point when the Pirani and capacitance sensors showed identical pressure readings.

4

Determination of glass transition temperature, water content, and water activity

The glass transition temperature of maximally freeze concentrated solution (Tg') of 2/3 sucrose, and 1/3 maltodextrin with a total dry weight of 20% (w/w) was analyzed using differential scanning calorimeter DSC (Mettler Toledo, Switzerland). Triplicates of 10 mg material were sealed in 40 µl aluminum pans. The samples were cooled to -70°C at a rate of 10°C/min, followed by a 5-minute equilibration and a subsequent heating step to 30°C at the same rate. The Tg' were determined using STARe Software according to ISO standard (ISO 11357–2:1999).

The water content of the dried pellets was analyzed directly after freeze-drying. The measurements were performed using Thermogravimetric analysis (TGA) with a TA Q500 (TA Instruments, New Castle, DE, USA). 2-3 crushed pellets from each batch were loaded onto an open platinum pan, and the temperature was then increased from 25°C to 200°C at a heating rate of 10°C/min. The weight decrease was recorded from 25°C to 125°C to avoid the inclusion of water released due to Maillard and caramelization reactions.

Water activity was measured at the same time point as the storage stability using a Rotronic HC-2 Water activity probe (PST, Ely, UK), measurements below 0.01 are denoted as <0.01 as values below this level are regarded inaccurate. All measurements are done with intact pellets without any signs of visible collapse or cracks.

Freeze-drying survival and storage stability

Freeze-drying survival was examined directly after harvesting the pellets from the freeze-dryer. 1 g of pellets were first dissolved in MRS broth and then diluted and plated using an automatic plater Easy spiral dilute (Interscience, France) on MRS agar and incubated at 37°C for 48 h. The CFU was counted using a scan 500 colony counter (Interscience, France) and compared to the initial cell concentration (defined using a flow cytometer). An accelerated stability study was conducted at 37°C and 75% RH. All pellets (including pellets with cracks and visual collapse) were divided into equal parts approximately 1g per sample and stored in plastic canisters with a drying agent (silica gel) and in vacuum-sealed aluminum bags. The storage stability was determined by analyzing CFU at each time point with freeze-drying survival as the reference point. Five time points were investigated for pellets stored in canisters, where a new canister was evaluated for each time point. The time points investigated were 7, 14, 28, and 56 days. Vacuum-sealed bags were investigated at 28 and 56 days.

The half-life of the bacteria was estimated from the viability data assuming exponential decay over the observation time:

$$C(t_{end}) = C(t_{start})e^{-\frac{t_2-t_1}{\lambda(t_m)}} \qquad\qquad [1]$$

$$\lambda(t_m) = \frac{t_{end}-t_{start}}{\ln(C(t_{start}))-\ln(C(t_{end}))} \qquad\qquad [2]$$

$$t_{1/2} = \frac{\ln(2)}{\lambda(t_m)} \qquad\qquad [3]$$

Where $C(t)$ is the number of viable bacteria (per gram) at time t, t_{start} and t_{end} are the starting and ending times of the observation period, and t_m is the average of the observation period. $\lambda(t)$ is the decay constant. The decay constant is assumed to depend on factors such as water activity, structural changes, diffusive equilibration processes etc.

Scanning electron microscopy

One intact pellet without any visible sign of collapse or cracks from each preparation protocol and batch was selected for scanning electron microscopy (SEM) analysis. The pellets were carefully divided into halves using a razor blade. The divided samples were then fixed to a sample holder and sputtered with a layer of gold-palladium (in a 60:40 ratio) with an expected film thickness of 9 nm. The pellets were investigated using a SEM microscope (JEOL JSM-6700F, Tokyo, Japan). 50x, 200x, and 800x magnification were used to study the pellet's structure. Additionally, a higher magnification of 2000x was used to investigate the bacteria embedded in the material.

X-ray microtomography

The X-ray microtomography (μCT) was performed on Zeiss Xradia Versa 520 (Zeiss, Heidelberg, Germany). One annealed pellet with no sign of macroscopic collapse or cracks was selected from each batch and condition. The selected samples were cut into ¼ wedges using a razor blade. The samples were then securely wedged into 200 μl pipette tips. The tips were sealed with parafilm to prevent moisture absorption. An overview scan of 1920μm x 1920μm x 1920μm and a local zoomed-in scan of 614μm x 614μm x 614μm were conducted on the top half of the wedge. The scanning parameters used are presented in Table 1. The image analysis follows the previously established methodologies addressed in (Bai Palmkron *et al.*, 2023a; Bai Palmkron *et al.*, 2023b).

Table 1: Parameters used for the µCT.

	Overview scan (2µm pixel size)	Local scan (0.64µm pixel size)
Source voltage	80 kV	80 kV
Source current	87uA	87uA
Source power	7W	7W
Exposure time per projection	0.3 s	3.0 s
Number of projections	1601	3201
Zoom (Lens)	4x	20x
Source to sample distance	9.03mm	9.03mm
Sample to detector distance	21.4mm	9.81mm
Effective pixel size	2.00µm	0.64µm

The greyscale image obtained from the tomography was treated with a 3D median filter of 4x4x4 pixels followed by a standard grey-level thresholding. Further quantitative image analysis was performed using the Python software package PoreSpy (porespy.org) to calculate the material thickness (referred to as local thickness) of the freeze-dried material. In PoreSpy, the local thickness procedure inscribes a number of 'blobs' with a diameter corresponding to the material thickness in the material. The counts of the blobs were presented as a frequency distribution, indicating the number of blobs at each diameter. However, the objective is to understand the distribution of the material thickness rather than a number of blobs. To accomplish this, the number distribution was transformed into a volume-weighted distribution.

The volume-weighted average of the material thickness is calculated from the volume-weighted average of the measuring 'blobs'.

$$d_{vol} = \frac{\int_0^V d\,dV}{\int_0^V dV} \approx \frac{\sum_{j=1}^J d_j V_j}{\sum_{j=1}^J V_j} \qquad [4]$$

Where d_{vol} is the material thickness, V is the volume of all material in the analyzed 3D volume. d_j is the diameter of the blobs. The volume-weighted average thickness is obtained from the blobs in each class j counted over J classes. V_j is the total volume of all particles in class j.

Results

Appearance after freeze-drying

The appearance of the pellets is shown in *Figure 1*. There were no noticeable changes in volume before and after freeze-drying. The annealed pellets displayed a more yellowish surface and were less fragile compared to the non-annealed. There was no sign of macroscopic collapse or pellet-to-pellet variation within the protocols except for the non-annealed pellets in Batch 2. Around 1/3 of the pellets in this batch had visual signs of collapse, where some of the pellets showed observable bubbles and cavities and a more uneven and shinier surface.
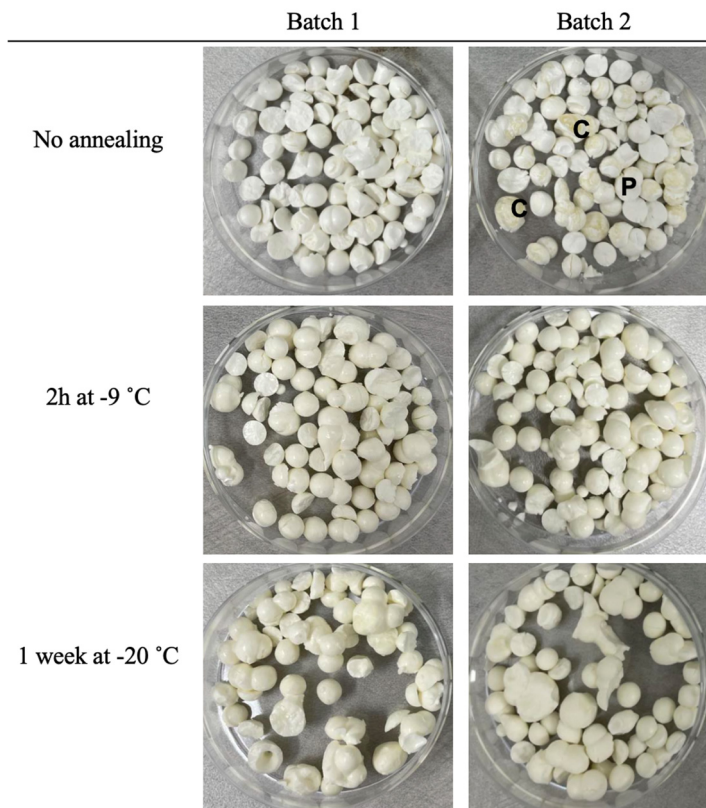

Figure 1: Appearance of freeze-dried pellets. Notice the difference between the non-annealed batches, where Batch 2 has significantly more collapse indicated by observable bubbles and cavities and a more uneven and shinier surface. C indicates visually collapsed, and P indicates visually intact pellets, respectively.

Water content, glass transition temperature and water activity

The water content and activity of the pellets are presented in *Table 2*. The results show that the water content of the dried pellets was 3.5 to 4.0%. There was a larger deviation for the non-annealed samples, while the annealed samples had a more consistent water content.

Table 2: The water content and water activity (during storage) for the individual batches.

Sample		Water content Day1 (%)	Water activity Day 1	Water activity Day 28	Water activity Day 56
Non-annealed (Canister)	Batch 1	3.3	0.029	<0.01	<0.01
	Batch 2	3.9	0.03	<0.01	<0.01
2 hour at -9°C (Canister)	Batch 1	3.6	0.027	<0.01	<0.01
	Batch 2	3.4	0.028	<0.01	<0.01
1 week at -20°C (Canister)	Batch 1	3.9	0.031	<0.01	<0.01
	Batch 2	4.0	0.031	<0.01	<0.01
Non-annealed (Vacuum-bag)	Batch 1	3.3	0.029	0.026	0.034
	Batch 2	3.9	0.03	0.056	0.081
2 hour at -9°C (Vacuum-bag)	Batch 1	3.6	0.027	0.037	0.042
	Batch 2	3.4	0.028	0.021	0.036
1 week at -20°C (Vacuum-bag)	Batch 1	3.9	0.031	0.037	0.042
	Batch 2	4.0	0.031	0.033	0.046

The onset of the glass transition temperature, Tg' for the formulation 20% (w/w) consisting of 2/3 sucrose and 1/3 maltodextrin was determined to be -25°C and the onset of the melting temperature, Tm, at -9°C. Due to the interference from the cells in the formulation, the glass transition temperature of the freeze-dried pellets could not be experimentally determined.

The water activity for all samples directly after freeze-drying was low at around 0.03. For the subsequent time points, the pellets stored in canisters with a drying agent had a water activity below 0.01 and were thus, too low to be measured accurately. The water activity for pellets stored in vacuum-sealed bags remained in a measurable range and increased over time. The water activity is presented in *Table 2*. It can be observed that the non-annealed pellets from Batch 2 had a notably higher water activity compared to pellets in Batch 1 after storage for 28 and 56 days in a vacuum bag.

Freeze-drying survival and storage-stability.

The freeze-drying survival and half-life during storage is shown for both batches and all annealing procedures in Table 3. The freeze-drying survival were highest for the non-annealed samples and the samples annealed for one week at -20 ˚C at around 80% of the initial viable cell concentration. The freeze-drying survival was lower for in pellets that had undergone a rapid annealing for 2h at -9 ˚C resulting in a survival of 65%.

Table 3: Summary of freeze-drying survival, the half-life during storage, and average material thickness based on tomography. Half-life is calculated according to eq. 1-3 using data from Figure 2.

Sample		Freeze-drying survival (%)	Half-life Time 0 to 1 month [days]	Half-life 1 month to 2 months [days]	Material thickness, Mode value (*Figure 5*) [μm]
Non-annealed (Canister)	Batch 1	75	4.0	6.4	0.5[a]
	Batch 2	87	6.0	11.9	N/A[b]
2 hour at -9˚C (Canister)	Batch 1	66	6.1	8.9	2.3
	Batch 2	64	4.5	7.3	2
1 week at -20˚C (Canister)	Batch 1	85	7.5	9.8	3
	Batch 2	73	7.5	10.4	3
Non-annealed (Vacuum-bag)	Batch 1	75	6.1	9.2	0.5[a]
	Batch 2	87	9.8	15.5	N/A[b]
2 hour at -9˚C (Vacuum-bag)	Batch 1	66	12.3	16.4	2.3
	Batch 2	64	10.4	12.1	2.0
1 week at -20˚C (Vacuum-bag)	Batch 1	85	13.5	20.4	3.0
	Batch 2	73	17.4	20.4	3.0

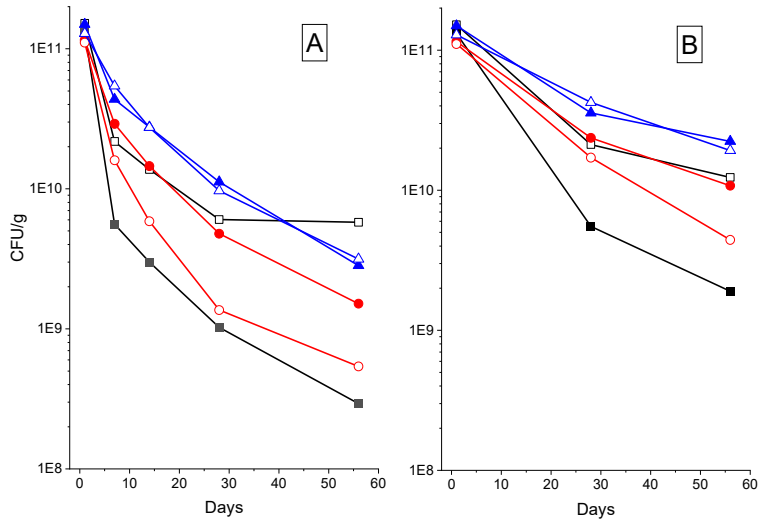[a] Estimated from SEM (Figure 3)

[b] Heterogeneous sample

Figure 2: Survival of freeze-dried Limosilactobacillus reuteri in pellets after storage at 37°C for 56 days. (Batch 1 ■, Batch2 □) Non-annealed, (Batch 1●, Batch 2 ○) annealed for 2h at -9°C, and (Batch 1 △, Batch 2 ▲) annealed for 1 week at -20°C. A) samples stored in a canister with desiccant, and B) samples stored in aluminium vacuum bags.

Structure of the freeze-dried pellets

SEM

SEM images were taken from the middle of the pellet at 200x and 800x magnification (Figure 3). An overview scan of the pellets at 50x magnification and a highly magnified image to detect the cells at 2000x are presented in the Supplementary Material.

The non-annealed samples have a dense fine structure with small pores around 5µm. The pores are aligned in a pattern pointing towards the centre of the pellet. The material thickness is estimated from the SEM images as being around 0.5 µm. There are parts of the non-annealed pellets, where microscopic collapse has occurred, and these parts have a much larger pore size and thicker material. The micro-collapse is inhomogeneous and randomly scattered throughout the pellet. Macroscopic collapsed pellets can be found in Batch 2 of the non-annealed pellets, as some of these pellets have visually deformed structures with bubbles, cavities, and a shinier surface (Figure 1).
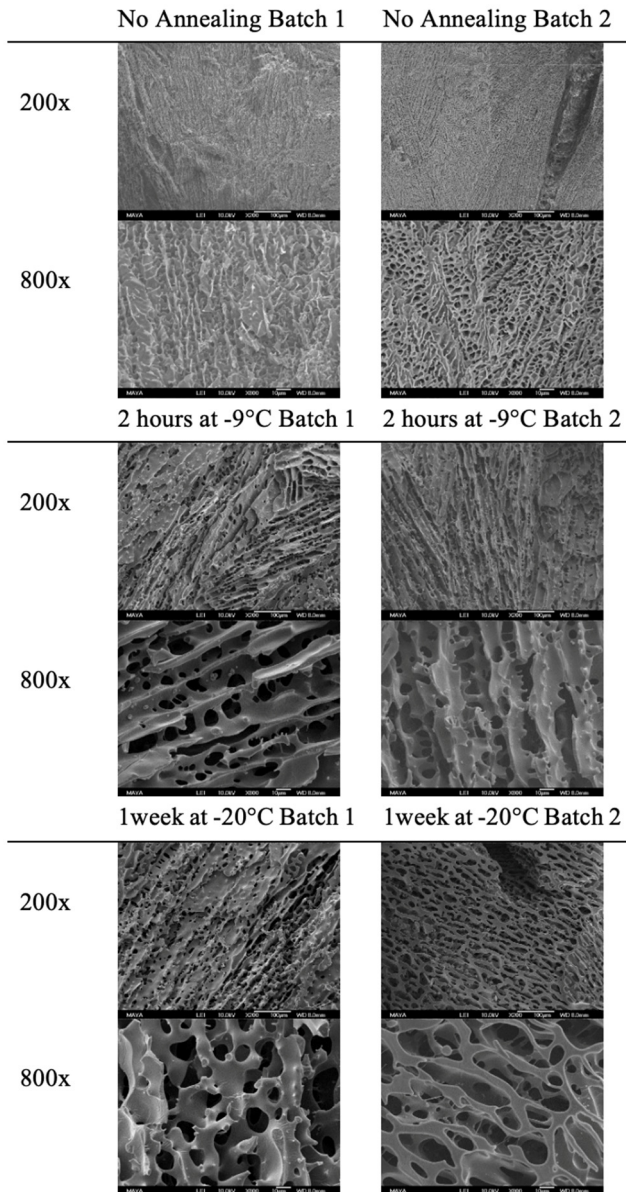
Figure 3: SEM images of the pellets' inner structure taken at 200x and 800x. One intact pellet without any signs of collapse or crack from each protocol and batch was chosen.

The annealed pellets had a coarser structure and thicker materials compared to the non-annealed pellets. The structure has a sheet-like arrangement, where the sheets are oriented towards the centre of the pellet. There is no visual macroscopic collapse amongst the annealed samples, but small regions of microscopic collapse can be detected. The different annealing methods gave similar overall structures, but there are however minor differences. The pellets annealed for 1 week at -20°C have notably thicker material and smoother structure compared to pellets annealed for 2 hours at -9°C. The representative material thickness estimated from the SEM images is >1 µm for pellets annealed for 2h at -9°C and >2 µm for pellets annealed for 1 week at -20°C.

X-ray microtomography

Due to limits in resolution, it was not possible to reconstruct a representative image of the fine and dense structure of the non-annealed pellet. Thus, only the annealed samples were investigated. The results are presented in *Figure 4*. It can be noted that the tomographic image reveals the same anisotropic pore character as the SEM image. The most important information acquired from tomography is the quantification of the material thickness, which was quantified in the 3D image using virtual spheres, 'blobs' embedded in the material. The analyses provided a number distribution of blobs that was converted to a volume-weighted distribution. A volume-weighted distribution is a more representative way to analyze the embedding capacity of the freeze-dried material (Bai Palmkron *et al.*, 2023a; Bai Palmkron *et al.*, 2023b). The results show that samples annealed for 1 week at -20°C had a mode value of 3 µm and a higher ratio of material thicker than 2.5 µm compared to samples annealed for 2h at -9°C which had a mode value of 1.5-2 µm, the results are shown in *Figure 5*.

In the previous investigation (Bai Palmkron *et al.*, 2023b), a similar quantification was made using a formulation consisting of maltodextrin where 1 h respective 4 h annealing at -7°C gave 2.0 µm respectively 2.4 µm in material thickness. Thus, the 3 µm thick structures obtained here after 1 week at -20°C can be considered a rather thick structure.

	Batch 1	Batch 2
2 hours at -9°C		
1 week at -20°C		
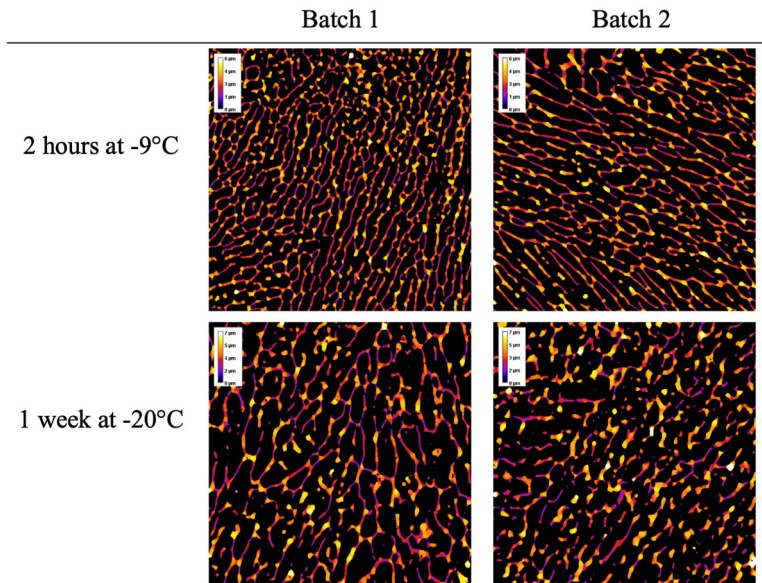
Figure 4: µCT slices of the color-coded local thickness variation, as quantified in 3D. Annealed samples at 2h, -9°C respectively at 1 week, -20 °C were investigated with tomography after drying.
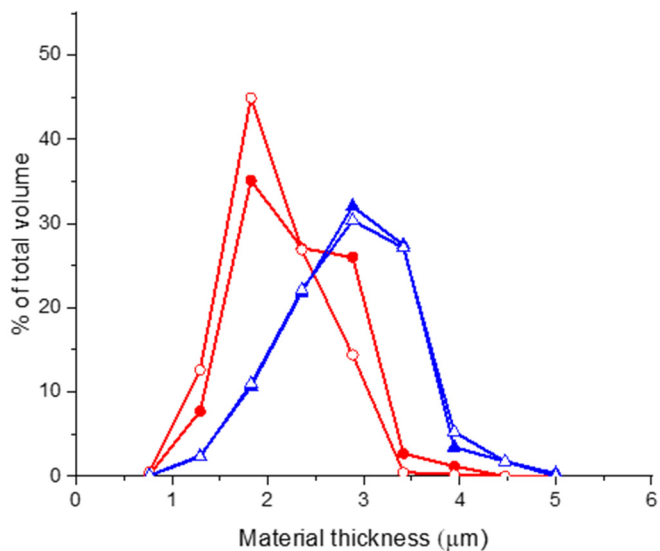

Figure 5: The volume-weighted material thickness distribution was obtained via image analysis of the µCT data sets of the samples, (Batch 1◦, Batch 2 ●) annealed for 2h at -9°C, and (Batch 1 ▲, Batch 2△) annealed for 1 week at -20°C.

14

Discussion

In this study, the structure of differently annealed pellets has been investigated using SEM and µCT to correlate the storage stability of a probiotic bacteria with the encapsulating material thickness. When evaluating the SEM images and µCT data, it is evident that non-annealed pellets have the thinnest material (below the tomographic resolution) and the pellets annealed at -20 ˚C for one week have the thickest material. The other major difference is the appearance of collapsed areas, where the annealed samples show little to no signs of microscopic collapse in the SEM and µCT images, while the non-annealed samples had extensive microscopic collapse and even macroscopic collapse. The non-annealed pellets in Batch 2 had the greatest extent of collapse where large cavities and dents were visually evident. Unfortunately, only intact pellets without visual signs of collapse were investigated using SEM or µCT, but based on previous experience (Bai Palmkron *et al.*, 2023b) and other studies (Ekdawi-Sever *et al.*, 2003), a visual collapse leads to much thicker material structures.

The emergence of structures and collapses is dependent on the freezing, relaxation, and annealing procedures (Bai Palmkron *et al.*, 2023b). The trajectory of these steps in a state diagram can be visualized in *Figure 6*. Due to the rapid freezing, a large number of very small ice crystals are formed, which grow as water diffuses from the freeze-concentrate to the ice crystals. The rapid cooling also results in non-equilibrium freezing where the freeze-concentrate drops below T_g before reaching a maximally freeze-concentrated solution, resulting in a freeze-concentrate with lower T_g than T_g'. When quenched pellets reside in temperatures above their T_g, water from the freeze-concentrate can migrate to the ice crystals. This increases the size and the total volume of ice crystals, further concentrates the freeze-concentrate, and increases its T_g. The relaxation process is rapid and occurs when the pellets reside inside the -30°C pre-cooled freeze-dryer. The rapid rate of relaxation makes it a difficult process to avoid in practice. Annealing refers to the process of ice crystal growth driven by Ostwald ripening and occurs at temperatures above the T_g' of the system. In this process, water is transferred from the small crystals to the larger crystals, resulting in larger more even-sized ice crystals. The annealing process does not increase the overall volume of ice crystals and should not be confused with relaxation where the water is transferred from freeze-concentrate to the ice crystals.

Quenched non-relaxed pellet possesses small ice crystals and a high proportion of freeze concentrate with a low T_g, resulting in an unstable material prone to
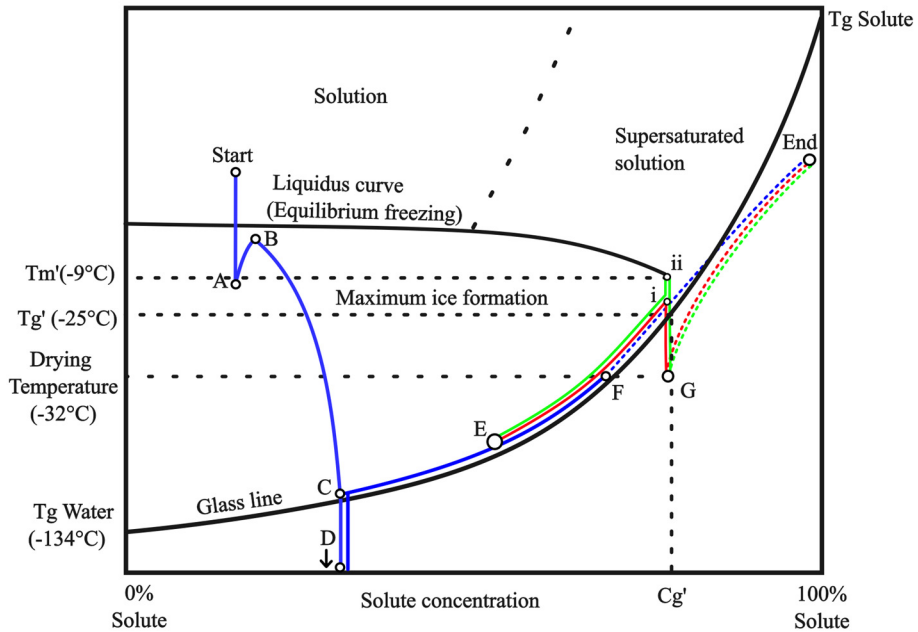
Figure 6: State diagram depicting the formulation comprising of 1/3 maltodextrin (DE 9) and 2/3 sucrose, has its Tg' experimentally measured, with other aspects assumed based on similarities to other systems. Trajectories in blue solid line represent the freezing and storage step for all pellets. A signify the nucleation of undercooled formulation, creating a two phase system comprising of ice crystals and freeze concentrate. The nucleation increases the temperature of the freeze concentrate (B), followed by rapid cooling and crystalization of numerous small ice crystals, further concentrating the freeze concentrate (C). Beyond point (C) the freeze concentrate is quenched and further crystalization is stopped (C-D). Upon storage, the temperature is raised to -80 °C, and water continues to diffuse from the freeze-concentrate to the ice crystals (termed relaxation) until the glass transition concentration at -80 °C is reached (E). The trajectories of the annealing process are signified by a solid red line for pellets annealed at –9°C (i) and a solid green line annealed at -20 °C (ii). Annealing results in a freeze concentrate composition corresponding to Cg'. The freeze-drying occurs at -32°C and is represented by dotted lines. This can contribute to further relaxation for the non-annealed pellets to point (F), while the starting point of drying for the annealed pellets starts at point (G). Notice the difference in the drying starting position between annealed(G) and non-annealed pellets (F). After the ice has been evaporated, the sample is further dried to the stable End point.

global and extensive collapse during drying (Bai Palmkron *et al.*, 2023b). This is evident in Batch 2 of the non-annealed pellets. While Batch 1 had sufficient time inside the -30˚C pre-cooled freeze-dryer to relax and become more stable. Collapse may also be induced by high mass transport resistance for a material consisting of a very fine structure and small pores. The high resistance leads to an increase in pressure at the sublimation front, this may lead to a temperature increase above Tg that causes movements in the material. Thus, collapse is more likely to be observed for the non-annealed pellets than for the annealed ones.

The loss of viability can in many cases be described by an exponential decay (Higl *et al.*, 2007) (equation 1). This aligns reasonably well with the information presented in Figure 2, although with a more rapid initial loss of viability. The slope can be described by the half-life period of the viability ($t_{1/2}$, equation 3). The $t_{1/2}$ values in *Table 3* are compared with the material thickness and presented in *Figure 7*. The results show a strong correlation between increasing material thickness and increased storage stability. Where the most annealed and collapsed pellets (thickest material) yielded the highest stability.
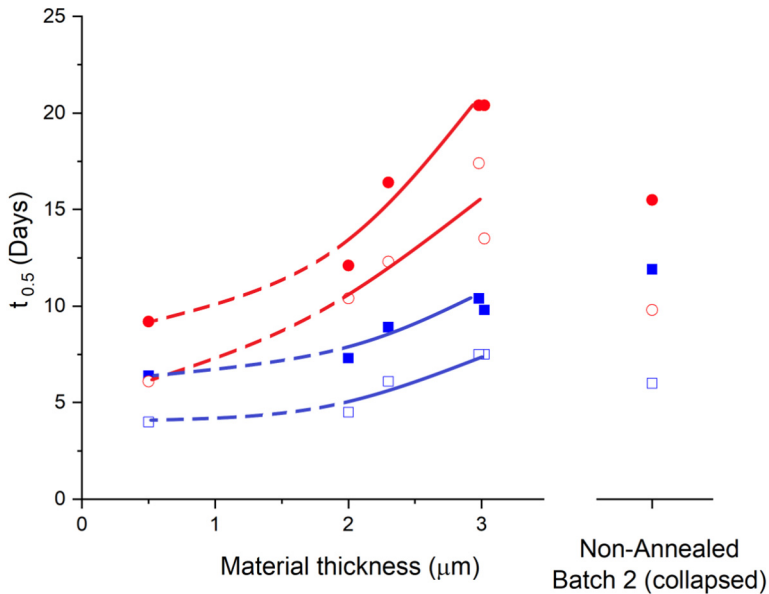

Figure 7: Stability of pellet freeze-dried Limosilactobacillus reuteri as a function of material thickness. The stability is observed as the half-time period of the viability (eq. 1-3) measured during storage at 37°C. Half-time period for (1 month □, 2 months ■) Stored in canister, (1 month O, 2 months ●) stored in a vacuum bag. The dimension of the material thickness has been measured using µCT and quantified using image analysis for all samples above 1.5 µm. For samples with thinner material, the material thickness was estimated from the SEM images and is therefore not fully comparable with the tomographic datasets. The non-annealed sample from Batch 2 had a macroscopically heterogeneous structure that could not be quantified in a meaningful way and is thus presented individually at the right panel in the figure.

The deviation in stability between the batches annealed at -9°C, 2h is considerably larger than the deviation between the batches annealed at -20°C, 1 week. The deviation is also evident when investigating the material thickness where Batch 1 has a slightly higher proportion of thicker material compared to Batch 2. The stability is therefore also higher for Batch 1. The reason for the deviation is unclear but can be due to a small difference in residence time during annealing. This aspect warrants further investigation. The large deviation in appearance and storage

stability between the non-annealed pellets in Batch 1 and Batch 2 is likely due to the difference in degree of relaxation. Batch 1 resided inside the -30˚C freeze dryer for 10-15 minutes longer compared to Batch 2. This is enough time for Batch 1 to become slightly relaxed, which would lead to improved mass transfer conditions (Ekdawi-Sever *et al.*, 2003; Nakagawa *et al.*, 2018). As a result, the short annealed (Batch 1) pellets maintain their microstructure while non-annealed (Batch 2) results in large collapse and a much thicker encapsulating material. The influence of a short relaxation (5-30 min) on the material thickness of quenched pellets is also evident in the work by Ekdawi-Sever et al. The study further revealed that collapsed pellets featuring thicker material exhibited increased storage stability, this correlation was linked to water content rather than the material thickness (where water content showed a covariance with material thickness)(Bai Palmkron *et al.*, 2023b; Ekdawi-Sever *et al.*, 2003). In his study, the water content varied from 1-8%, while the variation in water content in this study was low, between 3.5-4%. Therefore, the water content is considered to have a low impact on the storage stability in this study.

Apart from the impact of material thickness the results also show that the samples stored in vacuum-sealed aluminium bags have significantly higher stability than the samples stored in canisters with desiccant. A possible factor contributing to the increase in stability with increasing material thickness may be correlated to the protection against oxygen in the freeze-dried material. The encapsulating material is composed of amorphous sucrose and maltodextrin which are hydrophilic and should therefore result in slow diffusion of oxygen which is more hydrophobic. Hence, an increased thickness of the encapsulating material will act as a more efficient barrier against oxygen. Kurtmann et al observed a significant instability of freeze-dried *Lactobacillus acidophilus* under an oxygen-rich atmosphere, while it remained stable under an oxygen-depleted atmosphere. The bacteria were also more stable when there was an antioxidant present in the formulation. Kurtmann et al also showed that a high water activity (>0.1) can be detrimental to the storage stability (Kurtmann *et al.*, 2009). As the water activity remained low for all samples during storage, the water activity is considered to have a limited influence on storage stability.

Conclusion

This paper shows the importance of the material thickness of freeze-dried pellets on the stability of the encapsulated bacteria. Primarily, the storage stability showed a strong correlation with the material thickness. Further, the study shows the negative effect of oxygen on storage stability and indicates that thicker materials made of amorphous carbohydrates might hinder the transport of oxygen.

A range of material thicknesses can be obtained by using different annealing protocols and more extensive annealing results in a thicker material. Different degrees of relaxation between batches for the non-annealed pellets resulted in large deviations in structure and storage stability. The deviation between batches was shown to decreased with increasing annealing, where annealing at -20°C for one week resulted in a more consistent structure, compared to annealing at -9°C for two hours.

The benefits of applying extensive annealing are therefore both to increase the storage stability of the probiotic product and to gain control of the freeze-drying process to ensure a homogenous and reproducible product.

References

Badal Tejedor, M., Fransson, J., & Millqvist-Fureby, A. (2020). Freeze-dried cake structural and physical heterogeneity in relation to freeze-drying cycle parameters. *International Journal of Pharmaceutics, 590*, 119891. doi:https://doi.org/10.1016/j.ijpharm.2020.119891

Bagad, M., Pande, R., Dubey, V., & Ghosh, A. R. (2017). Survivability of freeze-dried probiotic Pediococcus pentosaceus strains GS4, GS17 and Lactobacillus gasseri (ATCC 19992) during storage with commonly used pharmaceutical excipients within a period of 120 days. *Asian Pacific Journal of Tropical Biomedicine, 7*(10), 921-929. doi:https://doi.org/10.1016/j.apjtb.2017.09.005

Bai Palmkron, S., Bergenståhl, B., Håkansson, S., Wahlgren, M., Fureby, A. M., & Larsson, E. (2023a). Quantification of structures in freeze-dried materials using X-ray microtomography. *Colloids and Surfaces A: Physicochemical and Engineering Aspects, 658*. doi:10.1016/j.colsurfa.2022.130726

Bai Palmkron, S., Bergenståhl, B., Håkansson, S., Wahlgren, M., Larsson, E., & Millqvist Fureby, A. (2023b). Quantification of structures in quenched annealed and nonannealed freeze-dried pellets using X-ray microtomography *manuscript*.

Bai Palmkron, S. B., Gustavsson, L., Wahlgren, M., Bergensthål, B., & Fureby, A. M. (2022). Temperature and Heat Transfer Control During Freeze Drying. Effect of Vial Holders and Influence of Pressure. *Pharmaceutical Research, 39*(10), 2597-2606. doi:10.1007/s11095-022-03353-4

Béal , C., & Fonseca, F. (2015). Freezing of Probiotic Bacteria. In P. Först & C. Santivarangkna (Eds.), *Advances in probiotic technology* (pp. 187-220). Boca Raton: CRC Press.

Champagne, C. P., Mondou, F., Raymond, Y., & Roy, D. (1996). Effect of polymers and storage temperature on the stability of freeze-dried lactic acid bacteria. *Food Research International, 29*(5), 555-562. doi:https://doi.org/10.1016/0963-9969(95)00050-X

Ekdawi-Sever, N., Goentoro, L. A., & Pablo, J. J. D. (2003). Effects of Annealing on Freeze-Dried Lactobacillus acidophilus. *Journal of Food Science, 68*(8), 2504-2511. doi:10.1111/j.1365-2621.2003.tb07052.x

Fonseca, F., Cenard, S., & Passot, S. (2015). Freeze-Drying of Lactic Acid Bacteria. In W. F. Wolkers & H. Oldenhof (Eds.), *Cryopreservation and Freeze-Drying Protocols* (pp. 477-488). New York, NY: Springer New York.

Giulio, B. D., Orlando, P., Barba, G., Coppola, R., Rosa, M. D., Sada, A., . . . Nazzaro, F. (2005). Use of alginate and cryo-protective sugars to improve the viability of lactic acid bacteria after freezing and freeze-drying. *World Journal of Microbiology and Biotechnology, 21*(5), 739-746. doi:10.1007/s11274-004-4735-2

Higl, B., Kurtmann, L., Carlsen, C. U., Ratjen, J., Först, P., Skibsted, L. H., . . . Risbo, J. (2007). Impact of water activity, temperature, and physical state on the storage stability of Lactobacillus paracasei ssp. paracasei freeze-dried in a lactose matrix. *Biotechnol Prog, 23*(4), 794-800. doi:10.1021/bp070089d

Kharatyan, T., Gopireddy, S. R., Ogawa, T., Kodama, T., Nishimoto, N., Osada, S., . . . Urbanetz, N. A. (2022). Quantitative Analysis of Glassy State Relaxation and Ostwald Ripening during Annealing Using Freeze-Drying Microscopy. *Pharmaceutics, 14*(6). doi:10.3390/pharmaceutics14061176

Kurtmann, L., Carlsen, C. U., Risbo, J., & Skibsted, L. H. (2009). Storage stability of freeze–dried Lactobacillus acidophilus (La-5) in relation to water activity and presence of oxygen and ascorbate. *Cryobiology, 58*(2), 175-180. doi:https://doi.org/10.1016/j.cryobiol.2008.12.001

Nakagawa, K., Tamiya, S., Sakamoto, S., Do, G., & Kono, S. (2018). Observation of Microstructure Formation During Freeze-Drying of Dextrin Solution by in-situ X-ray Computed Tomography. *Front Chem, 6*, 418. doi:10.3389/fchem.2018.00418

Roos, Y. H., & Drusch, S. (2016). Chapter 7 - Time-dependent phenomena. In Y. H. Roos & S. Drusch (Eds.), *Phase Transitions in Foods (Second Edition)* (pp. 215-273). San Diego: Academic Press.

Santivarangkna, C., Aschenbrenner, M., Kulozik, U., & Först, P. (2011). Role of Glassy State on Stabilities of Freeze-Dried Probiotics. *J Food Sci, 76*, 152-156. doi:10.1111/j.1750-3841.2011.02347.x

Santivarangkna, C., Higl, B., & Foerst, P. (2008). Protection mechanisms of sugars during different stages of preparation process of dried lactic acid starter cultures. *Food Microbiol, 25*(3), 429-441. doi:10.1016/j.fm.2007.12.004

Paper V

Synchrotron X-ray Microtomography for in-situ studies of the freeze-drying process in probiotics

THE PURPOSE OF THE PHD PROJECT
Freeze-drying is one of the most common ways to increase the shelf-life of probiotics and pharmaceutics. The impact of freeze-drying process on structure poses a significant challenge for probiotics, as inadequate cell encapsulation due to too thin material can harm the stability. The main purpose of this study is to follow the freeze-drying process in-situ to understand how the freezing, annealing and drying steps affect the final material structure. The study has affirmed the strength of using µCT imaging techniques to study freeze-dried probiotic products, which is of value for BioGaia AB.

USING A LARGE-SCALE INFRASTRUCTURE
Tomographic imaging techniques, both lab-based X-ray microtomography (µCT) and Synchrotron µCT (SRµCT) offer the potential to evaluate the 3D-structure of a freeze-dried product and to follow the evolution of the matrix during freeze-drying. Capturing the dynamic events of freeze-drying in 4D requires the of use synchrotron radiation in combination with an in-situ sample environment, offering a higher photon flux, thus decreasing the acquisition time. This study utilised a novel in-house designed freeze-drying sample environment designed for µCT at ForMAX beamline at MAX IV Synchrotron (Fig. 1) to investigate the structure during freeze-drying of a 20% malto-dextrin solution and pre-frozen pellets.

Figure 1. The sample environment under installa-tion at ForMAX

RESULTS AND IMPACT
To evaluate the efficacy of µCT as a characterization method for quantifying the material of freeze-dried samples, we performed tomography experiments using a lab-based µCT at the 4D Imaging Lab (Lund University, Lund, Sweden) and at the ForMAX beamline. The µCT experiments gave valuable insight into the structure of dry pellets, with a total scan time of 6 hours per sample, which is too slow to study kinetics in 4D.

A critical challenge was to achieve sufficient contrast between ice and freeze-concentrated solution. Using SRµCT at the ForMAX beamline a high spatial resolution and high contrast were achieved at a total scan time of only 45 s per sample. This enabled real-time capture of the structural changes during freezing and drying. Fig. 2 shows reconstructed 2D slices of various steps of freeze-drying. We were able to study both pre-frozen pellets and samples frozen directly in the freeze-dryer. The sample size was 3-4 mm in diameter. The sample holder temperature was varied from -25°C to 0°C during drying and the pressure varied between 40-65 Pa.
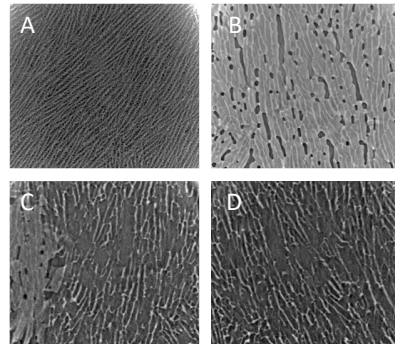

Figure 2. Reconstructed 2D slices of the same sample, captured at the ForMAX beamline, MAX IV Synchrotron. Sample directly frozen (A), annealed at -9 °C (B), partly dried with ice, (C), dried sample (D).

The results provided novel insights into the annealing process, revealing the transformation from a very fine frozen structure to a structure with larger ice crystals. Formation of cracks in the ice occurred due to the annealing process. The material changes only to a minor degree during drying, which also occurs faster in some parts of the samples. It was confirmed that the final ice crystal structure is the key factor for the structure of the dried product.

This project has given the PhD student good insight into planning and executing tomographic imaging experiments, and carrying out image reconstruction, processing, analysis and 3D-rendering. The method developed forms a large part of the thesis work.

Contacts: Shuai Bai Palmkron – PhD-student at Lund University, shuai.bai@food.lth.se
Marie Wahlgren – Supervisor at Lund University marie.wahlgren@food.lth.se
Björn Bergenståhl – Supervisor at Lund University bjorn.bergenstahl@foood.lth.se
Anna Millqvist Fureby – Supervisor at RISE, anna.fureby@ri.se
Emanuel Larsson – X-ray Tomography Expert at Lund University, emanuel.larsson@med.lu.se
Sebastian Håkansson – probiotics expert at BioGaia, sh@biogaia.se